Fall 2015

SUCTION-CONTROLLED CYCLIC TRIAXIAL TEST TO MEASURE STRAIN-DEPENDENT DYNAMIC SHEAR MODULUS OF UNSATURATED SAND

Ganna Suprunenko
University of New Hampshire, Durham

SUCTION-CONTROLLED CYCLIC TRIAXIAL TEST TO MEASURE STRAIN-DEPENDENT DYNAMIC SHEAR MODULUS OF UNSATURATED SAND

BY

GANNA SUPRUNENKO

B.S. Civil Engineering, Mykolayiv Building College, 2012

THESIS

Submitted to the University of New Hampshire

in Partial Fulfillment of

the Requirements for the Degree of

Master of Science

in

Civil Engineering

September, 2015

This thesis has been examined and approved in partial fulfillment of the requirements for the degree of Master of Science in Civil Engineering by:

Thesis Director, Dr. Majid Ghayoomi, Assistant Professor, Civil and Environmental Engineering

Dr. Jean Benoît, Professor, Civil and Environmental Engineering

Dr. Raymond Cook, Associate Professor, Civil and Environmental Engineering

On May 14, 2015

Original approval signatures are on file with the University of New Hampshire Graduate School.

ACKNOWLEDGEMENTS

I would like to thank my research advisor, Dr. Ghayoomi, for providing me with the opportunity that allowed me to pursue a Master of Science degree in the University of New Hampshire. I am grateful for his suggestions, time and effort during two years of my study.

Sincere gratitude to Dr. Benoit and Dr. Cook, who found time to be on my thesis committee, for comments and suggestions in improvement of my academic writing.

I recognize that this research would not be possible without the financial assistance of the National Science Foundation through the NSF CMMI grant No. 1333810 and the Department of Civil and Environmental Engineering (Teaching Assistantships, Summer TA Fellowship), and express my gratitude to those agencies.

I would like to thank the technicians Chris Levesque and Dave Kinney, CEPS Machinist Scott Campbell for their assistance in modification of the triaxial apparatus.

I would like to thank fellow graduate students, Geo-Institute Members for their friendship and wise advice.

Sincere thanks to my boyfriend, Laszlo Kindrat for his support and skillful help in developing Matlab codes for data analysis.

I am endlessly grateful for the encouragement, moral support and attention that my family provided me with.

TABLE OF CONTENTS

LIST OF TABLES

LIST OF FIGURES

LIST OF SYMBOLS

$(u_a - u_w)$ – matric suction

$(u_a - u_w)_b$ – soil air entry pressure

D_{max} –soil maximum damping

e_{max}- maximum void ratio

e_{min}- maximum void ratio

G_s – specific gravity of soil particles

G_{sec} –secant shear modulus

G_{tan} –tangent shear modulus

K_0 – coefficient of lateral earth pressure at rest

$K_{2,max}$ – empirical value based on relative density to calculate small strain shear modulus

R_s – radius of the maximum pore size or radius of the curvature of the contractile skin.

S_e – effective degree of saturation

T_s – surface tension of the air-water interface or the contractile skin

u_a – pore air pressure

u_w – pore water pressure

v_s – shear wave velocity

γ_r – reference shear strain

ε_a –axial strain of the specimen

ε_r –radial strain of the soil specimen

ε_v –volumetric strain of the specimen

θ_r – residual volumetric water contents

θ_s – saturated volumetric water contents

ρ_{dmax} – maximum unit density

ρ_{dmin} – minimum unit density

ρ_w – density of water

σ'_1 – principal effective stress

σ'_2 – intermediate effective stress

σ'_3 – minor effective stress

σ^s –suction stress

σ'_v – vertical effective stress.

τ_{max} – shear stress at failure

ψ_b – air-entry value.

ψ_m – matric suction

ψ_o – osmotic suction

c – cohesion

dr –change in radius of the specimen

D –soil damping

dV – volume change

e –void ratio

G –shear modulus

K - fitting parameter to relate volumetric water content to the effective stress parameter

m – van Genuchten fitting parameter

n – van Genuchten fitting parameter

N –number of cycles.

r –radius of the specimen

S- degree of saturation

z – depth of the soil

α –van Genuchten fitting parameter

γ – unit weight of the soil.

γ –shear strain of the specimen

θ – volumetric water content

λ – pore size distribution index

ν - Poisson's ratio

ρ –density of the material

σ – total stress

φ –angle of internal friction

χ – soil parameter that is related to water degree of saturation

ψ – total suction

ABSTRACT

SUCTION-CONTROLLED CYCLIC TRIAXIAL TEST TO MEASURE STRAIN-DEPENDENT DYNAMIC SHEAR MODULUS OF UNSATURATED SAND

by Ganna Suprunenko

University of New Hampshire, September, 2015

Recent advancement in unsaturated soil mechanics revealed the influence of the degree of saturation on dynamic properties of soils due to inter-particle suction forces. However, because of the complexities in states of stress and experimental modeling, most of the recent studies only focused on small-strain shear modulus. Cyclic triaxial system at the University of New Hampshire was renovated and modified for suction control to enable testing the soils with different degrees of saturation at medium to large strain levels. A set of strain- and stress-controlled cyclic triaxial tests were performed on dry, saturated, and partially saturated sand specimens. The measured moduli were consistent with the predicted values from the available empirical relations. Higher modulus was estimated in specimen with mid-range degrees of saturation. Although the results indicated the success of the newly developed suction-controlled system, there were challenges in testing process that needs to be addressed in future work.

CHAPTER I. INTRODUCTION

1.1 Motivation

Unsaturated soils are present mostly in the shallow part of the earth, where water table is located near the surface. The vadose water above the water table that is heavily influenced by capillary effects is under negative pore pressure. It is expected that this negative pore pressure and consequently the presence of suction stresses influence the soil mechanical properties. This includes the dynamic soil characteristics such as dynamic shear modulus and damping. However, conventional soil mechanics equations are based on dry or fully saturated conditions, which resulted in a gap in the geotechnical engineers' knowledge when it comes to unsaturated soil mechanics. For example, the response of different geotechnical systems that are located in surficial unsaturated soils will be different from those in dry or saturated soils.

Various dynamic loads, such as road and rail traffic, blasts, or earthquake will result in a different response in soil than from the static loading. For accurate analysis of soil behavior under dynamic loading, accurate estimation of dynamic soil properties is needed. Soil-structure interaction problems, for example, require two major parameters in estimation of dynamic response: shear modulus and damping ratio. Various researchers conducted series of tests, and formulated equations based on the experimental data (Seed and Idriss 1970, Hardin and Drnevich 1972, Seed et al. 1986) concluding that the shear modulus and damping are mostly influenced by the mean effective stress, relative density of the soil, and induced shear strain.

Experimental difficulties, such as direct measurement and maintaining matric suction caused delay in investigation and understanding the behavior of partially saturated soils. Only recently, researchers investigated the variation of small-strain shear modulus in unsaturated soils with different suction levels using bender element tests (Marinho et al. 1995, Ng et al. 2009, Ghayoomi and McCartney 2011) and resonant column tests (Mancuso et al. 2002, Mendoza et al. 2005, Khosravi and McCartney 2011). However, the effect of the degree of saturation on soil stiffness for medium to large strain levels is still under investigation.

1.2 The scope of the study

In this project, the existing cyclic triaxial system from Geotechnical Testing and Consulting System (GCTS) at the University of New Hampshire was renovated and modified for suction-control testing capabilities using axis translation technique. This system was successfully tested after implementing the following major changes to the original system: a new bottom platen with embedded High Air Entry Value (HAEV) ceramic disc that was machined and installed for precise control of matric suction, the axial loading piston was redesigned and constructed to enable cyclic reversals, and a DigiFlow flow pump was included in the system to apply and control the pore pressure, an independent Differential Pressure Transducer was used to monitor the suction.

After the completion of the system, a set of dynamic triaxial tests on F-75 Ottawa was scheduled and performed. In order to confirm the reliability of measured data, two main parts of the setup (triaxial system and the Flow Pump) were checked separately prior to conducting the tests on unsaturated soils. Using the GCTS system, dynamic tests on completely dry specimens were conducted and compared to results published in the literature. The hydraulic hysteresis of Ottawa F75 sand was measured with the Flow Pump and verified with the previous studies. The

results from both parts of the system showed good agreement with the existing research data and the full setup was used for the subsequent dynamic soil testing on saturated and unsaturated soils. These tests include both strain- and stress-controlled cyclic loading on sands with various degrees of saturation under different axial strain amplitudes. Overall, over 200 sand specimens were prepared and tested. This includes tests required for system calibration, troubleshooting test issues, problematic tests, and final acceptable tests. The objective was, first, to study the effect of degree of saturation on shear modulus and, second, to check the consistency of shear modulus reduction curves for unsaturated soils considering the changes in the effective stress equation.

1.3 Thesis outline

This thesis is presented in 12 chapters, starting with a brief introduction in Chapter 1. Chapter 2 is subdivided into two parts. The first part provides a theoretical background on dynamic soil properties and its use in geotechnical systems. Particular emphasis is given on shear modulus and damping ratio in sandy soils, which are described in the second part of the chapter. Typical equations for estimation of small strain shear modulus and shear modulus reduction curves are discussed.

Chapter 3 gives an introduction on unsaturated soils, explaining the importance of the study through the effective stress equations. Basic information on soil suction is presented, including techniques of measuring suction in laboratory. Wetting and drying paths of hydraulic hysteresis are discussed in detail, including description of three regimes in soil-water characteristic curve. Two main approaches for estimation of effective stresses in unsaturated soils are introduced in this chapter.

Chapter 4 provides information on physical and mechanical properties of the tested material. This includes sieve analysis, results on measuring maximum and minimum soil density, soil friction angle, and Poisson's ratio that were measured during this study, and soil-water retention curves for Ottawa F75 sand that was also measured as part of this project. Chapter 5 talks about existing triaxial apparatus in the Geotechnical Laboratory at the University of New Hampshire. Incorporation of the Flow Pump for testing partially saturated soils is discussed. Chapter 6 gives an explanation on the testing procedure that was used in this study. Sample preparation and triaxial cell assembly process are supported with figures for a visual representation. Three stages of the triaxial tests are explained including detailed description of cyclic strain and stress application.

Chapter 7 presents results of dynamic strain controlled tests on dry Ottawa F75 sand started with showing the representative hysteresis loops. Young's and shear moduli are plotted against strain for different confining pressures. Shear modulus reduction curves were built using three different formulas and plotted on top of normalized shear modulus data. The consistency of the data with available formulas from the literature was discussed.

Chapter 8 shows results for dynamic strain controlled tests on fully saturated soil specimens. Characteristic hysteresis loop of deviator stress versus axial strain is presented. Young's and shear moduli are calculated and plotted against axial and shear strain, respectively. The issue with increase of pore pressure is addressed and typical graphs are shown in this chapter.

Chapter 9 provides results from strain-controlled tests on partially saturated sand specimens. Dynamic shear moduli for different matric suction levels are plotted against shear

strain amplitude. Then, the effect of suction on shear modulus was discussed. In addition, the shear modulus reduction data are formed and discussed.

Chapter 10 shows results of stress-controlled tests on dry and partially saturated soils. Shear modulus reduction curve is plotted alongside the measured normalized values for all stress-controlled tests. The effect of strain level and degree of saturation on modulus were shown and discussed.

Chapter 11 focuses on the main discussion and summary of results. The data for all the acceptable tests are presented using the normalized shear modulus plots for various levels of saturation. Different marker types and coloring is used to distinguish between stress- and strain-controlled tests, as well as different levels of saturation. The change in shear modulus for soil under different degrees of saturation is presented and discussed in this chapter. Finally, conclusions from the thesis and recommendations for future research are given in Chapter 12

CHAPTER II. DYNAMIC SOIL PROPERTIES

2.1 Introduction

Soils can be subjected to various dynamic loads, such as earthquakes, blasts, road and rail traffic, wind, ocean waves, pile driving, or mining. These might be sinusoidal (e.g. machinery effects) or random in nature (e.g. earthquakes). The behavior of soils under these conditions is different from that under static conditions. Structural collapse, permanent deformation, or tilting of foundations are the most common results of inadequate dynamic resistance of soils. Dynamic load characteristics vary by the nature of their origin, therefore they result in different soil response.

Dynamic vibration in dry soils may lead to seismic compression while in fully saturated soil might lead to liquefaction. In the latter, the strength of the soil is reduced dramatically to the point where the soil is not able to sustain structures and it behaves as a fluid. Dynamic bearing capacity, soil-structure interaction, and earthquake resistance of structures are typical application of soil dynamics in geotechnical systems. Dynamic soil properties are key elements in the seismic design and performance assessment of geotechnical systems, where they are influenced by the state of stress of the soil and loading conditions. In order to seismically assess the response of a geotechnical system, motion characteristics have to be determined at different depths in the soil. Consequently, the dynamic properties of soils at different depths will be the controlling factor in these types of analysis.

Mohr circles have been traditionally used to show the state of stress in materials, where various points on the circle represent different stress combination states. These circles can be developed for both stresses and strains that help to understand the concepts of failure, stress and strain rotations, determine principal stresses and strains, as well as maximum shear stresses and strains. The maximum shear stresses and strains estimated from the Mohr circle, then, is used in dynamic analysis, where the Mohr circle evolves with continuous change of shear stresses and strains. Plotting the shear stress versus the shear strain throughout cyclic loading, a hysteresis loop is found. From this graph, dynamic properties of soils may be obtained, which will be characterized by the shape and the path of the loops, as shown in Figure 1.

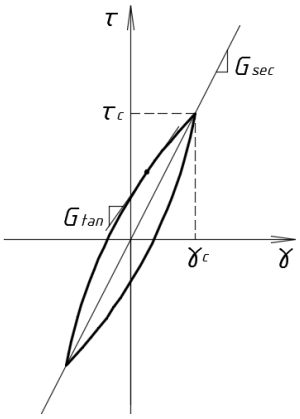

Figure 1 Hysteresis stress-strain relationship during cyclic loading (after Kramer 1996)

2.2 Shear modulus and damping ratio in sand

Shear modulus and damping are the two key dynamic properties of soils. Shear modulus representing soil stiffness in shear is determined from the slope of stress-strain curve. Damping is the phenomena that dissipate the energy in the system and reduces the amplitude of the motion. Parameters such as strain level, loading pattern and intensity, overburden pressure, and water content can affect these properties (Seed et al. 1970 and Kramer 1996). There exist a wide variety

of methods to determine these characteristics, both in-situ and ex-situ, or through empirical relations.

The typical hyperbolic hysteresis curve, shown in Figure 2, is used to estimate the shear modulus and damping values. The backbone curve, which forms a basis for the stress-strain response, is defined by two key values: 1) the modulus at very small strain (G_{max}) and the asymptote at large strain (i.e. shear strength, τ_{max}). Previous experience have shown that soils soften as shear stress application continues. Consequently, shear modulus at different strain levels (i.e. slope of the backbone curve), decreases by increasing the shear strain.

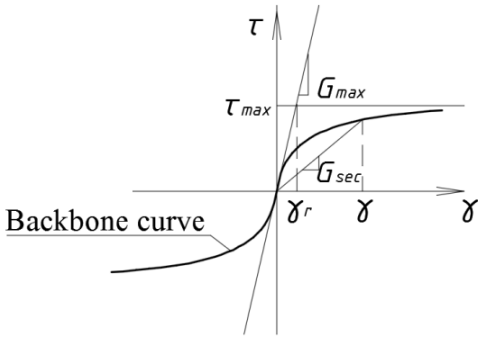

Figure 2 Backbone curve (after Kramer 1996)

The small strain shear modulus (G_{max}) is typically assigned to shear strains less than 10^{-4}% (Kramer 1996). It is referred to as the maximum modulus because it is the steepest slope in the stress-strain relation for a given overburden pressure and density. G_{max} is directly related to the soil shear wave velocity using the following equation

$$G_{max} = \rho v_s^2 \qquad (1)$$

where ρ is the total density of the material and v_s is the shear wave velocity that can be obtained by geophysical tests. Most of the geophysical methods are based on wave propagation theory and

are performed at shear strains lower than $3 \cdot 10^{-4}\%$. Seismic geophysical tests include generating stress waves and analyzing their travel time and path at different locations.

The small-strain shear modulus can be determined through different experimental laboratory techniques. The most common method is the resonant column test that uses an electromagnetic loading system for torsional or axial loading of cylindrical soil specimen. The soil element can be solid or hollow, and is subjected to consolidation before the cyclic load application with controlled amplitude and frequency. The test begins with the low frequency which gradually increases until the strain amplitude of the soil reaches its maximum value. In case of solid specimens under torsion, the shear strain varies from zero in the centerline of the sample to the maximum value at the outer edge. The resonant column test allows determination of shear modulus and stiffness of the soil specimen, as well as investigation of various effects such as mean effective stress or strain amplitude on dynamic soil properties.

Piezoelectric bender element test is another method for measuring shear wave velocity in the laboratory. Bender elements are designed as two piezoelectric materials bonded together so that applied voltage will cause one to expand and another to contract. This behavior will result in bending of the element and produce a voltage, which allows using these elements as both transmitters and receivers. During the test they are placed on the opposite sides of the specimen, and a voltage pulse is applied to one of them. Generated shear wave travels through the soil and reaches the receiver that produces another voltage pulse. The time difference is measured between the pulses and yields in shear wave velocity of the specimen by dividing over the distance between the bender elements. This method has a versatile application as it can be incorporated into direct simple shear, oedometer, conventional and cubical triaxial device.

Previous studies on dynamic soil properties of soils demonstrated that G_{max} is related to parameters like mean effective stress, stress history, void ratio, and soil mineralogy (Hardin and Drnevich 1972, Seed et al. 1970). Hardin (1978) proposed a general multiplicative form of G_{max} as follows:

$$G_{max} = A(OCR)^{K} f(e) P_a^{1-n} p'^{n} \tag{2}$$

where A and n are fitting parameters that vary for different soils, OCR is the over-consolidation ratio, p' is the mean effective stress, P_a is the atmospheric pressure, K is the hardening parameter related to the plasticity of soils PI, and $f(e)$ is the function of void ratio such as the following forms proposed by different Hardin and Black (1968) and Hardin (1978), respectively.

$$f(e) = \frac{(2.97 - e)^2}{1 + e} \tag{3}$$

$$f(e) = \frac{1}{0.3 + 0.7 \cdot e^2} \tag{4}$$

Following this format, several investigators proposed empirical equations to estimate the small strain shear modulus. Hardin and Black (1968) proposed Equation 5 for round-grained sand:

$$G_{max} = \frac{6908 \cdot (2.17 - e)^2}{1 + e} \cdot \sigma'^{1/2}_{o} \tag{5}$$

where e is the void ratio for sand, and σ'_0 is the mean effective stress in SI units.

They also presented Equation 6 for angular-grained sand.

$$G_{max} = \frac{3230 \cdot (2.97 - e)^2}{1 + e} \cdot \sigma'^{1/2}_{o} \tag{6}$$

where the mean effective stress can be calculated using the following formula

$$\sigma'_0 = \frac{1}{3}(\sigma'_1 + \sigma'_2 + \sigma'_3) \quad (7)$$

Further, Seed et al. (1970) proposed Equation 8 for sands.

$$G_{max} = 1000 K_{2,max} (\sigma'_m)^{1/2} \quad (8)$$

where $K_{2,max}$ is obtained from relative density or void ratio and σ'_m is the mean principal effective stress. σ'_m should be taken in psf. The parameter $K_{2,max}$ varies depending on the type of soil. Typical values are presented in Table 1.

Table 1 K-values proposed by Seed and Idriss (1970)

Relative density (%)	$K_{2,max}$
30	34
40	40
45	43
60	52
75	61
90	70

Since the shear modulus decreases as shear strains increase, shear modulus reduction functions have been developed linking the strain-dependent shear modulus to the induced shear strain in soils. Tangent shear modulus may be obtained at any point of the stress-strain graph, but secant shear modulus may be used as the approximation of the whole cycle, as shown in Figure 3. Due to the computational difficulties involved with tangent modulus, secant modulus has been widely used in geotechnical seismic analysis. As a result, it can express the general inclination of the loop, which depends on soil stiffness. Secant shear modulus is determined using the following equation

$$G_{sec} = \frac{\tau_c}{\gamma_c} \tag{9}$$

where τ_c is the shear stress and γ_c is the shear strain corresponding to the load cycle. The secant shear modulus depends on the cyclic strain. It is high at low strain amplitudes of loading, and declines as the amplitude rises.

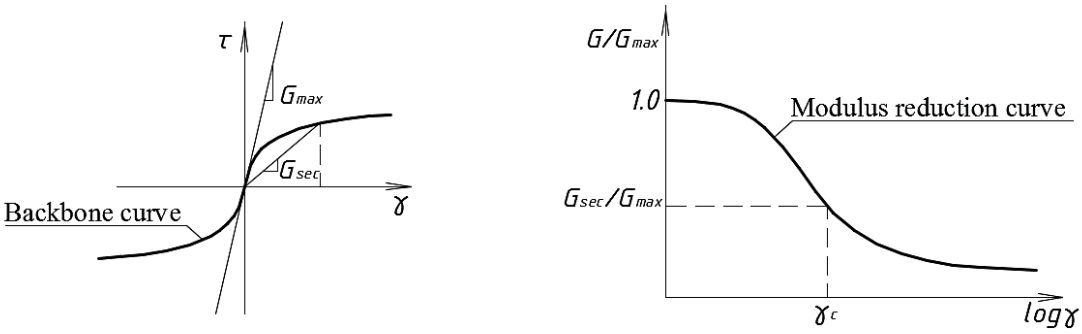

Figure 3 Modulus reduction (after Kramer 1996)

The steepest slope is at the origin of the graph. Therefore, it shows the highest value of shear modulus. In geotechnical earthquake engineering the ratio of $\frac{G_{sec}}{G_{max}}$ is called the modulus reduction ratio.

The medium to large strain shear modulus can be obtained using cyclic direct simple shear test, cyclic triaxial test, or torsional shear test. The former is the most common for liquefaction testing, as it can reproduce earthquake stress conditions with high precision. A small cylindrical specimen is confined between rigid platens or a series of rings stacked together to prevent lateral deformation. Shear stress can be applied from the top or bottom surfaces of the specimen, without any stresses on the vertical sides. Non-uniform distribution of stresses can have a significant effect on soil response, unless the diameter/height ratio of the specimen is increased.

In cyclic torsional shear device isotropic and anisotropic initial stress conditions can be created, followed by cyclic shear stress application on horizontal planes. Shear strains range from

zero along the axis to the maximum value at the outer edge of the specimen; therefore hollow devices are preferred over solid ones.

Due to the simplicity of the test and availability of the testing equipment, cyclic triaxial test is the most commonly used test for measuring shear modulus and damping ratio at medium to high strain levels. Cyclic load can be applied through stress- or strain- controlled program, where amplitude and frequency are set. To simulate different site conditions isotropic or anisotropic loading can be applied to the specimen. Axial strain and deviator stress measured in cyclic triaxial test can be used for computation damping ratio and shear modulus. System compliance does not allow measurements at shear strains lower than 0.01% in this testing equipment.

Ishibashi and Zhang (1993) proposed the following empirical relation to estimate the shear modulus reduction.

$$\frac{G}{G_{max}} = K(\gamma, PI) \cdot (\sigma'_m)^{m(\gamma,PI)-m_0} \tag{10}$$

where

$$K(\gamma, PI) = 0.5 \cdot \left\{1 + \tanh\left[\ln\left(\frac{0.000102 + n(PI)}{\gamma}\right)^{0.492}\right]\right\} \tag{11}$$

$$m(\gamma, PI) - m_0 = 0.272 \cdot \left\{1 - - \tanh\left[\ln\left(\frac{0.000556}{\gamma}\right)^{0.4}\right]\right\} \exp(-0.0145PI^{1.3}) \tag{12}$$

$$n(PI) = \begin{cases} 0 & \text{for } PI = 0 \\ 3.37 \cdot 10^{-6} PI^{1.404} & \text{for } 0 < PI \leq 15 \\ 7.0 \cdot 10^{-7} PI^{1.976} & \text{for } 15 < PI \leq 70 \\ 2.7 \cdot 10^{-5} PI^{1.115} & \text{for } PI > 70 \end{cases} \quad (13)$$

Since the hysteresis loops more or less form a hyperbolic curve, hyperbolic formula was fitted to the modulus reduction curves, as in the following equation (Hardin and Drnevich 1972).

$$\frac{G}{G_{max}} = \frac{1}{1 + \frac{\gamma}{\gamma_r}} \quad (14)$$

where γ is shearing strain, G_{max} is the small strain shear modulus, γ_r is the reference strain that can be computed using the following formula:

$$\gamma_r = \frac{\tau_{max}}{G_{max}} \quad (15)$$

where τ_{max} is the shear stress at failure that depends on the initial state of stress in the soil and can be calculated using Equation 16 (Hardin and Drnevich 1972):

$$\tau_{max} = \left\{ \left[\frac{1 + K_0}{2} \sigma'_v \sin\varphi' + c' \cos\varphi' \right]^2 - \left[\frac{1 - K_0}{2} \sigma'_v \right]^2 \right\}^{1/2} \quad (16)$$

In which K_0 is the coefficient of lateral earth pressure at rest, c' and φ' are static strength parameters, σ'_v is vertical effective stress.

Later Darendeli (2001) modified the formula by adding another material parameter "a", as in Equation 17

$$\frac{G}{G_{max}} = \frac{1}{1 + (\frac{\gamma}{\gamma_r})^a} \tag{17}$$

Based on an extensive set of torsional shear test data, Menq (2003) proposed the following empirical equations to estimate γ_r and a.

$$\gamma_r = 0.12 \cdot C_u^{-0.6} \cdot (\frac{\sigma'_m}{P_a})^{0.5 \cdot C_u^{-0.15}} \tag{18}$$

$$a = 0.86 + 0.1 \cdot \log(\frac{\sigma'_m}{P_a}) \tag{19}$$

where C_u is the coefficient of uniformity, P_a is atmospheric pressure, σ'_m is the mean effective stress. Reference strain in this equation is obtained in percentage.

The area of the stress-strain hysteresis loop is dependent on the breadth. It expresses the energy that was dissipated during the test, described as damping ratio. It was proved empirically that it happens even at very low strain levels, therefore damping is never zero. It depends on plasticity characteristics of the soil. Damping ratio for soils of low plasticity is higher than those of high plasticity if applying the same amplitude (Das, 1993). At the same time, with increasing strain amplitude the damping ratio also increases.

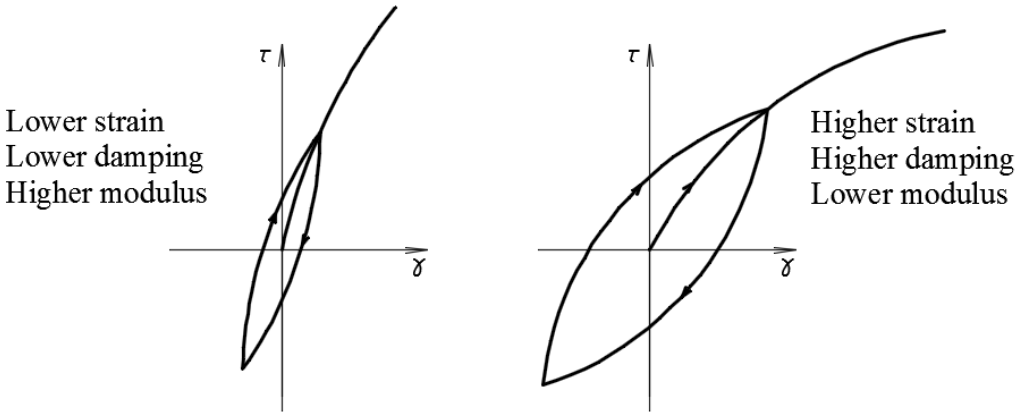

Figure 4 Effect of shear strain on dynamic soil properties (after Silver, and Seed 1969)

The relationship between damping ratio and shear modulus can be written as (Hardin and Drnevich, 1970)

$$D = D_{max}\left[1 - \frac{G}{G_{max}}\right] \tag{20}$$

Where D_{max} is the maximum damping (damping at large strain), G is the strain-dependent shear modulus, and G_{max} is the maximum shear modulus. D_{max} can be calculated in a cyclic test using the following formula (Seed and Idriss 1970)

$$D_{max} \approx 30 - 1.5\log_{10} N \tag{21}$$

where N is the number of cycles. In general, damping depends on several factors including confining pressure, cyclic strain, void ratio, number of cycles, frequency of loading, and soil structure and geologic age.

The relationship between shear stress and shear strain of soil can be described with equivalent linear model that is characterized by secant shear modulus and damping. Secant shear modulus shows the average value of the slope over the entire cycle of loading. For this purpose, two end points of the hysteresis loop should be connected to calculate the stiffness of the soil. More complicated models can be used in ground response analysis, and those allow prediction of the change in shear modulus taking the history of the soil into account.

CHAPTER III. UNSATURATED SOILS

3.1 Introduction

The soil layer in the ground may be divided into two parts with regards to water table: vadose and saturated zone. In geotechnical engineering, the zone between the water table and the ground surface serves to transfer water from the atmosphere to the groundwater and is called vadose zone. In this case the degree of saturation may vary from 0 to 100% with negative pore water pressure. Capillary fringe is a fully saturated zone immediately above the water table. Depending on the soil type it could be up to 10 meters thick. In this capillary zone air phase is discontinuous, while water phase may be assumed to be continuous. Desaturation or air-entry can occur in the upper portion of the soil body through cracks and fissures. Figure 5 shows the profile of saturated and unsaturated zone in the natural hydrologic cycle.

The groundwater table is highly influenced by changes of climate. The difference between downward and upward flux of water forms the soil profile in terms of groundwater table location. An equilibrium or hydrostatic condition might be reached with zero net flux, while evaporation equals precipitation. Apart from this, soils that are deposited in arid or semi-arid areas near the ground surface can have negative pore-water pressure. Shrinkage cracking of fine grained soil can occur in hot weather with evaporation, while wetting will result in closure of cracks and swelling. Uptake of water by plants and other vegetation may also dry the soil. Furthermore, future changes in climate on Earth may result in substantial shift of soil moisture regime.

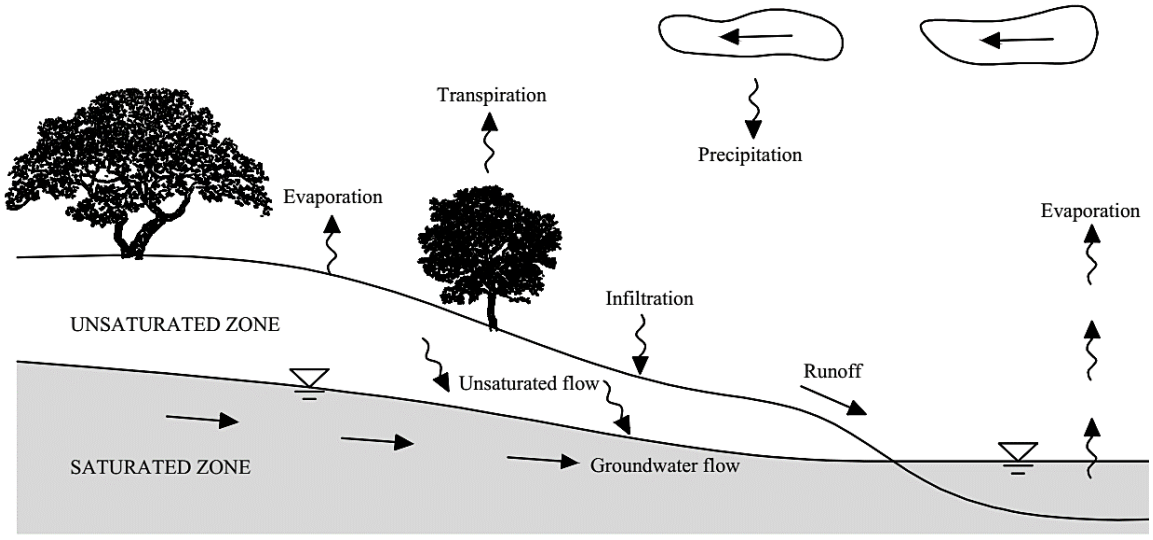

Figure 5 Schematic diagram of unsaturated soil environment (After Lu and Likos 2004)

Soils in nature tend to be fully saturated near the water table and become unsaturated closer to the ground surface. A significant part of the Earth is covered with arid and semi-arid regions. The change of degree of saturation through the soil profile is shown in Figure 6. The research on unsaturated soils was mostly conducted in region where the earth is rarely covered with saturated soils. In these areas water table might be far below ground surface and soil will be unsaturated. Soils such as collapsible, residual and swelling are problematic because of changes in the negative pore-water pressure that lead to changes in shear strength.

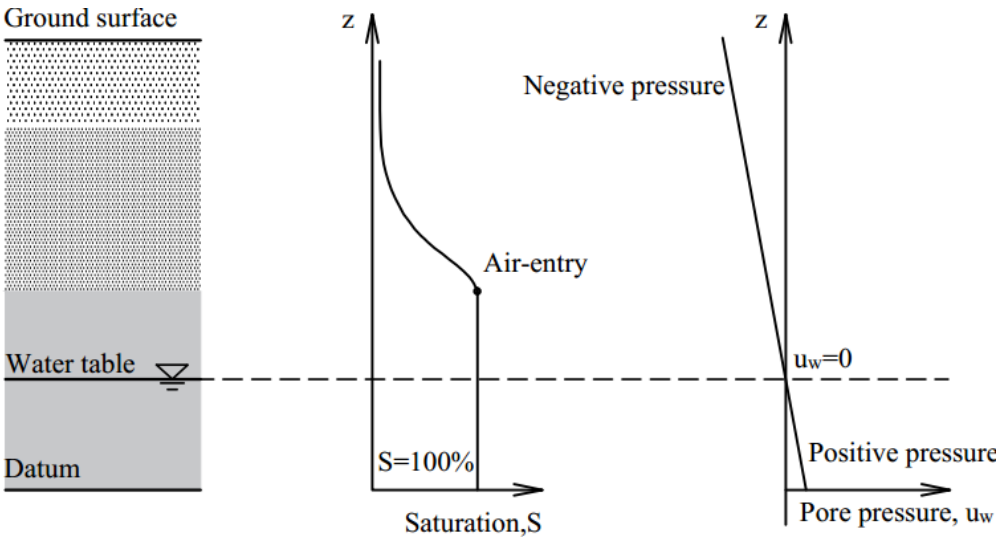

Figure 6 Saturation and pore pressure profiles for unsaturated soil zone (After Lu and Likos,2004)

Conventional soil mechanics is based on soils in either dry or fully saturated conditions. However, these are only two limiting conditions that are not applicable to the whole Earth surface. The representative element of soil volume consists of solid particles, water and air. However, for unsaturated soils the air-water interface should also be taken into account. It is represented by a thin membrane that stands separately from air or water phases and is called “contractile skin”, which contributes to a surface tension between the particles.

3.2 Soil suction

Unsaturated soil particles are connected through negative pore pressure and surface tension that can be referred to as suction stress. Forces that occur in saturated and unsaturated soils can be divided into three groups (Lu and Likos,2006):

- Active forces that propagate through soil grains (“skeletal”)
- Active forces concentrated at the inter-particle contacts (“local”)

- Passive particle contact forces that counterbalance the first two groups of forces

Saturated soils have local inter-particle forces that may include van der Waals attraction, electrical double-layer repulsion and the net attraction that arises at the grain contacts from chemical cementation. In unsaturated soils, in addition to physicochemical forces, negative pore-water pressure creates attractive forces and surface tension at air-water interface (Lu and Likos, 2006). For saturated soils pore-water pressure acts over the entire surface of grains, and it can be treated as a continuum medium. However, for unsaturated soils pore pressure can be described as three types of forces that act through liquid and air phases:

- Water pressure that acts on wetted areas of soil
- Air pressure that acts on dry portions of the soil grains
- Surface tension in air-water interface

Tensile stress in unsaturated soil is inversely proportional to the diameter of particle (Lu et al. 2007). For fine-grained soil tensile stress can be several kilo-Pascals, while for coarse grained soils it can reach only tens of Pascals. The primary mechanisms that can affect pore water potential in the soil are capillary effects, particle-pore water interaction (short-range adsorption), and osmotic effects. Short range adsorption is important mostly for fine-grained soils, and occur from electrical and van der Waals force fields. Negative charge on the outer surface of the clay minerals creates electrical fields, while molecule interaction between soil and water particles creates van der Waals forces. The effect of those fields is the most significant close to the particle surfaces and it decreases rapidly with distance. Therefore, soils with low water content that contain water mostly in thin films around particles are influenced by the short-range adsorption effects.

Capillarity and short-range adsorption effects can be defined as a matric suction, that is of the primary interest in the current study.

Osmotic effects occur as a result of solutes that can be dissolved in pore water. The solutes can be introduced externally (leaching processes) or occur naturally. Suction that arises from that effects is referred to as osmotic suction. For the entire drying and wetting process osmotic suction stays the same, unless the concentration of the solute changes.

Combined effects of short-range adsorption and capillary fringe can be combined into matric suction. However, the magnitude of inter-particle stress components depends on the soil type. For example, van der Waals attraction and double-layer repulsion are applicable for clays and silts with the particle size smaller than 10μm. Capillary attraction is active in all soil types and is represented by a function of water content and particle size. The peak value as a function of saturation occurs at relatively low degree of saturation (Lu and Likos, 2006).

Cementation forces are created from covalent and ionic bonds that occur between cementing agent and soil particles. Those forces are considered to stay constant regardless of the degree of saturation or particle size. Total soil suction may be described with the following equation (Fredlund, 2006):

$$\psi_t = \psi_m + \psi_o \tag{22}$$

where ψ_m is the matric component and ψ_o is the osmotic component of suction. In geotechnical engineering, measuring matric suction that is directly related to the negative pore pressure is imperative both in-situ and in laboratory.

3.3 Techniques of controlling suction in unsaturated soils

Vapor control technique is based of humidity control in the closed system. Bernier et al. (1997) installed oedometer cells inside a chamber with relative humidity control. Water molecules migrate through the vapor phase to the soil pores until equilibrium is reached. However, this process is highly dependent on diffusion and moisture equilibration takes a long time.

An osmotic technique was used by Delage and Cui (2008a) with the sample placed in a membrane permeable to water, while a solution with polyethylene glycol (PEG) molecules was circulated behind the membrane. The PEG molecules are not able to penetrate the membrane, resulting in application of osmotic suction. The concentration of the solution affects the suction application. The advantage of this technique is that there is no need for pressure application even for high suction levels.

The most commonly popular technique for measuring suction in the laboratory is axis translation technique (Hilf 1956). This method started to develop with pressure plate apparatus in the middle of the XIX century (Richards 1941, Gardener 1956). The procedure includes liquid phase control through a saturated interface, saturated High Air Entry Value (HAEV) disc and artificial increase of the air pressure in the soil sample. This technique proved to be reliable and provide judicious results. It gives data points even at elevated suction levels, as well as nearly saturated conditions. Basic concept of the axis translation technique is shown in Figure 7.

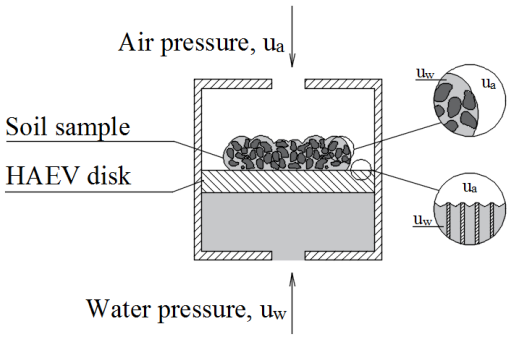

Figure 7 Axis-translation technique

Water pressure is applied from the bottom of the specimen through a HAEV ceramic disc, while air pressure can be artificially increased from the top of the specimen. The difference in pressure at the bottom and at the top of the specimen is measured with a differential pressure transducer. Although, the pressure induced to the sample at the boundaries does not represent the real picture, it needs to equilibrate through the soil to give reasonable results of matric suction. To control the volume of water moving in and out of the specimen and to monitor the equilibrium suction stage a feedback loop is required.

3.4 Soil-water characteristic curve

The water content in an unsaturated soil system affects the physical and physicochemical mechanisms that influence the soil suction. Soil-Water Characteristic Curve (SWRC) represents a constitutive function between matric suction and degree of saturation. It describes thermodynamic potential of pore water in the soil to free water as a function of volume of water adsorbed by the soil system (Lu et al. 2007).

Soil-water characteristic curve can describe wetting and drying process of the soil sample that form a hysteresis. Soils that experience evaporation or drainage as a result of the drying

process tends to retain more water than that of the same suction level under a wetting process, which can be caused by capillary rise or infiltration. Hysteretic behavior is a result of particle and inter-particle mechanisms that happen in the soil. Those may include nonhomogeneous pore size distribution, swelling and shrinkage in fine grained soil or entrapped air. Occluded air bubbles will prevent soil from reaching fully saturated condition after the wetting process. Figure 8 shows four regimes that may be defined in a soil-water characteristic curve.

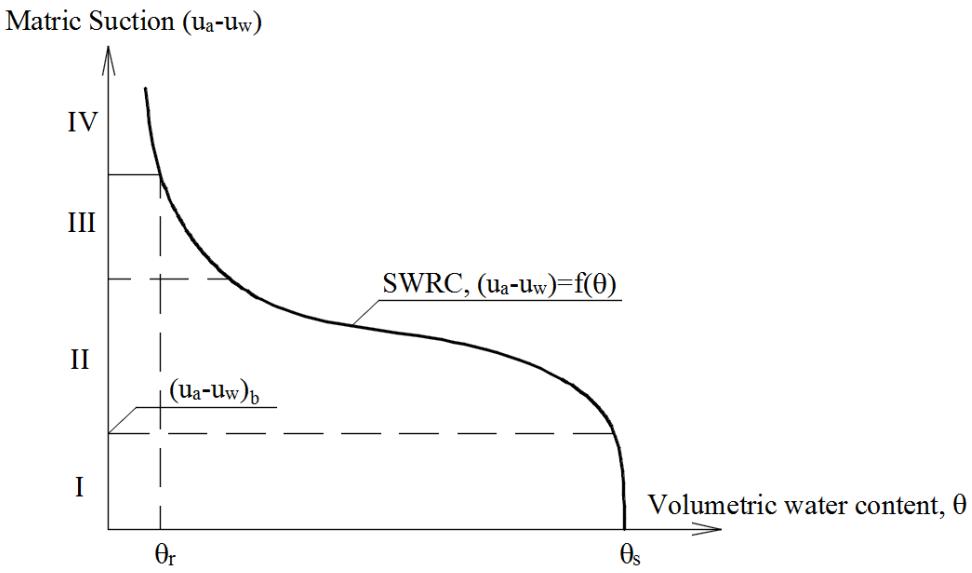

Figure 8 Regimes of soil-water characteristic soil (after Lu and Likos 2006)

For Regime I, soil remains saturated regardless of the negative pressure and can be considered as an equivalent continuum medium. The upper boundary of that stage is known as air-entry pressure. During Regime II water in soil pores is mostly represented by capillary menisci between particles of soil. Rapid decrease of water content under increasing suction is affected by pore size and pore size distribution of the soil.

For Regime III, the water decreases to the small film at the surfaces of the particles. The last stage is known as “residual” regime, when small amount of pore water is held as hydration of

the soil particles. During this regime large increase in matric suction would not result in significant water content change. For sandy soils residual water represents monolayer coverage and is less than a few percent by mass (Lu and Likos 2006). The amount of water adsorbed during regimes II-IV depends on the particle size and the change in density of soil minerals near the surface of the particles.

The transition between the regimes depends on the type of soil. Figure 8 shows the change of soil-water-air interface during the hydraulic hysteresis. The shape of SWRC will show the influence of soil properties, such as density, pore size and grain size distribution, mineralogy, clay content and organic material content on the pore water retention behavior.

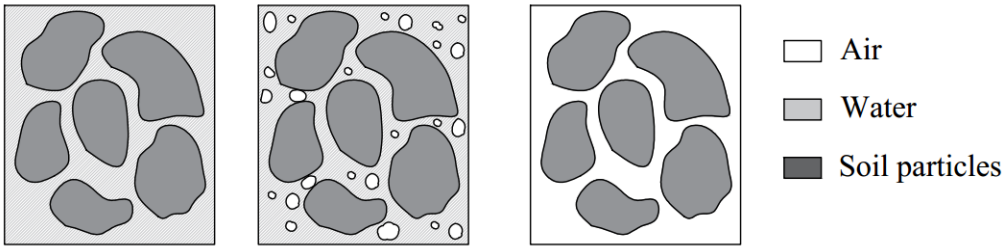

(a) (b) (c)

Figure 9 Soil phase constituents a) Saturated, b) Unsaturated, and c) Dry

Because of the high cost in direct measurements of hydraulic hysteresis, several researchers developed different models to fit experimental data and plot SWRC for soils. Such models require specification of certain points of the graph (air-entry pressure, saturation and residual saturation) and several empirical constants that are used for describing the shape of the curve.

A dimensionless parameter that characterizes water content in the sample is created for modelling purposes and can be described as:

$$S_e = \frac{\theta - \theta_r}{\theta_s - \theta_r} \tag{23}$$

where S_e is the effective degree of saturation, θ is volumetric water content, θ_s and θ_r are saturated and residual volumetric water contents, respectively. Different SWRC models use such fitting parameters that are related to physical properties of the material (e.g. air-entry pressure and pore-size distribution). There can be two or more fitting parameters to describe the hydraulic behavior of soil for SWRC. More accurate representation of the soil behavior over a wide range of matric suction can be illustrated with models that have three fitting parameters.

Brooks and Corey (1964) after a series of experimental measurements developed a model that can be expressed with the group of equations:

$$\begin{aligned} S_e &= 1 \quad \text{for } \psi < \psi_b \\ S_e &= \left(\frac{\psi_b}{\psi}\right)^{\lambda} \quad \text{for } \psi \geq \psi_b \end{aligned} \tag{24}$$

where S_e is the effective degree of saturation, ψ is matric suction, λ is a pore size distribution index to fit model to experimental data and ψ_b is the air-entry value. The hydraulic behavior of coarse grained soils can be described with this model, as even low suction levels will result in drainage of water. However, as water content of the specimen approached the residual value, this model does not give reasonable values. Because of inability to capture the change in shape of SWRC the Brooks and Corey model can lead to discontinuity of data and numerical instability.

The van Genuchten (1980) model incorporates three fitting parameters and can be described with an equation

$$S_e = \left[\frac{1}{1 + (\alpha\psi)^n}\right]^m \tag{25}$$

where α, n and m are fitting parameters, and

$$m = 1 - \frac{1}{n} \tag{26}$$

Three parameters allow capturing the inflection of the SWRC and therefore demonstrate a better representation of the data through a wide range of suction levels.

The change in matric suction with respect to degree of saturation is shown in the Figure 10. It can be concluded from the figure that prior to air entry pressure the soil remains saturated. During transition regime, that can be considered as desaturation, the drainage of the soil pores occurs. Water in the soil is present in thin films around particles under short-range interaction mechanisms. Residual part of the curve represents water content that is retained by molecular bonding. For coarse-grained soils this water can be extracted only under high temperature, e.g. drying the soil sample in the laboratory oven. However, this method would not remove residual water in fine-grained soils.

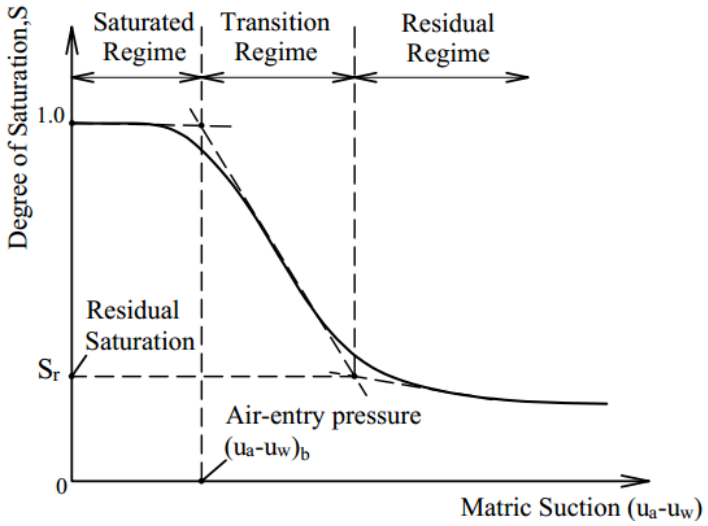

Figure 10 Soil water regimes with respect to the matric suction (after Lu and Likos,2004)

3.5 Effective stress in unsaturated soil

Unsaturated soil element consists of three phases: solids that are represented by soil particles, liquid that is typically water, and gas (pore air), while saturated or dry soils are two-phase systems that consist of solids and liquid or solids and gas only, respectively. For this reason the states of stress are different for unsaturated and saturated soil samples. The pressures of the pore water and air phases have a significant impact on the state of stress acting on the particle contacts and on soil behavior in general. Such natural processes, in addition to evaporation and precipitation, can change the amount of air and water phase in the soil that can considerably change the effective stress. Slope failures that occur after extensive precipitation is one of the examples of change in effective stress and performance of geotechnical engineering systems.

In unsaturated soils, pore water can sustain negative pressures that will result in tensile forces that will increase effective stress and will hold the soil particles together. Several researchers worked on different approaches to represent the effective stress in unsaturated soil. Bishop (1959) suggested using the following effective stress equation for soils with different degrees of saturation:

$$\sigma' = (\sigma - u_a) + \chi(u_a - u_w) \tag{27}$$

where σ' is the effective interparticle stress, σ is the total stress, u_a is pore air pressure, u_w is pore water pressure, $u_a - u_w$ is matric suction, and χ is a soil parameter that is related to water degree of saturation, which can be used as the effective stress parameter ranging from 0 to 1. In case of completely dry soil this parameter equals 0, while for fully saturated soil it is 1.The net normal stress is represented by the first term in the equation, while the second term, i.e. $\chi(u_a - u_w)$, represents suction stress.

Describing the dependency of the effective stress parameter, χ, on the degree of saturation has been a challenging task for researchers over the past 40 years. Theoretical and empirical studies have been performed to produce relationships between the two parameters. The difficulty of the research has been the inability to measure or control χ directly during experiments.

Bishop (1954) proposed a way to obtain χ value from the stresses measured in direct shear or triaxial test at failure of the soil specimen. This includes adapting the failure envelope equation for the effective stress relation in unsaturated soils.

$$\tau_f = c' + [(\sigma - u_a) + \chi(u_a - u_w)] \tan \phi' \tag{28}$$

where τ_f is shear strength, c' is effective cohesion intercept and ϕ' is effective friction angle.

The effective stress parameter can be evaluated from Equation 28 and written as:

$$\chi_f = \frac{\tau_f - c' - (\sigma - u_a)_f \tan \phi'}{(u_a - u_w)_f \tan \phi'} \tag{29}$$

Khalili and Khabbaz (1998) proposed an empirical equation as follows:

$$\chi = \left(\frac{u_a - u_w}{(u_a - u_w)_b}\right)^{-0.55} \quad \text{for } (u_a - u_w) > (u_a - u_w)_b$$
$$\chi = 1 \quad \text{for } (u_a - u_w) \leq (u_a - u_w)_b \tag{30}$$

where $(u_a - u_w)_b$ is the soil air entry pressure.

Several investigators tried to connect the soil water retention curve, which basically correlates matric suction and the corresponding degree of saturation of the soil specimen, to the effective stress parameter. As a result, a relationship between χ and the degree of saturation or χ and SWRC parameters could be established.

For example, Vanapalli and Fredlund (2000) proposed the following equation for χ:

$$\chi = S^K = (\frac{\theta}{\theta_s})^K \tag{31}$$

where S is the degree of saturation, K is a fitting parameter to get the best fit between predicted and measured values, θ is the volumetric water content, θ_s is the saturated volumetric water content.

Suction stress approach was proposed by Lu and Likos (2006) to use a single stress variable in analysis of unsaturated soils without the need to identify χ, independently, as follows

$$\sigma' = (\sigma - u_a) - \sigma^s \tag{32}$$

where $\sigma^s = -(u_a - u_w)S_e$, σ^s is the suction stress, and S_e is the normalized or effective degree of saturation. According to van Genuchten (1980) soil water characteristic curve model, the normalized degree of saturation can be determined through the following equation (Lu et al. 2010):

$$S_e = \left\{\frac{1}{1 + [\alpha(u_a - u_w)]^n}\right\}^{1-1/n} \tag{33}$$

where α is the inverse of air entry pressure for saturated soil and n is pore size distribution parameter for unsaturated soil. By matching experimental soil-water retention curve to the predicted one, those parameters may be obtained. The phenomena of flow and stress in granular materials can be described through the closed-form equation that has been proposed. Thus, the equation for effective stress in unsaturated soils becomes:

$$\sigma' = \sigma - u_a + \frac{u_a - u_w}{(1 + [\alpha(u_a - u_w)]^n)^{1-\frac{1}{n}}} \tag{34}$$

This equation can be used for soils with different levels of saturation, which makes it an extension to general soil mechanics effective stress concept.

All parameters necessary for calculation of effective stress for unsaturated soil are listed in the Table 2.

Table 2 Parameters used for calculation of the effective stress in unsaturated soil

Matric suction	$u_a - u_w$
Net normal stress	$\sigma - u_a$
Suction stress	σ^s
Effective stress parameter	χ
Air-entry pressure of the soil	$(u_a - u_w)_b$
Volumetric water content	Θ
Saturated volumetric water content	θ_s
Residual volumetric water content	θ_r
Effective degree of saturation	S_e
van Genuchten fitting parameters	α, n, m

CHATER IV. MATERIAL TESTED AND SPECIMEN PREPARATION

4.1 Physical properties

The soil selected for this study is a fine grained sand with high amount of silicon dioxide (SiO_2 >98%). The original version was obtained by hydraulic mining from the sandstone in Ottawa, Illinois, but it is currently manufactured industrially. The sand is composed of nearly pure quartz with naturally rounded grains that is used in oil and gas markets and in mortars for testing hydraulic cement.

Grain size distribution was performed in the geotechnical laboratory at the University of New Hampshire with accordance to the procedure outlined in ASTM C136-06 "Standard Test Method for Sieve Analysis of Fine and Coarse Aggregates". Dry Ottawa sand was sieved to measure the particle size distribution. Three tests were performed and the average result shown in Table 3 and Figure 11 were considered in calculations.

Table 3 Sieves used for sieve analysis of Ottawa F75

Sieve number	Sieve Opening, mm
Sieve 12	1.7
Sieve 16	1.18
Sieve 20	0.85
Sieve 40	0.425
Sieve 50	0.3
Sieve 100	0.15
Sieve 140	0.106
Sieve 200	0.075

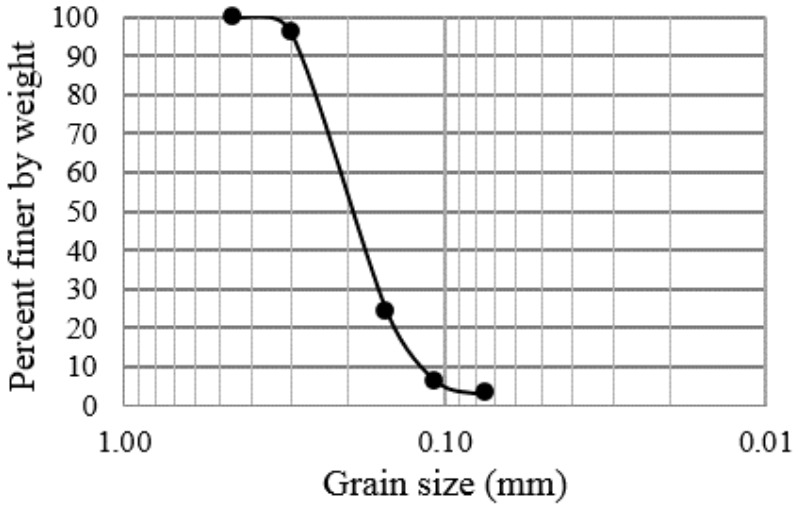

Figure 11 Grain-size distribution for Ottawa F-75

Grain size distribution curve can be characterized by several parameters, such as

Coefficient of uniformity

$$C_u = \frac{D_{60}}{D_{10}} \tag{35}$$

Coefficient of curvature

$$C_c = \frac{(D_{30})^2}{D_{10} \cdot D_{60}} \tag{36}$$

where D_{60} , D_{10} , D_{30} is a grain diameter (in mm) that corresponds to 60, 10 and 30% passing respectively.

Based on Figure 11, the coefficient of uniformity C_u was found to be 1.83, while the coefficient of curvature C_c was 1.09. A series of tests were performed to determine maximum and minimum density of Ottawa sand according to ASTM D4254 “Standard Test Method for Minimum Index Density and Unit Weight of Soils and Calculation of Relative Density” and ASTM D4253

"Standard Test Method for Maximum Index Density and Unit Weight of Soils Using a Vibratory Table".

Before running the tests to obtain maximum and minimum dry densities, the volume of the mold should be calibrated based on the following methods:

- Direct measurement
- Water-filling method

For the latter method the mold should be filled with water completely. Then, the mass of the water required to fill the mold is measured. Using thermometer, the temperature of water is determined to the nearest degree. The measured mass of water should be multiplied by a temperature coefficient from ASTM D4254 to obtain the volume. The measured volumes of the mold are compared below

$$V_{water} = 1657.83\ cm^3 \qquad V_{direct} = 1682.27\ cm^3 \qquad (37)$$

The volume obtained after water-filling method is assigned to the mold, as it reflects the condition of the mold more accurately.

The following procedure was used to determine the minimum dry density:

1. The soil was mixed for obtaining even distribution of the particles.
2. A spout in a steady stream was used to place the soil as loose as possible. The pouring device was moved in a spiral path to the center of the mold, thereby creating uniform thickness for each layer.
3. The mold needs to be filled 25 mm above the top.

4. Avoiding any shaking movements, the trimming operations were performed by using straightedge.

It is necessary to determine the mass of the soil plus mold and calculate the mass of the soil filling the mold. The results should be recorded from which the minimum unit density can be calculated using $\rho_{dmin} = \frac{M_s}{V}$, where M_s is the mass of the dry soil and V is the volume of the tested dry soil that was taken as volume of the mold. Maximum void ratio that corresponds to the minimum density can be calculated as:

$$e_{max} = \frac{G_s \cdot \rho_w}{\rho_{dmin}} - 1 \qquad (38)$$

where G_s is the specific gravity of soil particles, e_{max} is the maximum void ratio and ρ_w is the density of water. Specific gravity for Ottawa F75 sand is $G_s = 2.65$ (Ghayoomi et al.,2011) and density of water is $\rho_w = 1000\ {}^{kg}/_{m^3}$. As a result, a minimum density of 1540.11 kg/m^3 corresponding to a maximum void ratio of 0.72 was calculated.

Maximum density of 1718.77 kg/m^3 with corresponding minimum void ratio of 0.54 was calculated. The measured maximum and minimum void ratios of Ottawa sand are compared in Table 4.

Table 4 Comparison of the obtained minimum and maximum void ratio with literature data

	Current study	Saldago et al. (2000)	Dakoulas and Sun (1992)	Mesri and Vardhanabhuti (2007)	Ghayoomi et al. (2011)
e_{min}	0.54	0.48	0.57	0.52	0.49
e_{max}	0.72	0.78	0.95	0.85	0.8

The calculated maximum dry density value is lower than values found in the literature. The source of error could be using of equipment for shaking sieves instead of a shaking table, and not adjusting the volume of the mold after shaking. Minimum density was obtained by pouring sand in the mold through a large funnel, keeping the distance of 19 cm between the funnel and the sand surface. The smaller value for density could be achieved through zero pluviation when no distance between the funnel opening and the sand surface is kept. For the test performed in this study zero pluviation was not possible to perform because of the mold height. Therefore, minimum and maximum densities were taken from Ghayoomi et al. (2011). A summary of physical properties of Ottawa sand is presented in Table 5.

Table 5 The geotechnical properties of Ottawa F75

Property	Description
Mineralogy	99.8% SiO_2
Specific gravity	2.65
C_c	1.71
C_u	1.01
e_{max}, e_{min}	0.80, 0.49
ρ_{max}, ρ_{min}	1781, 1469 kg/m^3

4.2 Friction angle

In order to determine the friction angle of F-75 Ottawa sand at 45% relative density, three static triaxial tests were performed with different cell pressure. Confining pressures applied in the triaxial apparatus represent soils at different depths in the ground. Vertical effective stress of dry soil can be calculated as

$$\sigma'_V = z \cdot \gamma \tag{39}$$

where z is the depth of the soil and γ is the unit weight of the soil. The mean effective stress at the specific depth can be calculated as:

$$p' = \frac{\sigma'_V + 2 \cdot K_0 \cdot \sigma'_V}{3} \tag{40}$$

where σ'_V is vertical effective stress and K_0 is earth pressure coefficient at rest.

The mean stresses in the field can be represented by the cell pressure in a triaxial system, $p = \sigma_3'$. Three confining pressures of 50, 100 and 200 kPa approximately in the range of mean stresses for 5, 10 and 20 meters-depth soil were selected for this analysis, respectively. Conventional triaxial system is capable of conducting experiments with approximate axial strain levels ranging from 10^{-2} to 1%. For static tests, sand specimens were loaded until failure. Then, Mohr circles at failure were plotted and the tangent of the failure envelope was determined. The graphical representation of results can be observed in Figure 12.

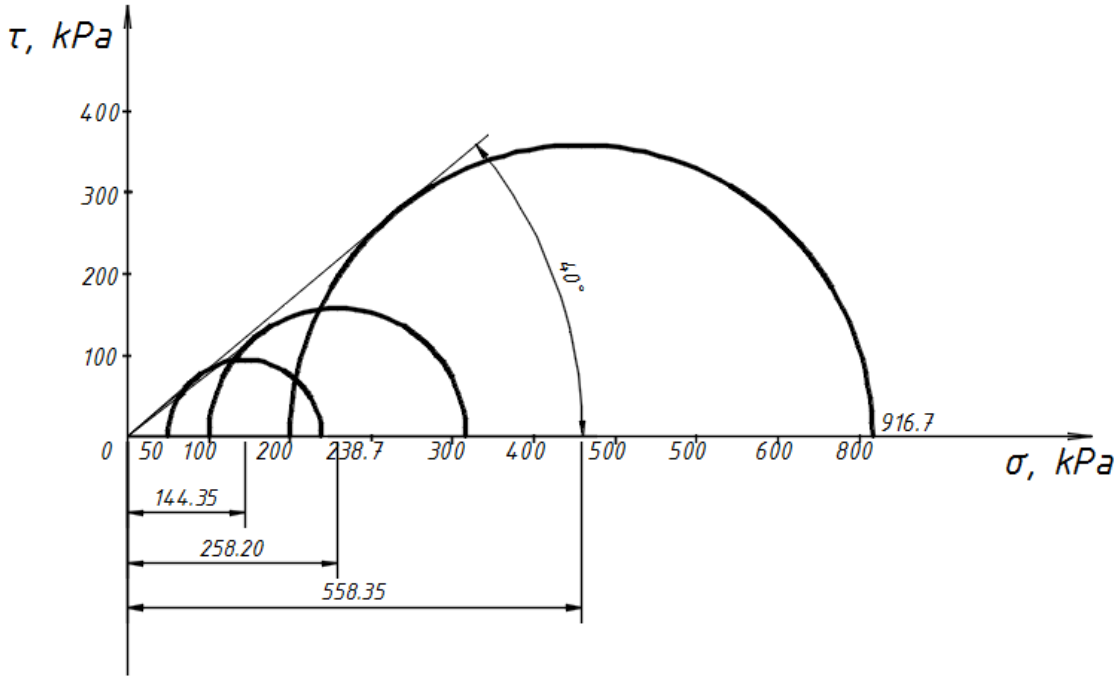

Figure 12 Failure envelope for Ottawa F75 sand

Drained angle of internal friction can be determined using fundamental formula from soil mechanics:

$$\sin\phi = \frac{\sigma_a - \sigma_r}{\sigma_a + \sigma_r} \tag{41}$$

where σ_a is the axial stress at failure and σ_r is the radial stress. A summary of triaxial data at failure is presented in Table 6.

Table 6 Static triaxial test data

σ_r, kPa	σ_a, kPa	Diameter of the circle, kPa	$\frac{\sigma_a+\sigma_r}{2}$, kPa	$\Phi_{average}$
50	238.7	188.7	144.35	40^o
100	416.4	316.4	258.2	
200	916.7	716.7	558.35	

4.3 Poisson's ratio

The value of Poisson's ratio for Ottawa F-75 was measured in the geotechnical laboratory using the triaxial test. Initial volume of water in the graduated cylinder connected to the cell was recorded before application of the axial stress. Static triaxial test was performed until reaching the axial strain of 5%. After that the test was stopped, readings of the final volume of water in the burette were taken. The average volumetric strain of the specimen was calculated using the following equation:

$$\varepsilon_v = \frac{dV}{V} \tag{42}$$

Where dV is the volume change in the burette representing the displaced water due to the soil deformation, which was corrected for the volume of loading bar entered into the triaxial cell, and V is the total volume of the specimen. In addition, values of the axial strains were taken from the CATS software that operated the triaxial system.

Corrected height and volume were calculated using the following equations

$$\begin{aligned} H_2 &= H - dH \\ V_2 &= V - dV \end{aligned} \tag{43}$$

Corrected area and radius was calculated as follows

$$\begin{aligned} A_2 &= \frac{V_2}{H_2} \\ r_2 &= \sqrt{\frac{A_2}{\pi}} \end{aligned} \tag{44}$$

The change in radius was determined through the following equation

$$dr = r_2 - r_1 \tag{45}$$

Using the values calculated in previous steps, radial strain of the soil specimen could be calculated

$$\varepsilon_r = \frac{dr}{r_1} \tag{46}$$

Then, the Poisson's ratio was calculated using the equation below

$$\nu = -\frac{\varepsilon_r}{\varepsilon_a} \tag{47}$$

where ε_r is the radial strain of the specimen and ε_a is the axial strain of the specimen.

In addition, empirical equation proposed by Seed and Duncan (1983) can also be used for Poisson's ratio calculation given the friction angle:

$$\nu = \frac{4 - 3\sin\Phi}{8 - 4\sin\Phi} \tag{48}$$

Obtained results and values calculated through empirical correlations are presented in Table 7

Table 7 Poisson's ratio for dry soil for different confining pressures

	Cell pressure		
	50 kPa	100 kPa	200 kPa
ν, measured	0.29	0.37	0.35
ν, empirical	0.38		

Due to uncertainty in the adapted methodology in Poisson's ratio measurement and nonlinearity of soil behavior, Poisson's ratio was taken as 0.38 which equals to the empirically calculated value.

4.4 Soil Water Retention Curve

Soil-Water Characteristic Curve (SWRC) or Soil-Water Retention Curve (SWRC) for Ottawa F-75 sand was determined using the DigiFlow Pump through axis translation technique. By maintaining the difference between air and water pressure in the specimen through the pores of High Air Entry Value (have) ceramic disc the matric suction was calculated. The top of the specimen was open to the atmospheric pressure, while the Flow Pump extracted water from the bottom through HAEV disc by applying negative pressure. More detailed description of the procedure can be found in Chapter 7. The outflow of water from the specimen was measured by the pump sensor and allowed to calculate the specimen volumetric water content and subsequently the level of saturation of the soil.

The sand specimen was prepared using dry pluviation technique with e=0.66 and the confining pressure during the test was maintained 50 kPa. The result of the SWRC tests is shown in Figure 13.

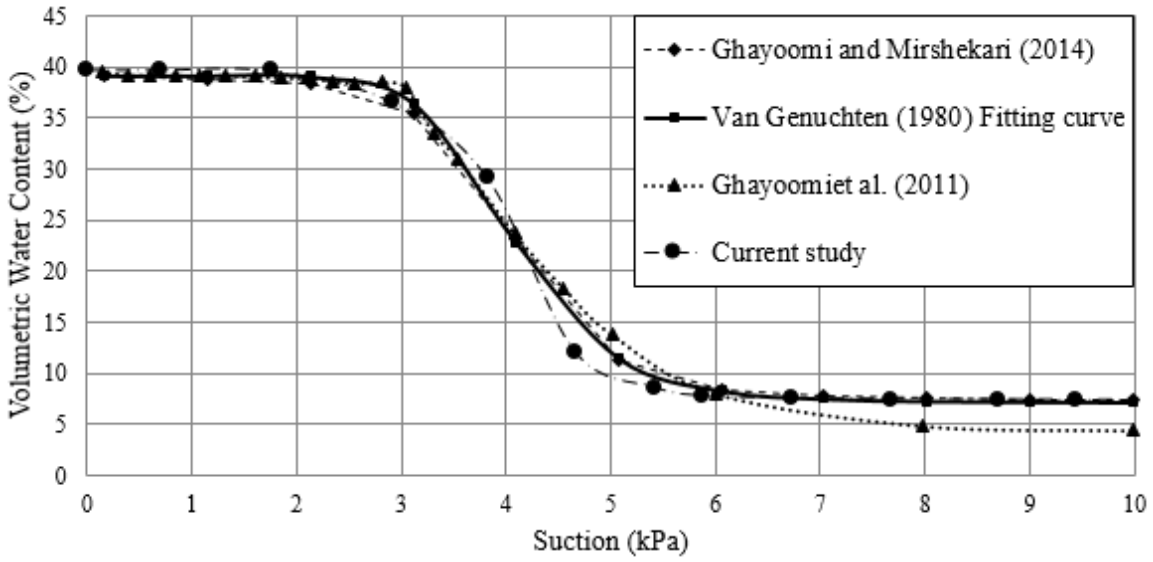

Figure 13 Soil-water retention curve for Ottawa F75 sand

The experimental data was compared to those published on previous studies for Ottawa F-75 sand samples with relative density of 45%, which corresponds to void ratio 0.66. In addition to that, van Genuchten model was fitted to the data and the associated fitting parameters were obtained and presented in in the following table.

Table 8 van Genuchten fitting parameters for Ottawa F-75 sand samples

α	n	θ_r	θ_s
0.25	9	0.072	0.392

CHAPTER V. MODIFIED TRIAXIAL APPARATUS AND PROCEDURE FOR SUCTION (DEGREE OF SATURATION) CONTROL

5.1 Introduction

One of the goals of this research was to develop a new device that could be used for measuring shear modulus of sand specimens with different levels of saturation. To achieve this goal, a new bottom platen for the triaxial cell was developed and constructed to install a High Air Entry Value (HAEV) ceramic disc and a flow pump for measurement of level of saturation was incorporated into the system. Details of the improved apparatus and the procedure for testing are presented in this chapter.

5.2 Apparatus

A GCTS triaxial system in the Geotechnical Laboratory at the University of New Hampshire is able to perform static and dynamic tests on dry or saturates soil samples. The current system is computer-controlled, which is opposite to the manual-controlled, which allows performing more complex testing programs and minimizing operator errors. The system consists of a Pressure Control Panel, a Digital System Controller, a Load Frame and a Triaxial Cell.

The Pressure Control Panel PCP-3000 is operated by a hydraulic oil pump and is able to introduce 1000 kPa pressure and 800 cm^3 of volume change to the soil. A hydraulic servo valve is able to apply cyclic loading to the sample with different wave forms up to 10 Hz frequency. Control parameters such as actuator movement, back pore pressure and cell pressure can be controlled manually if needed; however, for different stages of the test as saturation, consolidation or shearing

the system allows programming and controlling those parameters automatically. Through the CATS software that operates the GCTS SCON-1000 Digital System Controller, an automatic control over pressure drain valves could also be established. A CATS software screenshot for dynamic loading phase of the test is shown in Figure 14.

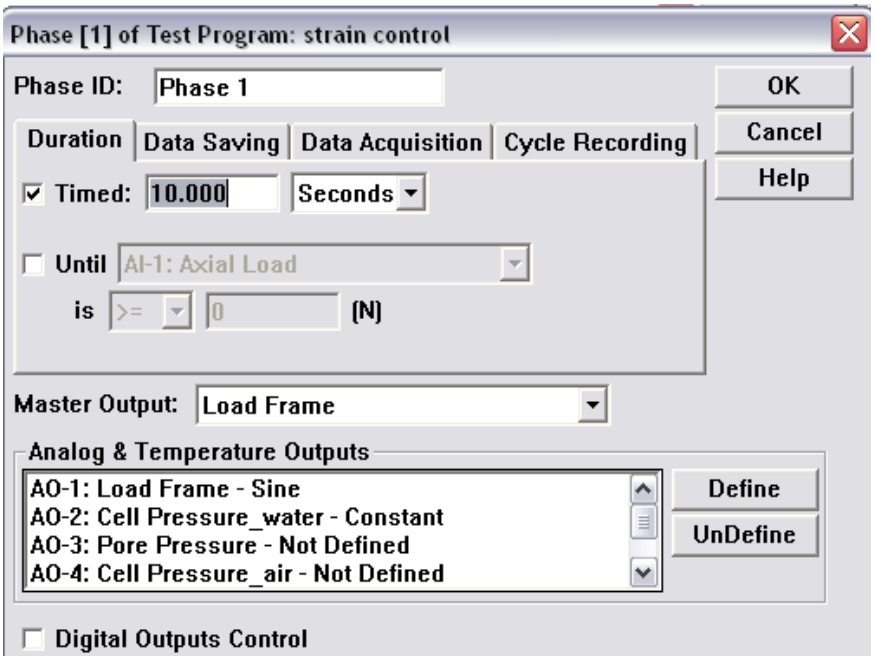

Figure 14 Programming triaxial system for cyclic loading

The pressure control panel is connected with the triaxial cell through “quick connection” of ¼ in. pressure resistant plastic tubes. All sensors are connected to separate analog inputs in GCTS SCON-1000 Digital System Controller that create closed feedback control loop. “Military standard” connectors are used for electrical wires to ensure proper insulation and avoid possible noise from the hydraulic pump during operation. The triaxial system setup in Geotechnical Laboratory is shown in Figure 15.

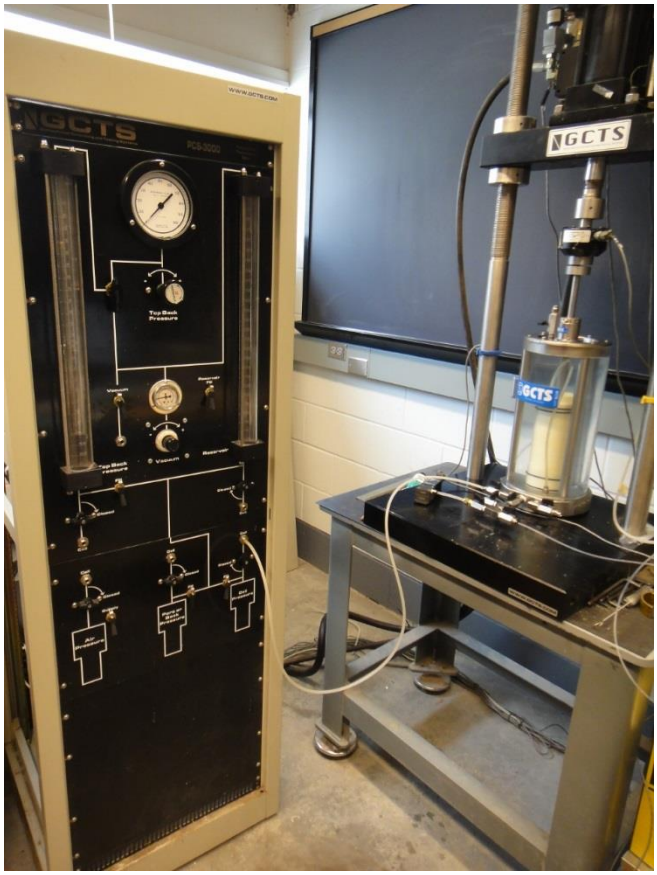

Figure 15 Overall view on the triaxial system

5.3 Modification of the triaxial cell for unsaturated soils

The GCTS triaxial system was improved for testing soils with different levels of saturation by incorporating the DigiFlow flow pump. For matric suction application and monitoring, the bottom of the triaxial cell had to be modified by installing a High Air Entry Value (HAEV) ceramic disc.

Axis translation technique for unsaturated soils requires constant measurement of matric suction, which is possible only by separate handling of water and air pressure. Conventional tests on unsaturated soils are performed using High Air Entry Value (HAEV) disks, instead of regular

porous stones that are used in saturated testing. Direct measurement of negative pore pressure is possible through control of air and water phases simultaneously.

Small pores of relatively similar size form a HAEV disk. The HAEV disk used in this study was made of sintered kaolin and manufactured by Soil Moisture Equipment Corporation, California. The disk serves like a membrane that separates air and water phase by preventing air to flow through. A 'bridge' between water in the soil specimen and measuring system is established through water in the ceramic disc. The measuring systems stays fully saturated, while soil is turned to a three phase system (solids, air and water). The separation between air and water phases is successful up to a point of an air entry value of the disk that refers to the maximum matric suction that the disc can operate with. After reaching this value, the air can pass freely through the disc to the measuring system and cause false measurements of the pore-water pressure.

The air entry value of the disc is a function of the surface tension and the maximum size of the pores in the ceramic disc (Fredlund and Rahardjo 1993, Lu and Likos 2004). Uniform openings in a ceramic material can behave as a capillary medium in case of contacting with moisture. According to Kelvin's equation the air entry value of the disc can be calculated using the equation

$$(u_a - u_w)_d = 2\frac{T_s}{R_s} \tag{49}$$

where $(u_a - u_w)_d$ is the air entry value of the material, T_s is the surface tension of the air-water interface or the contractile skin that is taken with respect to temperature and R_s is the radius of the maximum pore size or radius of the curvature of the contractile skin.

Pore size of the material has a significant effect on the air entry value. Therefore, if the openings are smaller the air entry value is higher. Consequently, the small radii of the material may reduce the speed of water interacting with sensors. Figure 16 shows a magnified image of HAEV ceramic disc confined between air and water phases.

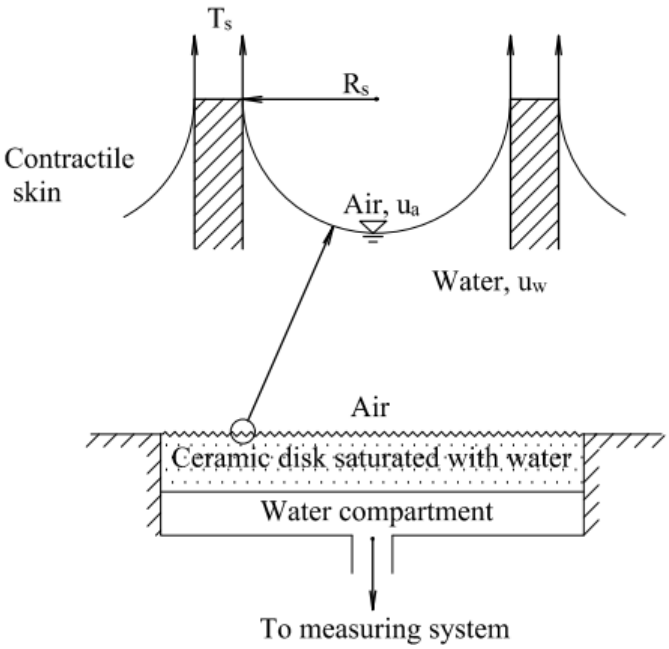

Figure 16 Air-water interface for HAEV disk (After Fredlund and Rahardjo, 1993)

The properties of the ceramic disk that was used in this research project are presented in Table 9.

Table 9 HAEV characteristics of the material used in this research

Type of disk	Approximate diameter ($*10^{-3}$ mm)	Coefficient of permeability with respect to water, k_d (m/s)	Approximate porosity	Thickness
½ bar	6.0	$3.11*10^{-7}$	50% by volume	0.281 in.

Depending on the type of material tested, different disc might be needed. With increasing the air entry value, the coefficient of permeability of the disc decreases. The point of water occlusion for Ottawa F-75 was observed to be less than 10 kPa, therefore HAEV ceramic disc with a relatively low air entry value was used.

The disk had to be installed in the bottom platen of the triaxial cell. The design of the modification was developed and presented in Appendix D. Water flow is supported by two grooves for increasing the area of penetration through the ceramic disk that is installed using LORD Epoxy Adhesive. The epoxy had to be water and pressure resistant, without allowing any air to pass through. Ceramic surface had to be previously covered with LORD AP-134 adhesion enhancer/surface modifier to increase adhesion. Modification of the bottom platen for triaxial cell is shown in Figure 17.

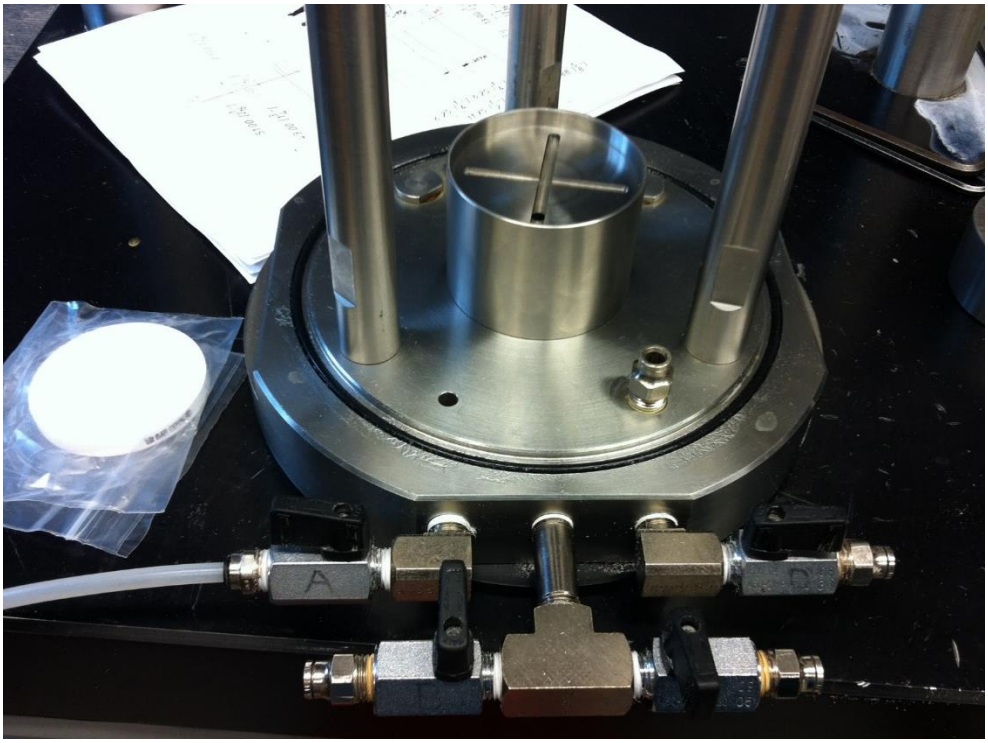

Figure 17 Modification of the triaxial cell for unsaturated soil testing

5.4 Incorporation of the flow pump

Precise control of the flow rate and pore water pressure is achieved through the flow pump developed by the GEOTAC company. The design of this equipment is very similar to a syringe that induces various water flows in and out of the specimen. A solid steel reservoir with a capacity of 80 mL is filled with water and connected to the circular piston. By operating the stepper motor, the piston will slowly move with a threaded rod into the reservoir and induce the flow to the specimen. Sealing rubber “o”-ring is placed between the piston and reservoir.

The flow pump is capable of applying the flow rates in the range of $3.96 \cdot 10^{-6}$ to $7.92 \cdot 10^{-12}$ m^3/s. The flow pump is connected to the bottom of the specimen, inducing the pressure to the soil. By operating the stepper motor it is possible to flush or withdraw water from the specimen

through the ceramic disc at the bottom. A pressure sensor with a capacity of 100 psi is attached to the flow pump.

The pump can operate through volume or pressure control and allows selecting the rate of flow, total volume and direction. Pressure control allows constant application, or ramping that is particularly useful for unsaturated soil testing to prevent damage of the high air entry value disk.

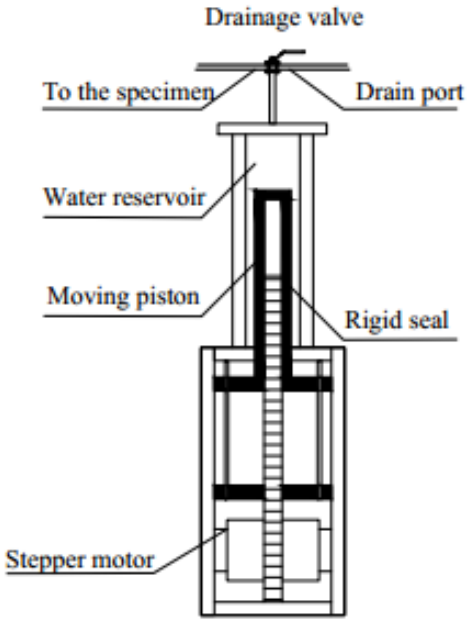

Figure 18 Schematic view of the flow pump

The valve from the top of the specimen is open to the atmosphere to maintain atmospheric pressure. This method represents real field conditions without imposing excessive air pressure on the sample. However, air pressure can also be controlled independently throughout the unsaturated soil testing.

For a more accurate measurement of matric suction, an additional pore pressure sensor was added to the system. Validyne Differential Pressure Transducer (DPT) includes two connection ports that measure the difference between the two sources of air or water pressure. One port is

connected to the bottom of the specimen for water pressure, while another was kept open to the atmosphere. However, in case of air pressure application to the specimen this second port must be linked to the top of the specimen for air pressure.

Typical view on Flow Pump software that demonstrates constant pressure control is shown in Figure 19.

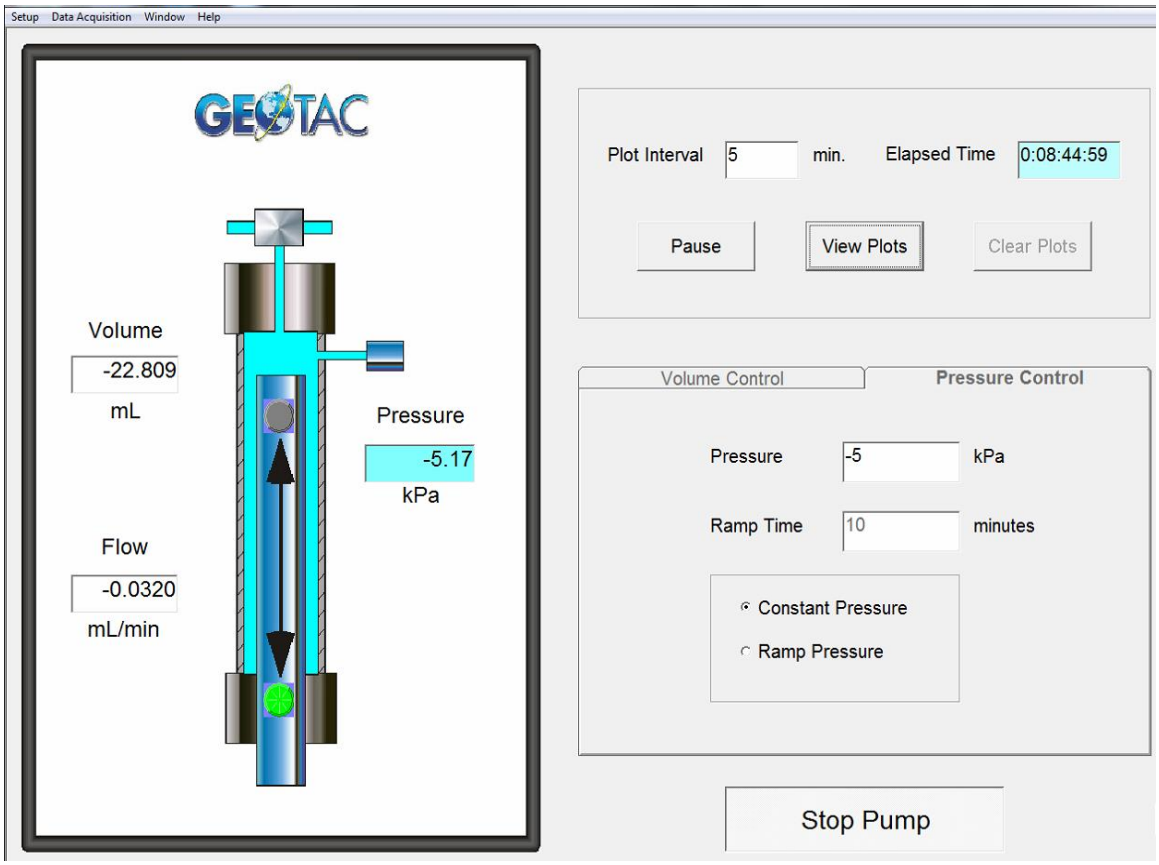

Figure 19 Schematic view of the DigiFlow software

CHAPTER VI. EXPERIMETAL PROCEDURES FOR DYNAMIC TRIAXIAL TESTING ON UNSATURATED SOILS

6.1 Introduction

In this chapter a detailed description of the testing procedures and methodologies are presented. This includes specimen preparation, cyclic triaxial testing, and the flow pump application and axis translation technique for suction control. The goal of this study is to measure shear modulus for various degrees of saturation and shear strain levels.

6.2 Assembling the triaxial cell for testing

The triaxial system in the Geotechnical laboratory at the University of New Hampshire includes a pedestal for triaxial cell with the loading mechanism, the hydraulic pump, the GCTS PCS-3000 Control Panel and the SCON-1000 Digital System Controller. Figure 20 shows the cell base, metal pieces for cell assembling, bolts, vacuum grease, rubber o-rings, hex wrenches on the pedestal with loading mechanism. For preparing specimens in unsaturated and fully saturated soils, the system was fully water saturated and all the connections and tubes were bleeded to eliminate possible air bubbles trapped in the system. High pressure vacuum grease and rubber “o”-rings were used in all tests to ensure full isolation of the specimen from the cell water.

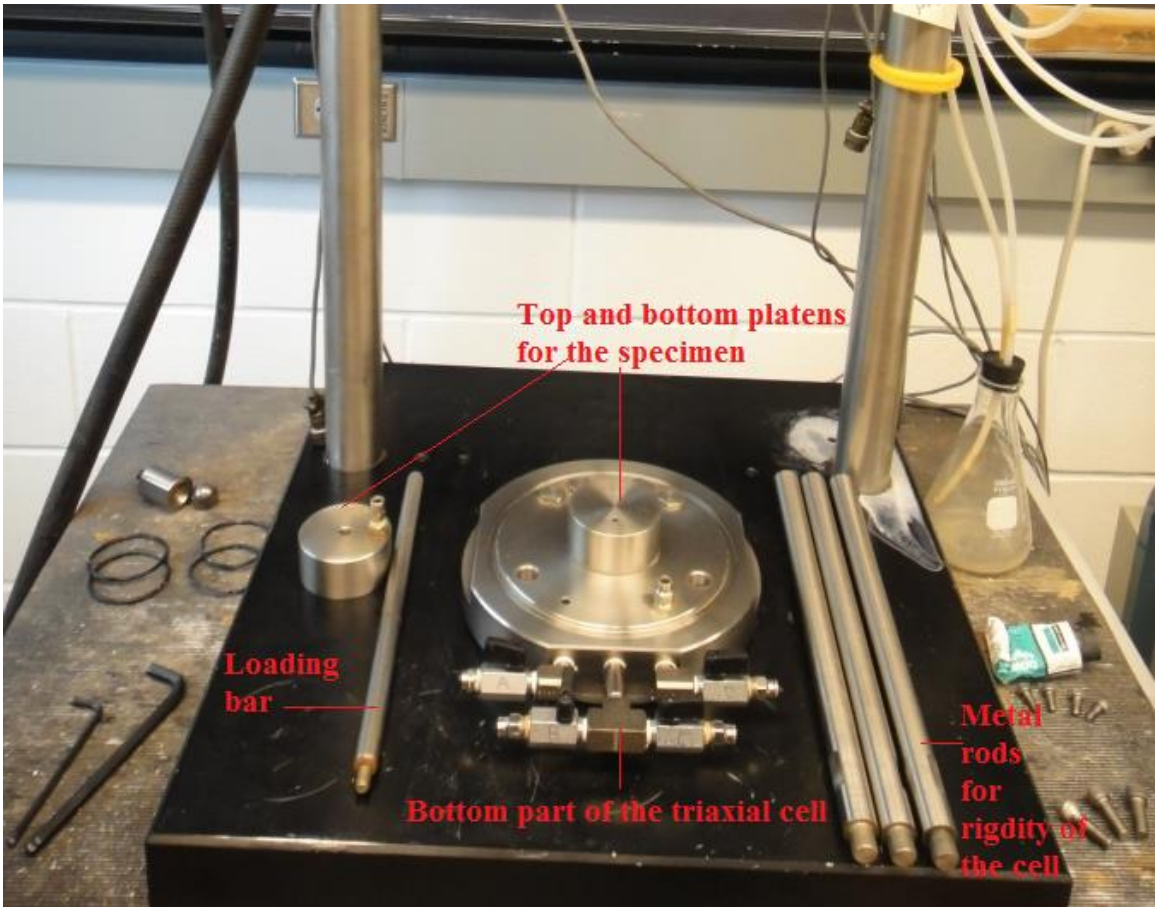

Figure 20. Disassembled triaxial cell

6.3 Sample preparation

To prepare a sample of Ottawa F-75 sand, the soil was first dry pluviated through a funnel ("Sand Raining"). Detailed description of the method can be found in ASTM D4253-83. For preparing a soil sample with a relative density of 45%, Ottawa F-75 sand was rained through a funnel with an opening of 0.12 in., from 15 in. above the soil surface. Figure 20 shows the specimen preparation process for the triaxial test. By measuring the dimensions of the specimen and the weight of the sand needed to prepare it, the void ratio and relative density can be calculated.

After the sand was poured into the mold, vacuum was applied to keep the specimen in shape prior to the application of radial stress. Figure 22 shows the process of assembling the triaxial cell and filling it with water for subsequent application of the cell pressure.

Figure 21 Dry pluviation of Ottawa F75 sand

Upon filling the cell with water, cell pressure water output was turned on in the CATS software and 20 kPa of confining stress was applied to the soil. Then, the vacuum was turned off the specimen, the trapped vacuum was released, and the first stage of triaxial test could start.

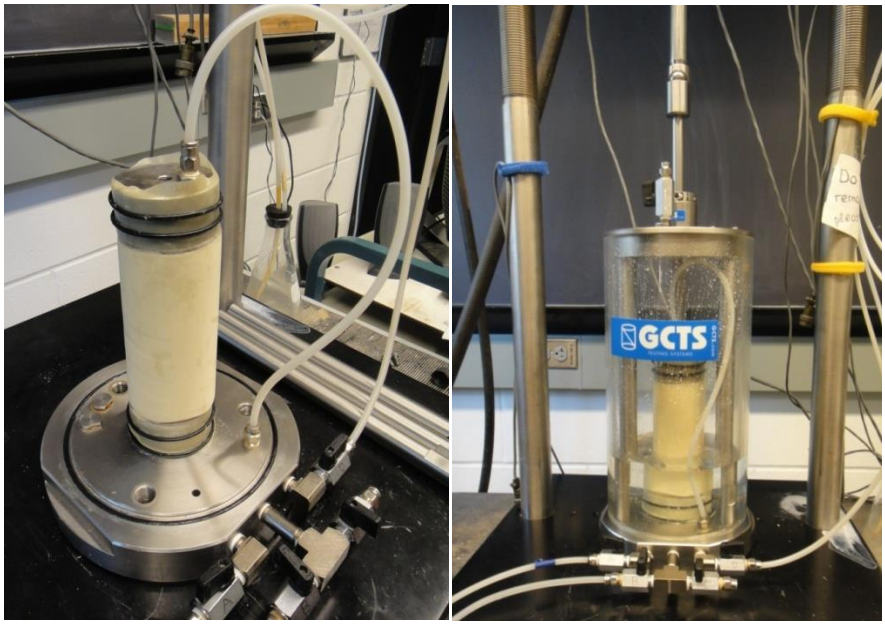

Figure 22 Assembling the triaxial cell

6.4 Triaxial test

Triaxial test can be performed on any type of soil, which makes it a most common test due to versatile purposes. In this test, soil specimen is sealed in the membrane and placed in the triaxial cell, typically filled with fluid for further pressure application. Intermediate and minor principal stresses are equal to the cell pressure ($\sigma_2 = \sigma_3$). Common cylindrical specimens for triaxial testing have a length to diameter ratio of 2. Typical triaxial cell is shown in Figure 23. Vertical load is applied through the ram acting on the top platen of the specimen for even load distribution, where the vertical pressures, represents the major principal stress on the soil element (σ_1). The soil water pressure can be controlled independently and the pore water pressure can be measured before, during, and after the test.

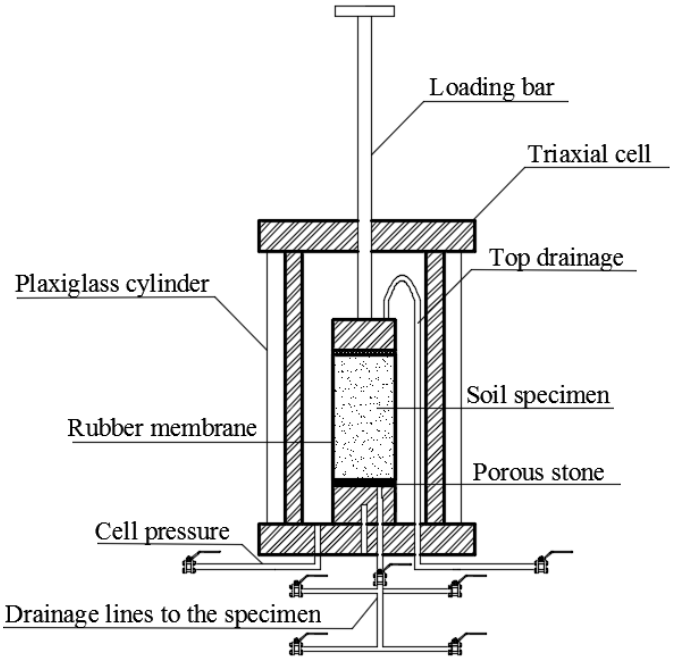

Figure 23 Common triaxial cell

Generally, triaxial tests can be classified in accordance with drainage allowance during separate stages of the test, application of cell pressure and increase of deviator stress:

- Unconsolidated-Undrained test (UU): This test does not allow any dissipation of pore pressure at any stage of the test. At first, the specimen is subjected to increase in cell pressure, and then the principal stress difference applied immediately. This test is usually performed on undisturbed samples obtained from the field.

- Consolidated-undrained tests (CU): The test allows drainage during application of lateral stress, so the specimen is fully consolidated due to the cell pressure. However, during the increase of deviator stress no drainage is allowed. In any type of undrained tests deformation occurs at constant volume, assuming that soil particles and water are incompressible. Such tests should be performed slowly to ensure a uniform pore pressure distribution thought the specimen.

- Consolidated Drained tests (CD): Drainage conditions are retained during all the test stages to ensure full consolidation under the all-round stress and omit excess pore pressure during the application of axial loading. The rate of testing may change depending on the size of the sample and permeability of soil, to prevent any possible increase in pore pressure.

Typical soil element in triaxial stress state is shown in Figure 24.

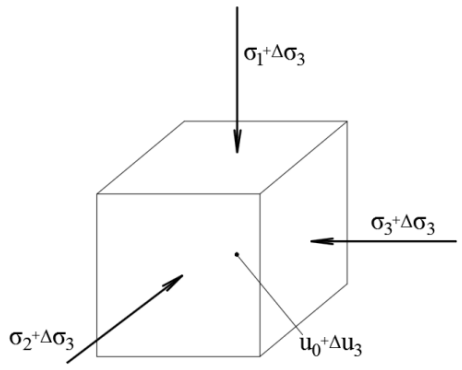

Figure 24 Soil element under cell pressure stress increment

In any type of test, field drainage conditions should correspond to those applied in the test. For example, undrained tests represent low permeable soils that would not let significant dissipation of pore pressure during stress change. Drained conditions will imitate the response of permeable soils or the soil behavior after many years of completion of construction, when excess pore pressure is zero.

A conventional triaxial test consists of

- saturation stage
- consolidation stage
- shearing stage

6.4.1 Saturation stage

Except for the dry tests, the specimen in the triaxial cell was saturated from the bottom to the top by flushing de-aired water from the tank inside the GCTS PCS-3000 Control Panel. Ensuring that no air bubbles were observed coming from the top of the specimen, the gravitational saturation process was stopped. Then, the final saturation process was progressed through back-pressure saturation and B-value check.

Applying back-pressure (increased water pressure to the specimen) assist in dissolving the small air bubbles trapped in the soil. This is done through an increase in water pressure while keeping it lower than the cell pressure. This process was being done in stages, giving enough time to the pressure to equilibrate and dissolve the air (about 20-30 min). Then, the specimen drainage valve was closed and the Skempton B-value parameter was measured.

$$B = \frac{1}{1 + n \cdot \frac{C_V}{C_S}} \tag{50}$$

where C_V is the compressibility of pore fluid under an isotropic pressure ramping, C_S is the compressibility of the soil skeleton under an isotropic stress ramping, n is the porosity.

Assumption of fluid incompressibility is made for fully saturated soil samples, so that $\frac{C_V}{C_S} \to 0$, and pore pressure parameter, $B \to 1$. In unsaturated soils with the pore air present in a mass, compressibility of pore fluid is not zero and $B < 1$. The change of pore pressure parameter with variation of degree of saturation can be seen in Figure 25.

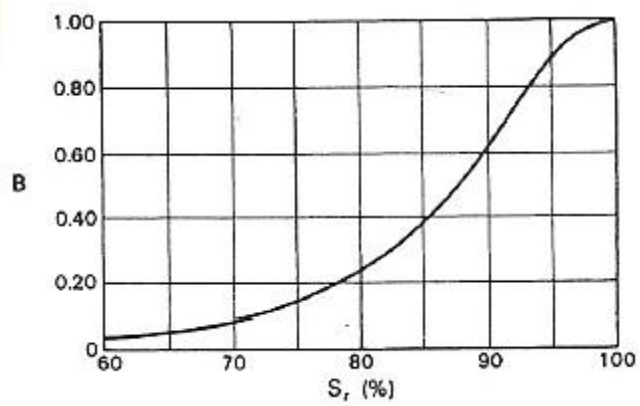

Figure 25 Relationship between B and degree of saturation (Craig's soil mechanics 2004)

B-value check can be performed in triaxial apparatus by increasing (or reducing) the all-round pressure by $\Delta\sigma_3$ and measuring the difference in pore pressure Δu. B-value is calculated using the following formula

$$B = \frac{\Delta\sigma_3}{\Delta u} \tag{51}$$

Where $\Delta\sigma_3$ −increase of the cell pressure, Δu −corresponding increase of the pore pressure.

The detailed process is described in Chapter 7. To perform a B-value check, a quick increase of 15 kPa in the cell pressure was applied while monitoring pore water pressure. This was done after each stage of back pressure saturation. This process was repeated until a B-value higher than 0.95 was achieved. Throughout the back pressure saturation, the cell and pore pressures were increased while keeping the effective stress constant. It is important to note that effective stress during saturation should never exceed effective stress for the actual test, to achieve a normally consolidated soil before shearing. However, this might be less significant in sandy material. After reaching a target B-value, the next stage of triaxial testing was performed. The purpose of the study was to execute consolidated drained tests that do not allow excess pore pressure to build up and require consolidation stage before shearing.

6.4.2 Consolidation stage

For fully saturated specimens the pore pressure was kept constant and the cell pressure was increased to reach the target effective stresses of 50, 100 and 200 kPa. For dry specimens, the saturation part of the test was skipped and a confinement pressure of 50, 100 and 200 kPa was applied after turning off the vacuum from the specimen. To ensure proper consolidation, a specimen was left for 30 minutes under a certain effective stress, while the drainage valve was open.

6.4.3 Application of the matric suction

For testing unsaturated soil, after the consolidation stage, the cell and pore pressures were brought down to 50 and 2 kPa, respectively. The value of the pore pressure was adjusted in accordance with the height of the specimen to reach 0 kPa pressure at the top of the specimen. The valve at the top was opened to the atmosphere, introducing the air pressure that is assumed to be 0 kPa. The average matric suction ($u_a - u_w$) was taken as the average value measured at the middle of the specimen.

For the purpose of studying the hydraulic behavior of Ottawa F75 sand samples with the relative density of 45%, drying and wetting tests were conducted and SWRC was calculated. In addition to the pressure sensor on the flow pump, a Differential Pressure Transducer (DPT) recorded the difference between the negative pore pressure at the bottom of the specimen and the atmospheric pressure with high precision.

To start with the drying path, the specimen and all the system were fully saturated with no air bubbles trapped in any connections. The pump can operate through pressure or volume control regime. The target suction value was set for the pump, and it started withdrawing water from the

bottom of the sand specimen through the HAEV ceramic disc. Upon reaching the desirable suction value the flow pump stops and gives time for the specimen to equilibrate. The pump restarts automatically when suction value at the bottom of the specimen is lower than the target one, due to water movement from the top of the specimen to the bottom. This equilibration may take up to 12 hours to complete. When the soil sample reached the point of equilibrium, the volume of withdrawn water is recorded to get the first point on SWRC that shows values of matric suction versus the degree of saturation calculated from volumetric water content. This procedure was repeated several times with an increment of 1 kPa in matric suction in order to build a complete graph. For each value of matric suction the system was left to equilibrate until the volume of withdrawing water was less than 0.002mL/min. Residual volumetric water content for Ottawa F75 sand with initial void ratio of 0.66 was observed at 9 kPa of matric suction, where an increase in matric suction resulted in minimal change in water content. The result of the test was presented in Figure 26.

In order to obtain the wetting path in SWRC, the direction of the pump piston was reversed to deliver de-aired water to the bottom of the soil specimen. Similar increments in pore water pressure were applied during wetting path and the specimen was allowed to equilibrate.

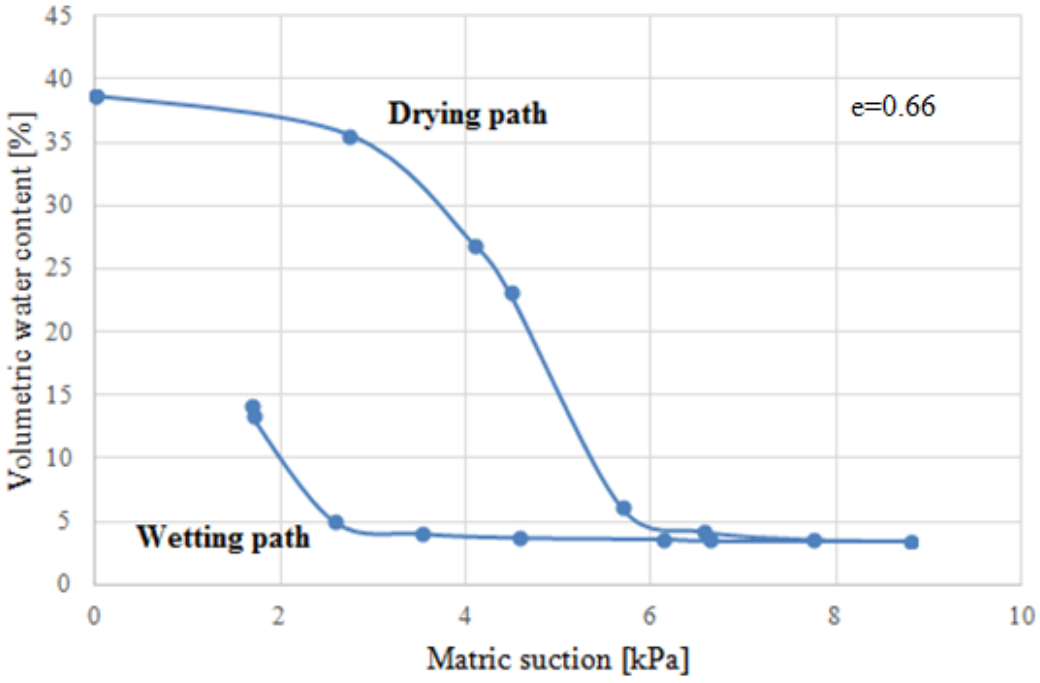

Figure 26. Drying and wetting path for Ottawa F-75 sand specimen

6.4.4 Shearing stage

In static triaxial tests, shearing stage was performed by applying axial loading using the vertical piston. Angle of internal friction for Ottawa F-75 sand samples with a void ratio of 0.66 was determined through triaxial compression tests for three different confinement pressures and results were presented in Figure 12. For determination of dynamic soil properties, cyclic load was applied using either stress- or strain-control mechanisms.

The controlling mechanism for dynamic loading is the actuator that is run by a cyclic waveform. GCTS system supplied by CATS software can support load application in sine, triangular and square forms. The impact of the waveforms on the response is out of the scope of this study; sine wave form was chosen and applied in this study.

The initial starting point of the wave can be absolute or relative, and such parameters as Peak to Peak Amplitude, Frequency, and Delay should be specified. Figure 27 shows a screenshot from the CATS software prior to dynamic testing.

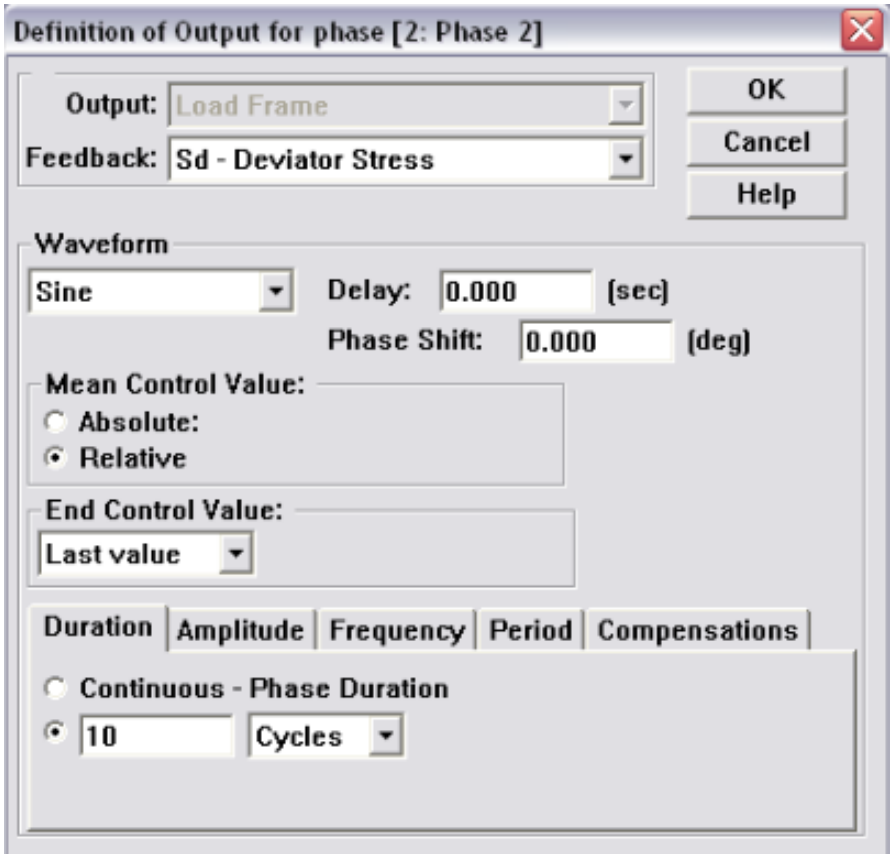

Figure 27 Setting parameters for cyclic testing in CATS software

The duration of dynamic loading stage is defined by a number of cycles performed by the Actual Actuator. Earthquake motion has irregular characteristics, but dynamic soil testing is performed with uniform amplitudes of stress application. For such testing, earthquake-induced loading is converted into an equivalent series of stress cycles that are applied uniformly. In this study each dynamic test is represented by 10 cycles with a frequency of 1 Hz, which corresponds to an earthquake with a magnitude of 7 (Seed et al., 1975a).

Typical load cycles during strain- and stress- controlled tests are shown in Figures 28 and 29, respectively.

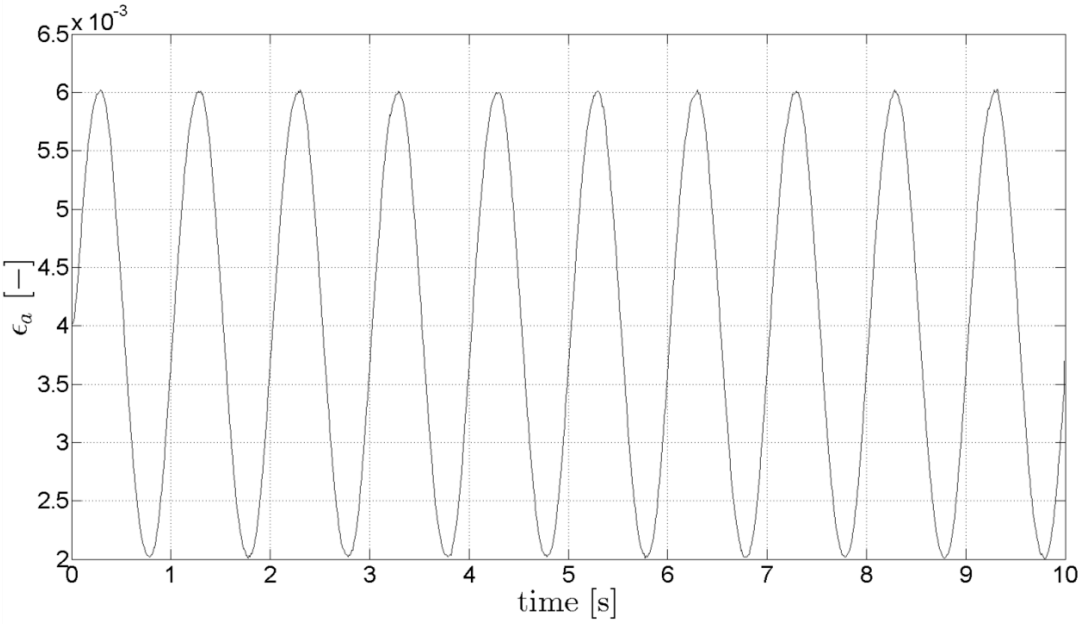

Figure 28 Cyclic strain application for one measurement

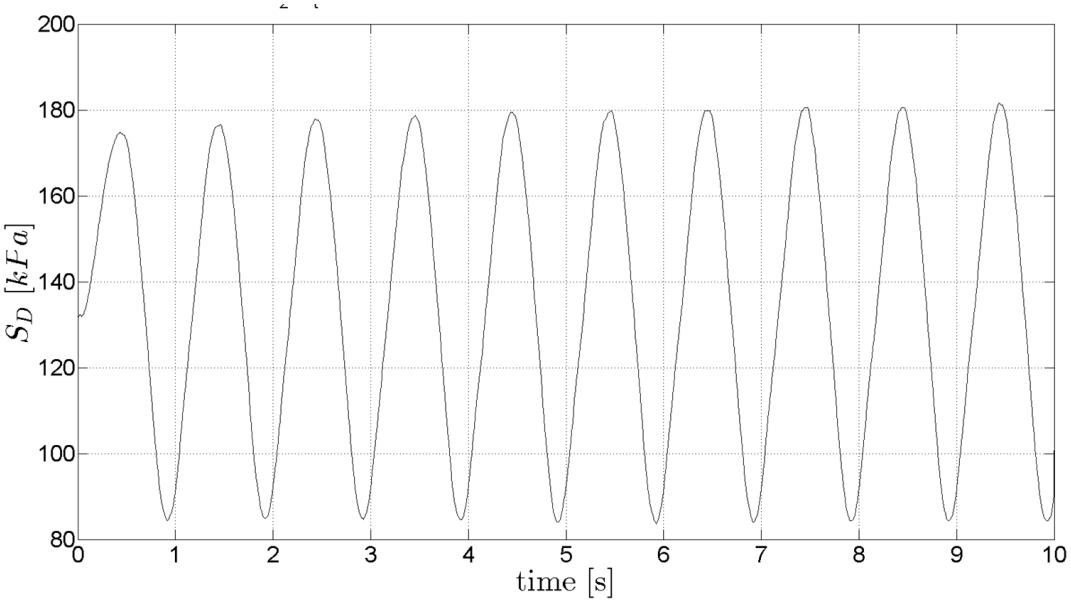

Figure 29 Cyclic stress application for one measurement

For dynamic stress control test, initial "seating" stress of 50 kPa is applied for all the specimens, which was equivalent to approximate seating strain of 0.2%. The purpose of the seating stress was to avoid tension in the specimen during cyclic loading. Thus, soil specimens experienced several compression and extension stress states throughout the tests.

Upon the completion of the cyclic triaxial test deviator stress versus axial strain hysteresis loops can be plotted. Most of the plots presented in this thesis are plotted using Matlab2014. The representative loops for strain- and stress-controlled tests are shown in Figures 30a and 30b, respectively. Most of the tests in this study were performed using strain-controlled approach that enabled a direct control of strain level. However, stress-controlled tests were performed with approximately similar conditions for comparison and confirmation purposes.

The detailed procedure on the specimen preparation and setting test parameters in CATS Software are described in the Appendix F.

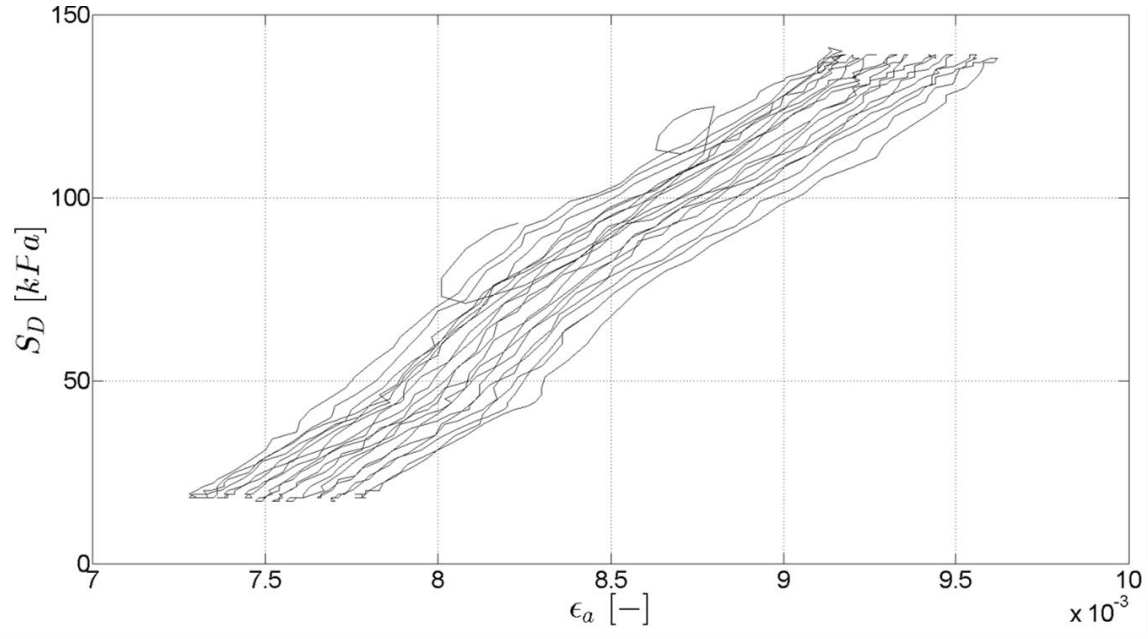

a)

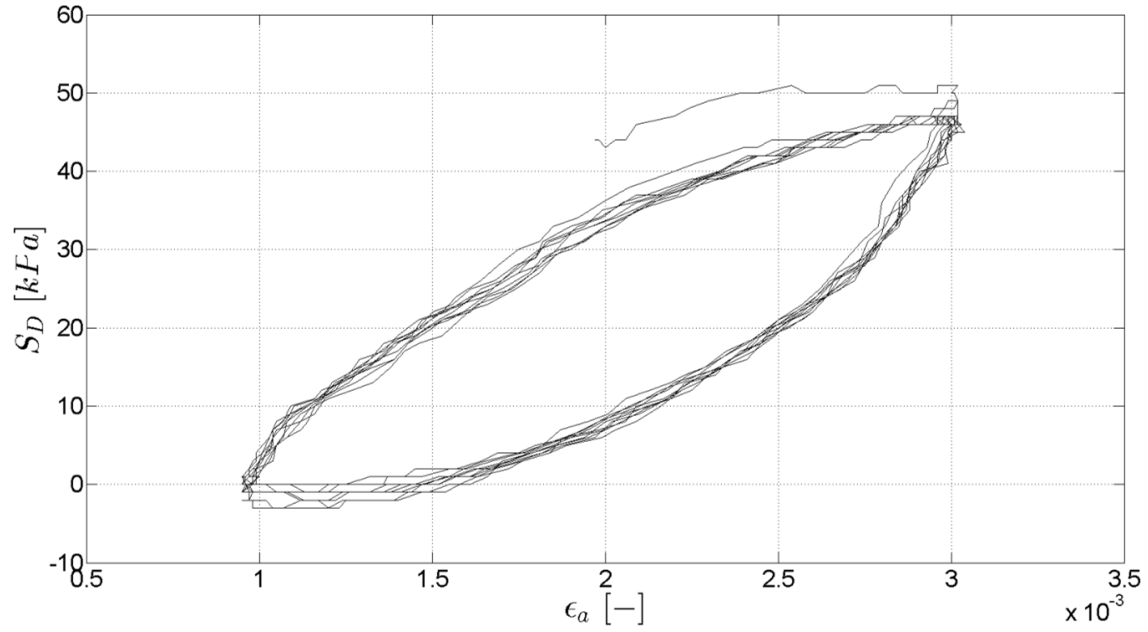

b)

Figure 30 Typical hysteresis loops for cyclic test a) stress-controlled b) strain- controlled

CHAPTER VII. RESULTS: STRAIN-CONTROLLED TESTS ON DRY SAND

A series of cyclic tests were performed on dry Ottawa F-75 sand during the early phase of the study. Thus, it is expected that some of the tests do not follow the ideal expected trends due to the difficulties in testing systems and data acquisition. Tremendous efforts were made to troubleshoot these problems and renovate the system. The effects of different strain levels, levels of saturation, and confining pressures were monitored and are discussed in this chapter. Although cyclic tests were performed under both strain- and stress-controlled conditions, this chapter only focuses on strain-controlled test data.

Soil specimens with a relative density 45% and corresponding void ratio of 0.66 were prepared by dry pluviaton method, and then were tested under three different confinement pressures. Typical hysteresis loops for strain-controlled test on dry sand are shown in Figure 31.

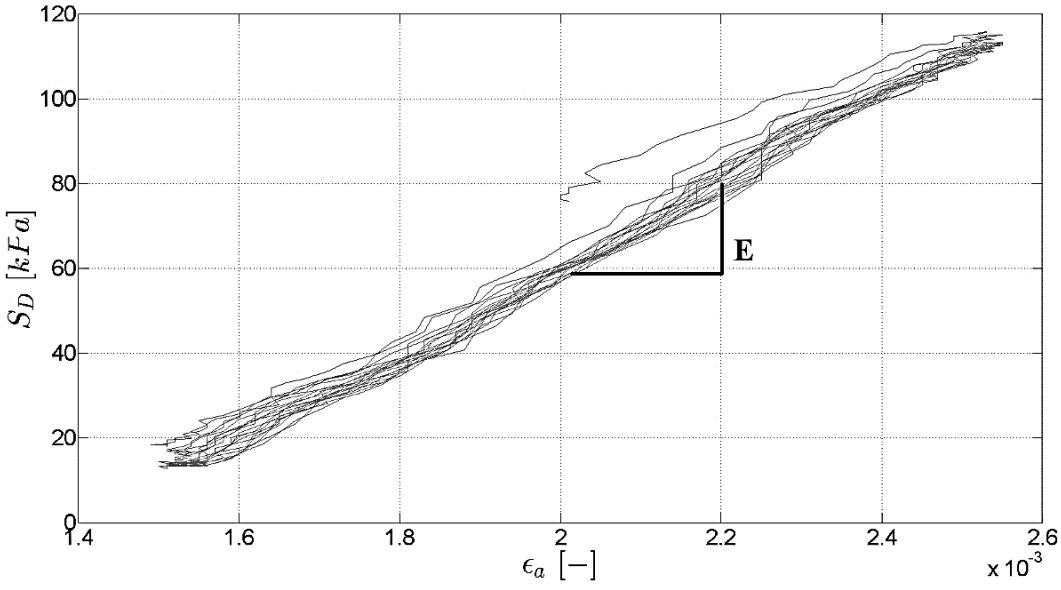

Figure 31 Representative hysteresis loop for strain-controlled cyclic triaxial test

Young's modulus of fine-grained sand was taken as a slope of the stress-strain hysteresis loops.

$$E = \frac{\Delta\sigma_d}{\Delta\varepsilon_a} \tag{52}$$

where $\Delta\sigma_d$ is the amplitude of deviator stress and $\Delta\varepsilon_a$ is the amplitude of axial strain. Young's modulus was plotted against axial strain amplitude and shown in Figure 32.

Typical triaxial test equipment is used for measuring soil properties from medium to high axial strain levels (10^{-4} to 10^{0}). In the early stage of testing, trials on small amplitudes of strain showed noisy results that could not be considered for determination of dynamic soil properties. Typical results from the test are shown in Figure 32 and Figure 33. Conducting tests with the single amplitude of axial strain of 0.005% and 0.01 % was beyond the limits of system accuracy.

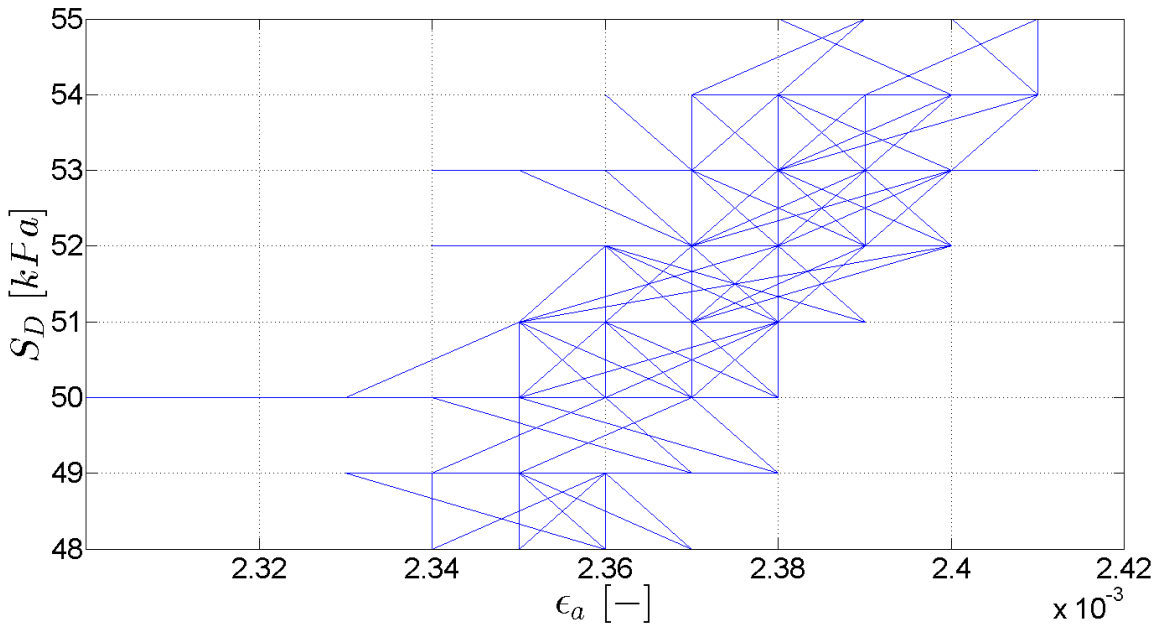

Figure 32 Triaxial test results for 0.005% axial strain amplitude

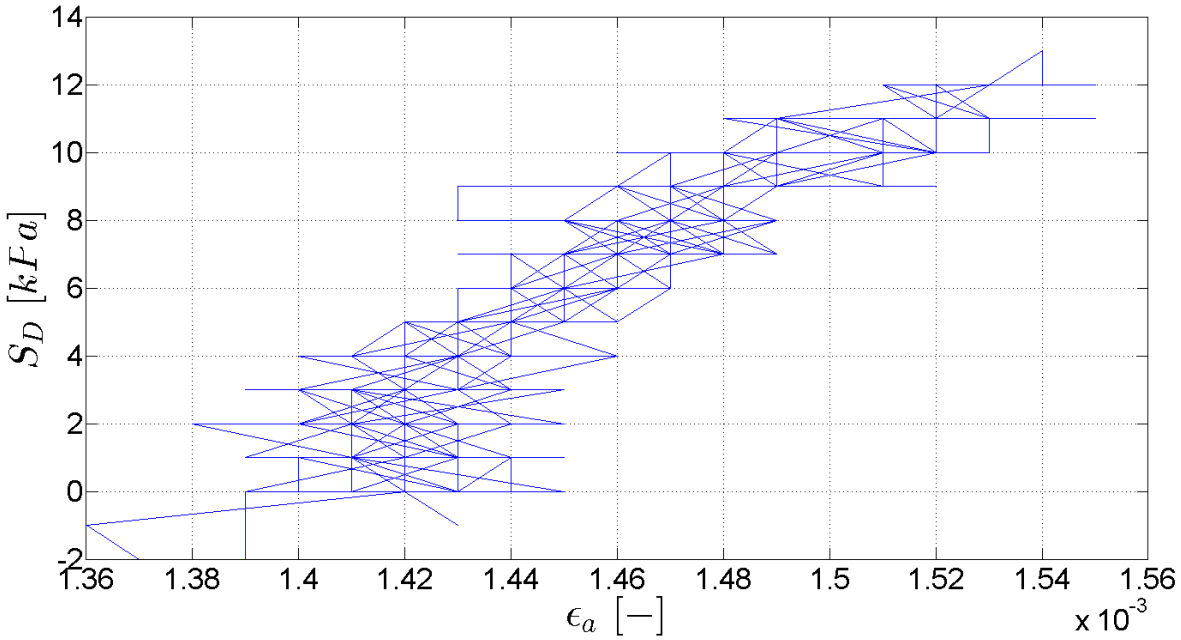

Figure 33 Triaxial test results for 0.01% axial strain amplitude

The slope of the line that connects two peaks of the loop was taken as Young's modulus. The first cycle was different from the consecutive ones by the slope of the loading portion of the loop. Therefore, the average value for 9 full loops of the test was taken for further analysis. Young's modulus for different cycles was changing, indicating that the soil was undergoing permanent deformations. The variation of the modulus for 0.05% of axial strain is presented in Figure 34. The variation of the modulus for 0. 5% of axial strain is presented in Figure 35. Kokusho (1981) performed a series of cyclic triaxial tests and stated that shear modulus for wide strain rate can be calculated from Young's modulus through the equation below

$$G = \frac{E}{2 \cdot (1 + \nu)} \tag{53}$$

where E is Young's modulus and ν is Poisson's ratio. Knowing that shear modulus can be calculated as the ratio of shear stress over shear strain, $G = \frac{\Delta\tau}{\Delta\gamma}$, the following relationship was derived assuming a constant cell pressure

$$\Delta\gamma = \Delta\varepsilon_a \cdot (1 + \nu) \tag{54}$$

$$\Delta\tau = \frac{\Delta\sigma_d}{2} \tag{55}$$

For better visualization of the results, data associated with different confinement pressures were separated, and shear modulus were plotted against the corresponding shear strains for 50, 100, and 200 kPa confining pressures in Figures 37, 38, and 39, respectively.

In order to minimize human error and improve the data analysis, all calculations were performed in Matlab2014 software. The code is attached in the Appendix C.

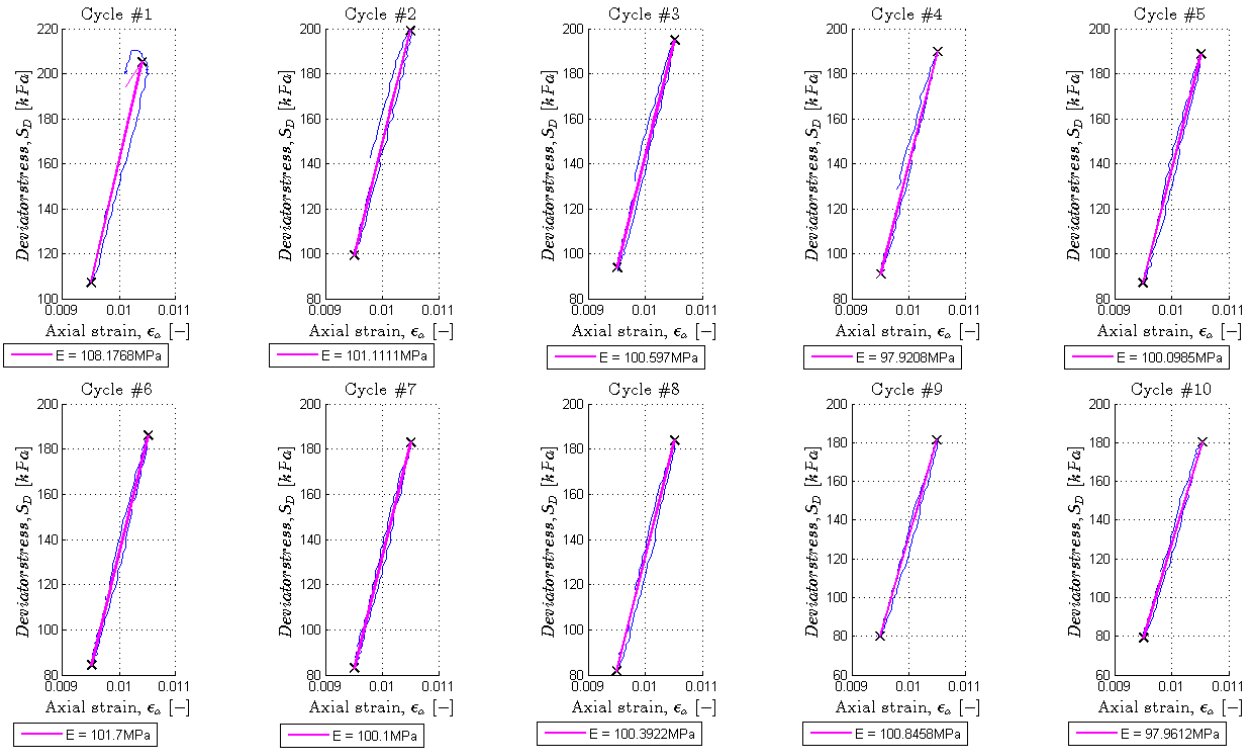

Figure 34 The change of Young's modulus for different cycles of the test for 0.05% axial strain amplitude

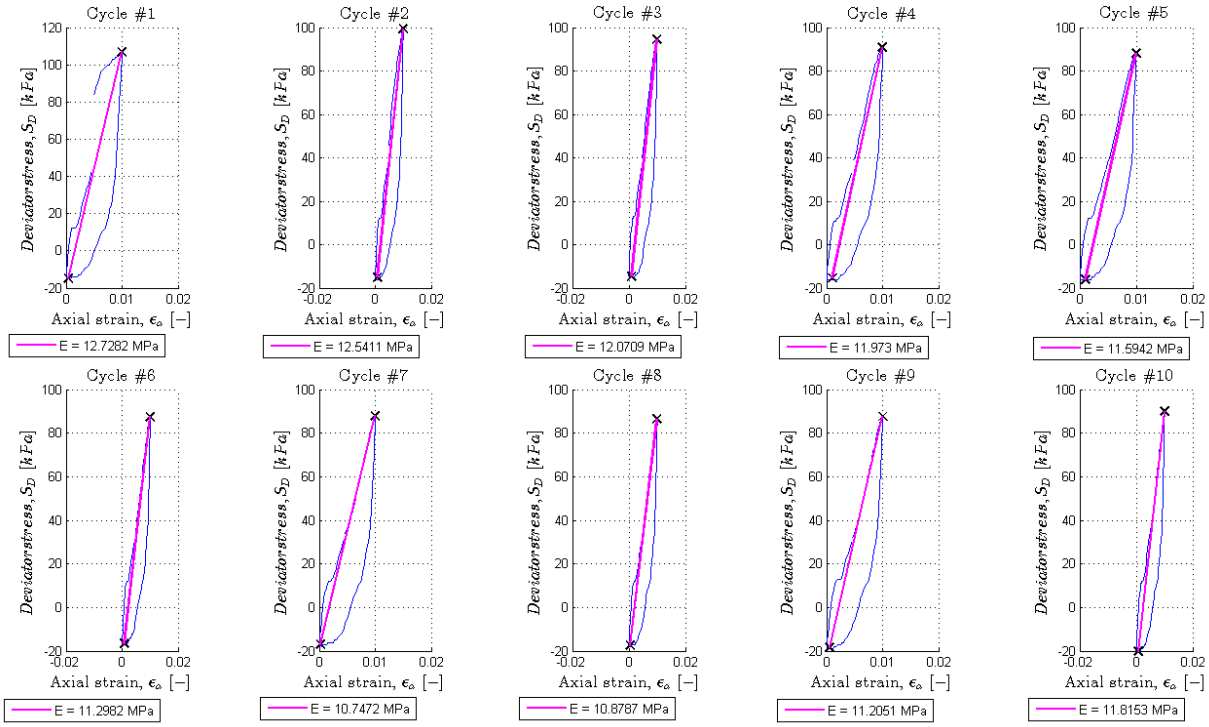

Figure 35 The change of Young's modulus for different cycles of the test for 0. 5% axial strain amplitude

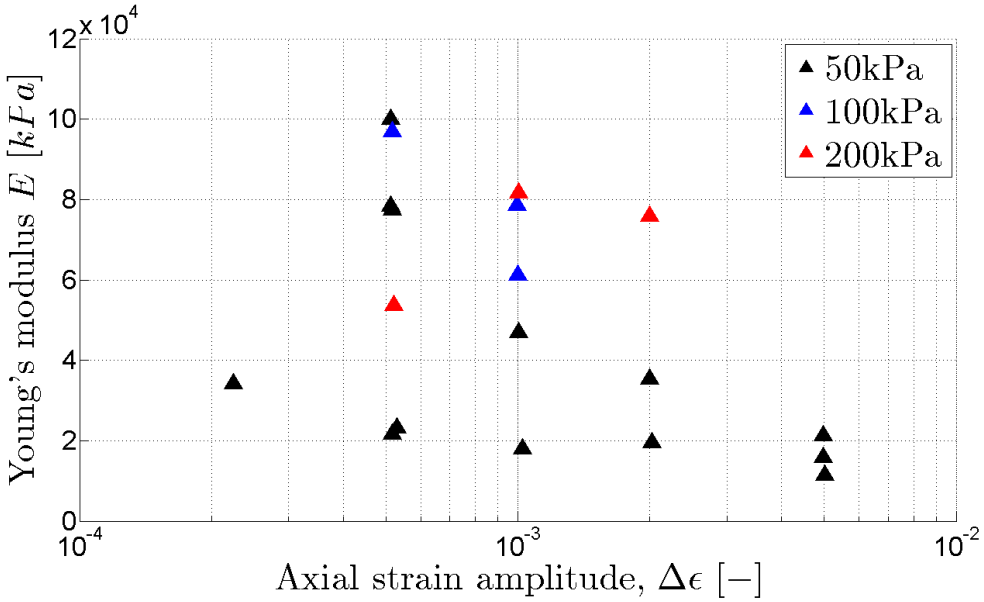

Figure 36 Young's modulus of dry sand specimens versus axial strain for 50 and 100 kPa confining pressures

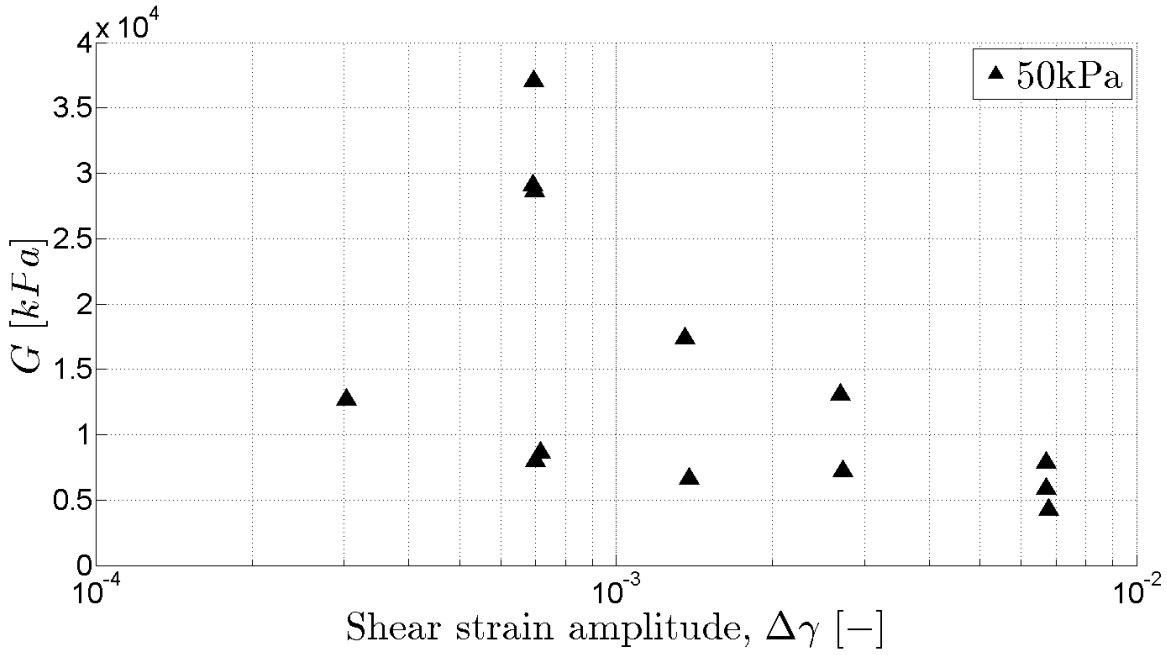

Figure 37 Shear modulus of dry sand specimens versus shear strain for 50 kPa confining pressure

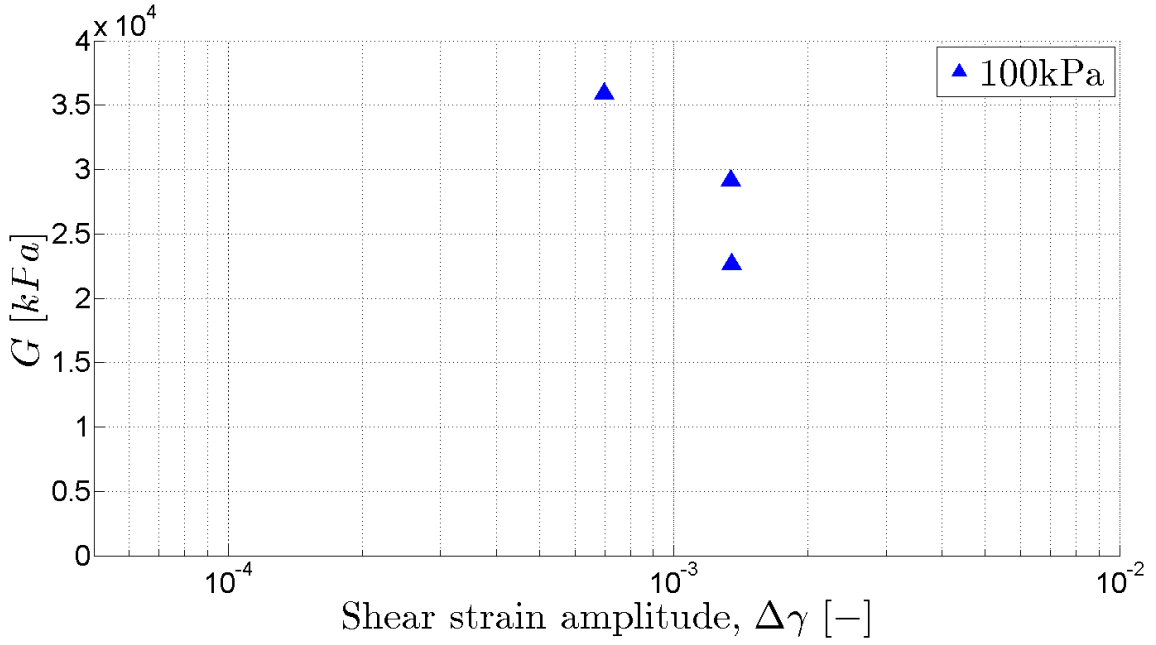

Figure 38 Shear modulus of dry sand specimens versus shear strain for 100 kPa confining pressure

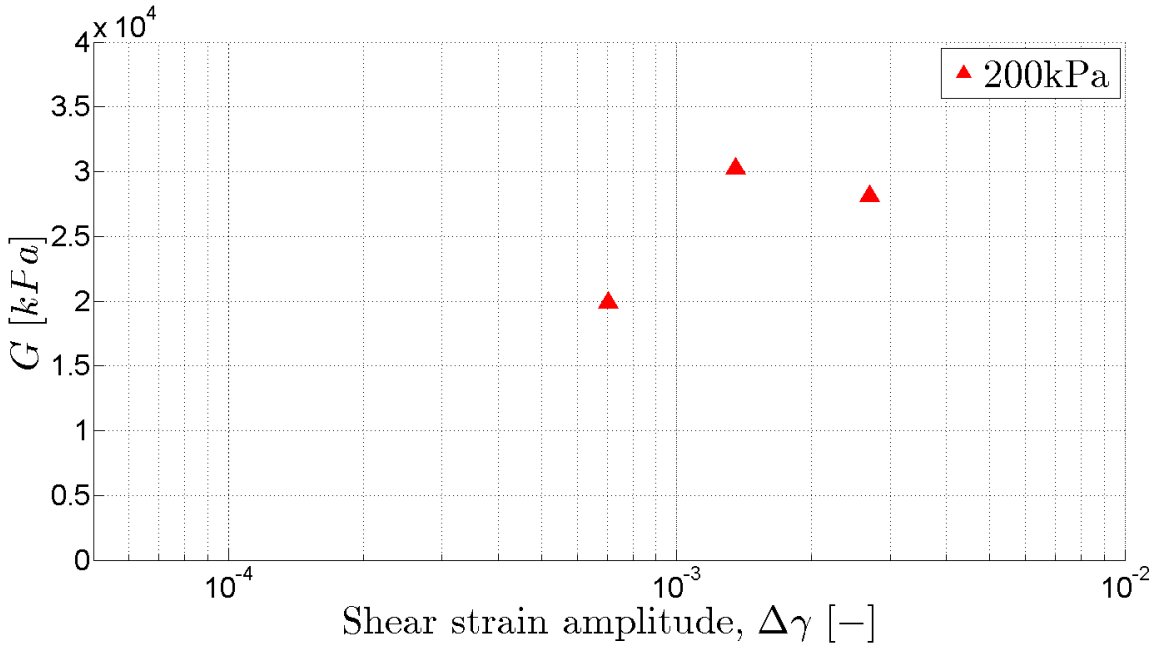

Figure 39 Shear modulus of dry sand specimens versus shear strain for 200 kPa confining pressure

In order to better understand the soil behavior under cyclic loading, obtained shear modulus was normalized to the small strain shear modulus calculated from the Equation 8 proposed by Seed et al. (1970). As discussed in Chapter 2, shear modulus reduction curve (the ratio of strain-dependent shear modulus to small-strain shear modulus) is a good representation of change in dynamic properties with change in strain amplitude. Those equations proposed by Hardin and Drnevich (1972), Darendeli (2001) and Menq (2003) were used for comparison and plotted with the experimental data on Figures 40, 41, and 42 for 50, 100, and 200 kPa, respectively.

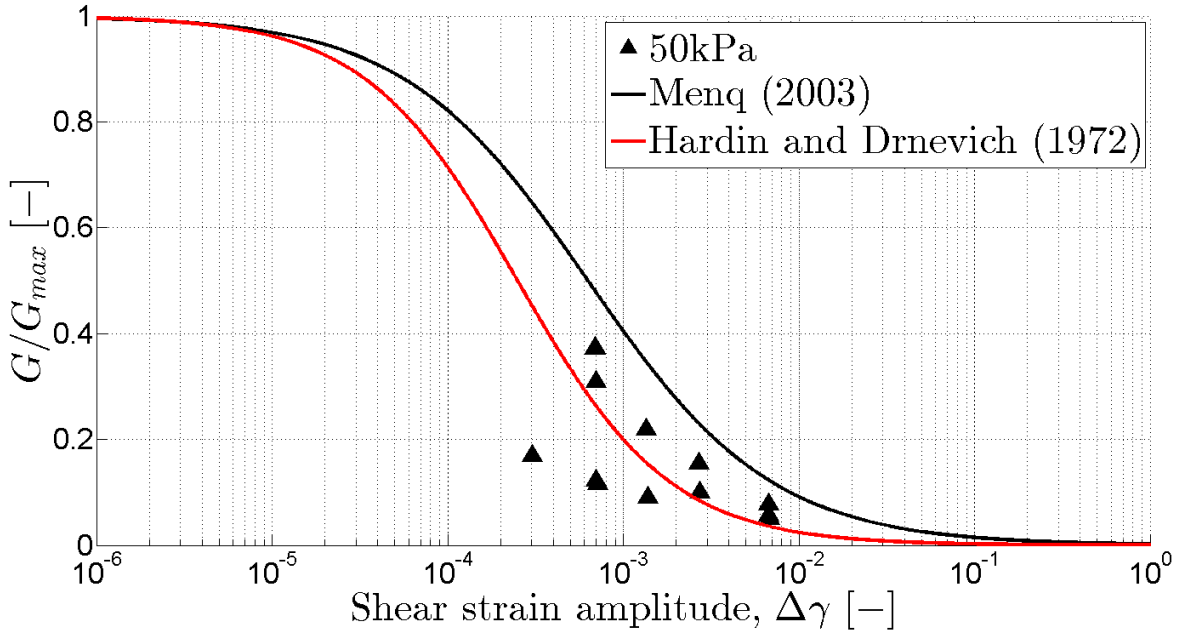

Figure 40 Normalized shear modulus versus gamma for 50 kPa confining pressure

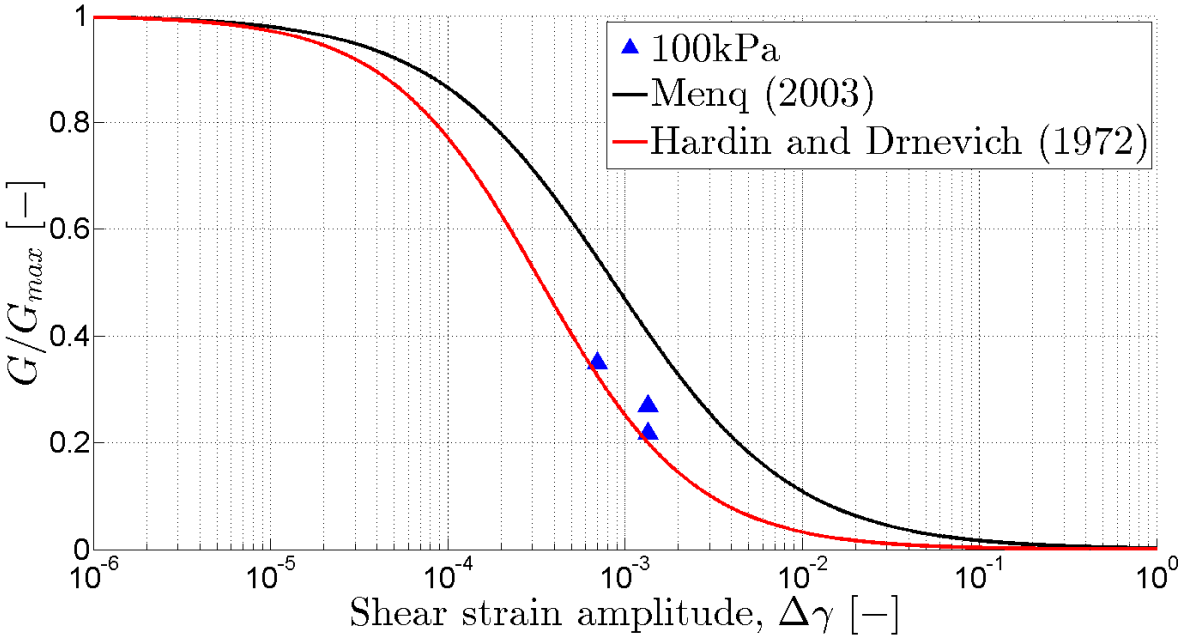

Figure 41 Normalized shear modulus versus gamma 100 kPa confining pressure

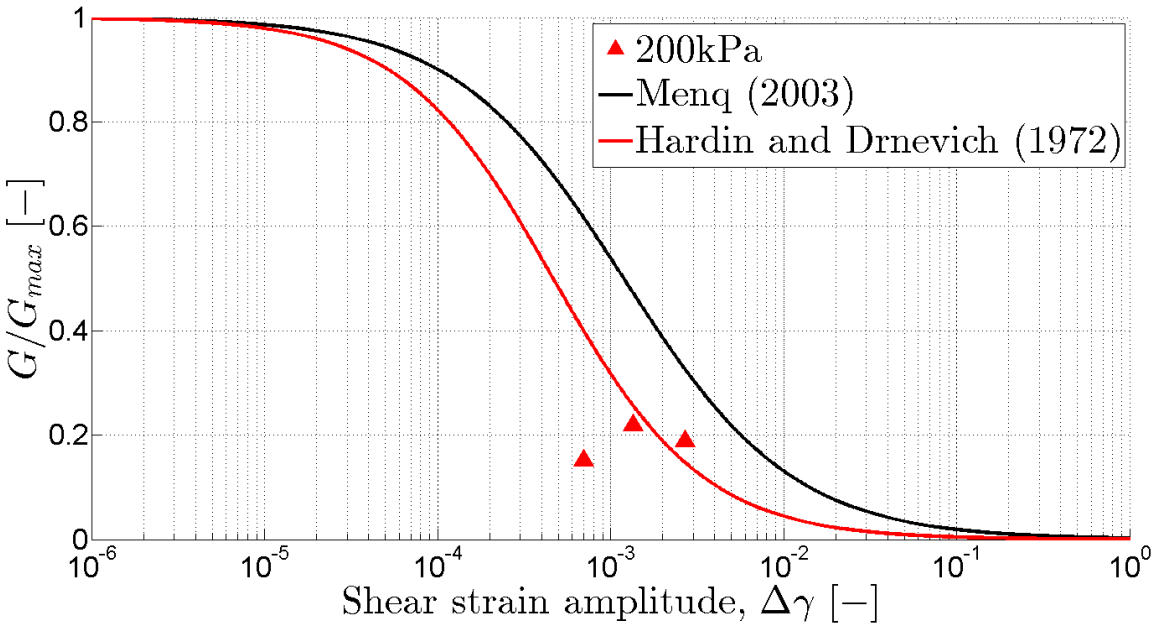

Figure 42 Normalized shear modulus versus gamma 200 kPa confining pressure

The effect of confining pressure on dynamic soil properties was also studied. The change in shear modulus for different cell pressures was plotted for 0.05 and 0.1% strain amplitude on Figures 43 and 44, respectively. The general trends in data points confirm the theory that shear modulus increases with the increase in confining pressure with half power of the effective confining pressure. Concluding from Equation 8 proposed by Seed and Idriss (1970) the relation of small strain shear moduli for different confining pressures can be written as

$$\frac{G_{max-\sigma'_1}}{G_{max-\sigma'_2}} = \left(\frac{\sigma'_1}{\sigma'_2}\right)^{0.5} \tag{56}$$

Assuming that all the specimens were prepared to the same relative density using the same soil, and with and approximate assumption that the shear modulus reduction only depends on shear strain, for similar shear strain values the equation can be re-written for strain-dependent shear modulus relation

$$\frac{G_{\sigma'_1}}{G_{\sigma'_2}} = \left(\frac{\sigma'_1}{\sigma'_2}\right)^{0.5} \quad (57)$$

For axial strain amplitude of 0.05% reference points for 50 and 100 kPa were taken and the trend was extended to reach another confining pressure, as shown in Figure 43. The trends approximately confirm the expected effect of confining pressure on shear modulus. Similarly, for axial strain amplitude of 0.1% the general trend was simulated for 50, 100, and 200 kPa confining pressures. Table 10 below summarizes the values that were calculated, and the results are plotted in the Figures 43 and 44. For the rest of study on saturated and unsaturated soils, the specimens were tested only under 50 kPa.

Figure 45 shows the complete set of G/G_{max} data for dry sand under different confining pressures.

Table 10 Back calculated values of Shear Modulus

	Confining Pressure (kPa)		
Strain level (%)	50	100	200
	Shear Modulus (MPa)		
0.05	***28***	39.6	56
	25.4	***36***	51
0.1	***17.5***	24.7	35
	15	21.2	***30***

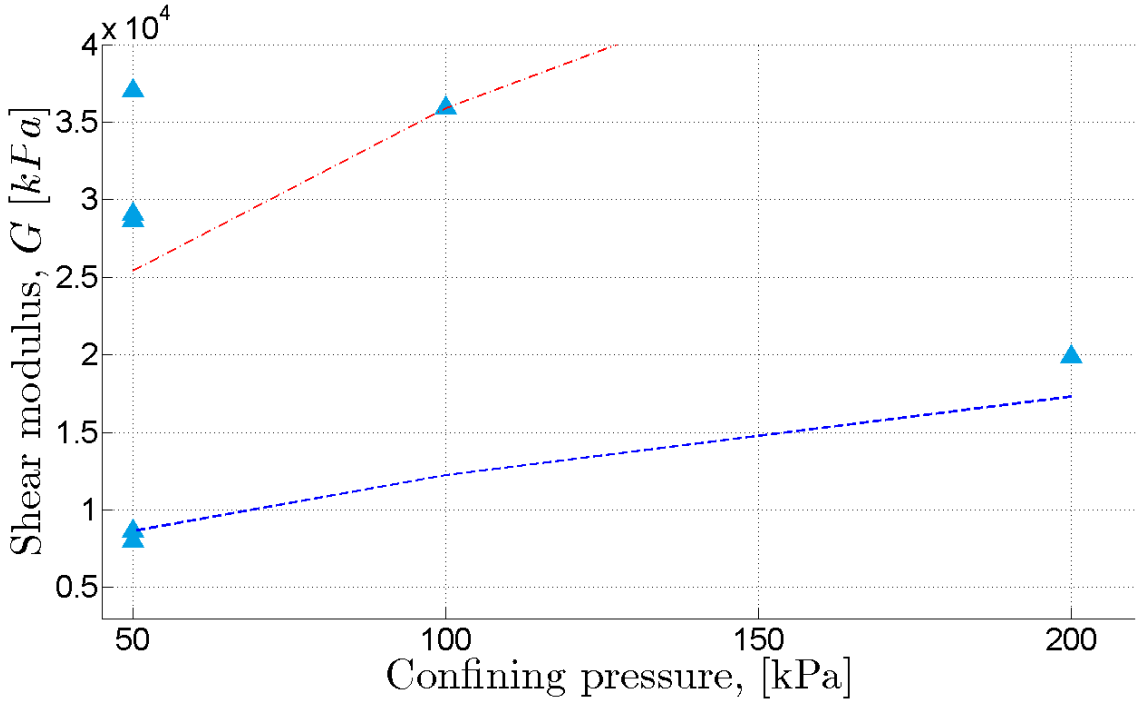

Figure 43 Shear modulus versus confining pressure for 0.05% of axial strain

Red line shows back calculated shear modulus with the initial point at 200 kPa cell pressure, while the initial point for the blue line was taken at 50 kPa cell pressure. Both trends show increase of the values of shear modulus with increase of confining pressure.

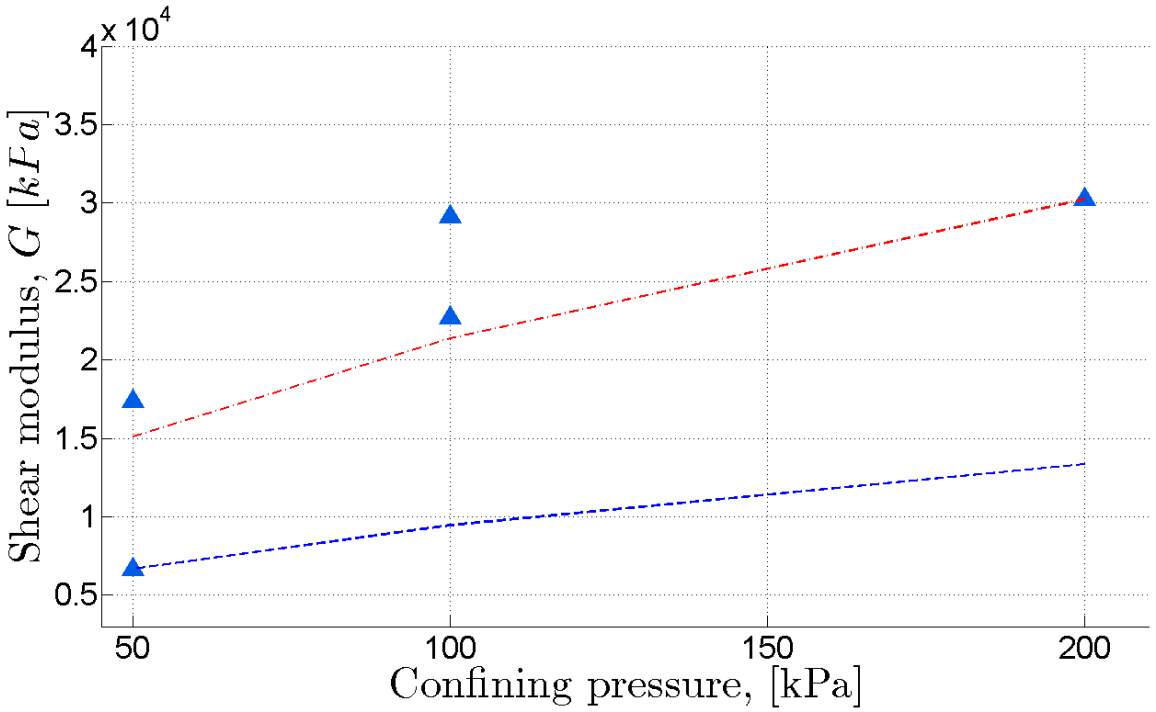

Figure 44 Shear modulus versus confining pressure for 0.1% of axial strain

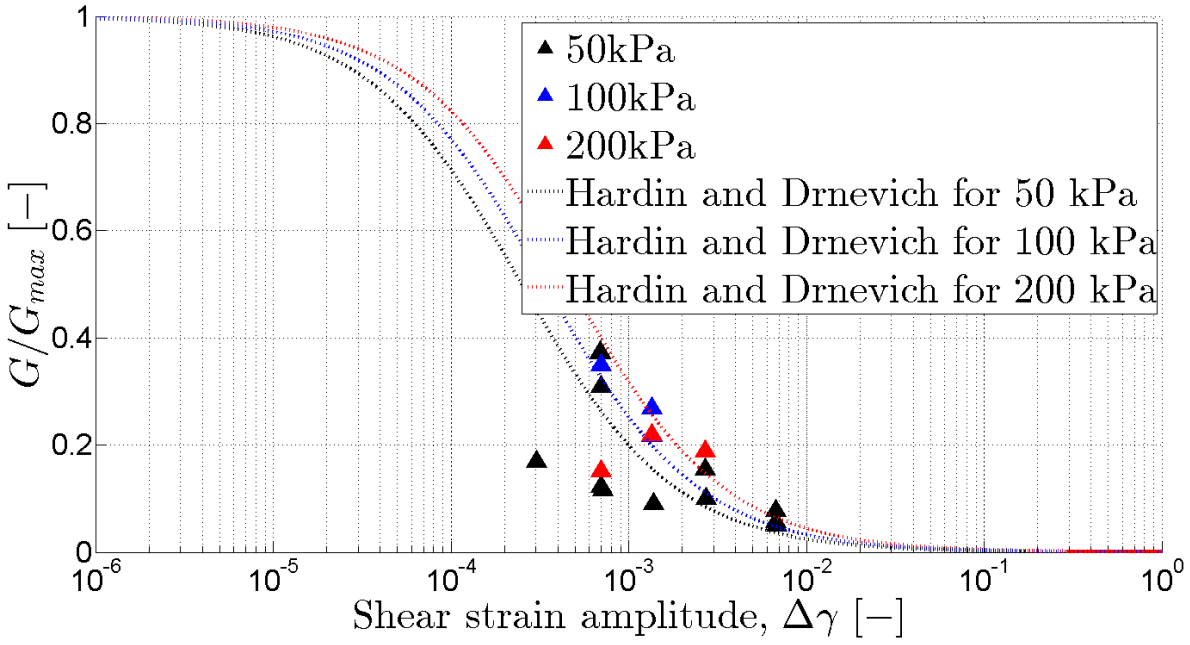

Figure 45 Shear modulus reduction curves for dry specimens

CHAPTER VIII. RESULTS: STRAIN-CONTROLLED TESTS ON FULLY SATURATED SAND

Strain- controlled cyclic triaxial tests were performed on saturated sand specimens and results are presented in this chapter. The specimen preparation and testing technique were exactly similar to the tests on dry sand. A typical set of hysteresis loops obtained from the tests are shown in Figure 46. Because of the water inside the specimen, the loops are broader than those of dry sand samples, demonstrating higher level of energy dissipation. This could be explained by a higher damping inside fully saturated soil samples due to the lubrication effects.

The goal of the study was to perform saturated tests under drained conditions, where pore pressure should be kept constant by continuous application of back pressure or suction to the soil specimen. However, because of the rapid rate of loading one can observe an increase water pressure with subsequent dissipation. The Flow Pump was operating under pressure control mechanism, but the maximum outflow rate that it can support is 3mL/min that was not always sufficient during cyclic test to dissipate the excess pore pressure immediately.

As mentioned in Chapter 6, dynamic triaxial test provides reasonable results for the shear strain amplitude 10^{-4} to 10^{0}, which corresponds to medium and large strain levels. Figure 47 shows the increase of pore water pressure during cyclic loading in a typical series of tests. It can be concluded from the graph that the general trend of the pore pressure built-up tends to increase.

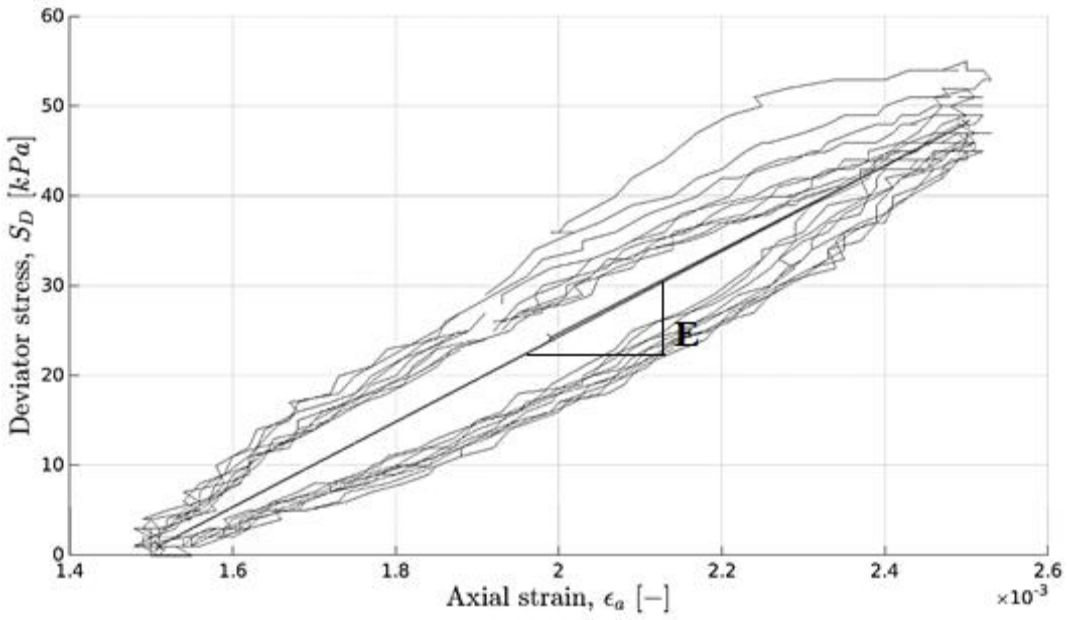

Figure 46 Representative hysteresis loop for strain-controlled cyclic triaxial test

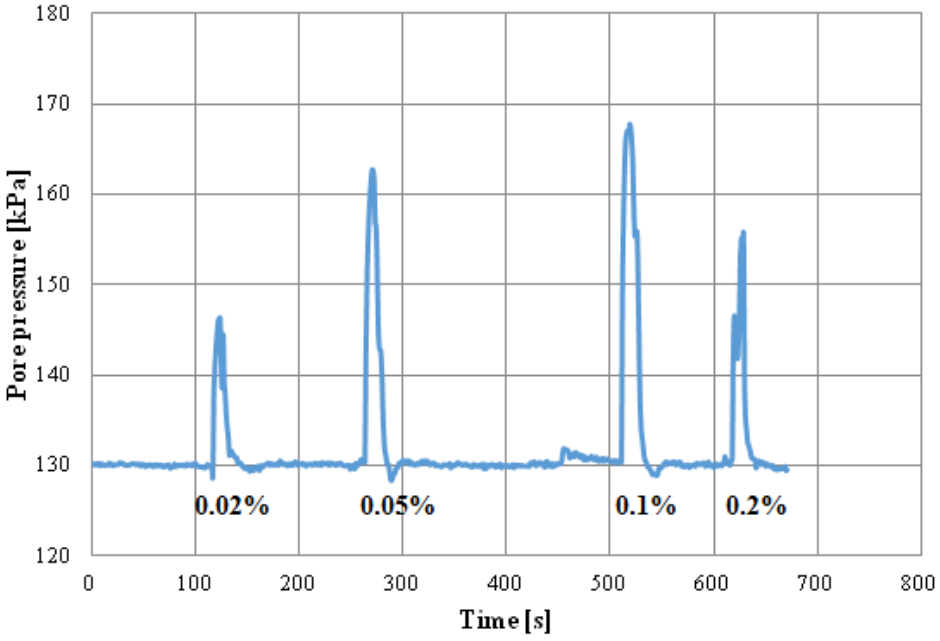

Figure 47 The increase of pore pressure during saturated triaxial test

The excess pore pressure ratio should be calculated using the following formula

$$r_u = \frac{\Delta u}{\sigma'} \tag{58}$$

Where Δu is the pore pressure change and σ' is the effective stress in the beginning of the test. In case when pore pressure is equal to confining pressure, $r_u = 1$ and effective stress is equal to 0, which represents a liquefied case. The r_u values for this set of tests are presented in Table 11.

Table 11 Pore pressure ratio for tests with different strain levels

ε_a , (%)	0.02	0.05	0.1	0.2
r_u , (-)	0.3	0.62	0.76	0.5

Because of the increase in pore pressure the tests were considered "partially drained". This situation is very similar to what happens to sand layers during earthquakes. In such cases, despite the high permeability of the material the fast rate of loading does not allow enough time for equilibration of pore water pressure dissipation and generation. Similar results has been reported in other studies (Dashti et al. 2010).

Similar to the tests on dry sands, the Young's modulus and subsequently the shear modulus variation with respect to shear strain are presented in Figures 48 and 49, respectively. In addition, for better visualization of data G/G_{max} values were calculated and plotted alongside the empirical curves, as shown in Figure 48. Although the values are approximately close the proposed band, they are on the lower side of the band. This can be attributed to the smaller measured shear modulus due to the generation of some excess pore water pressure, which reduced the effective stress and, in turn, the stiffness.

Another reason for the values to be lower than the modulus reduction curve, is decrease of shear modulus with each cycle. Because of the energy dissipation in saturated soil, the change in Young's modulus can reach 50% between first and tenth cycles. The difference is more significant for higher strain levels. The variation of the modulus is presented in Figure 48 and 49.

The results from dry and saturated strain-controlled tests are used for further analysis and comparison with tests on soil samples with different levels of saturation that are presented in Chapter XI.

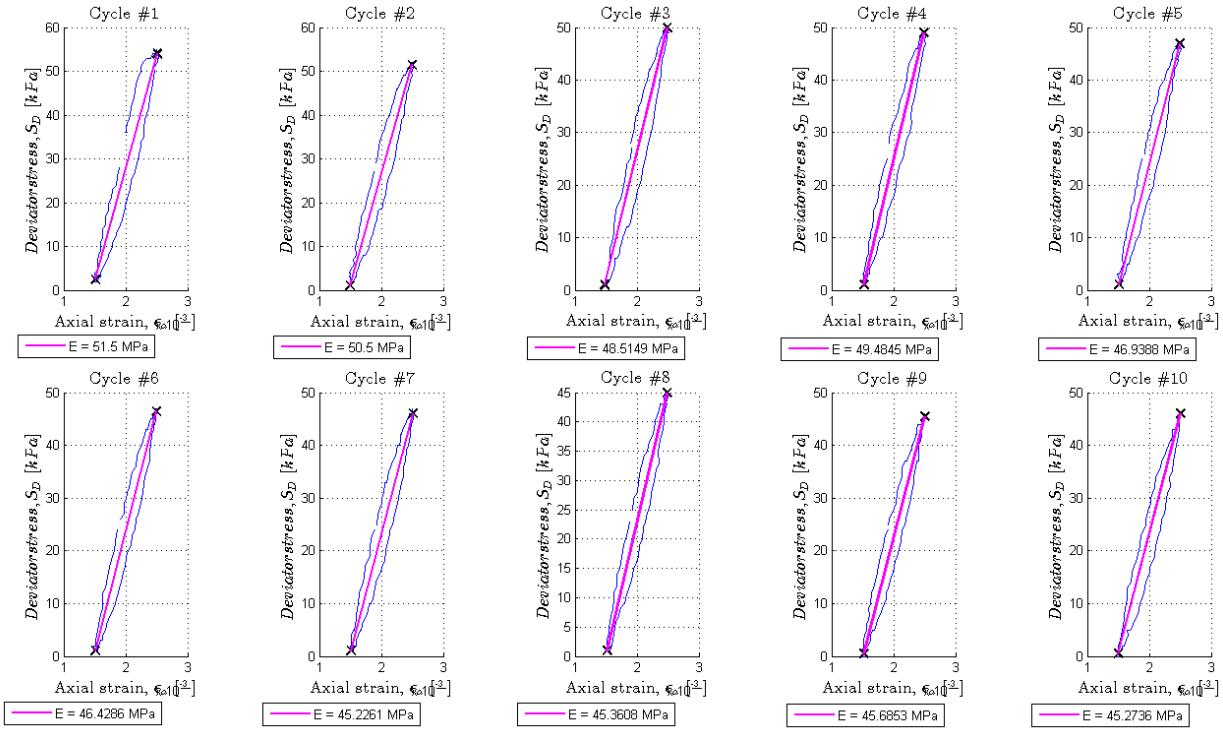

Figure 48 Young's modulus variation for 0.05% axial strain amplitude

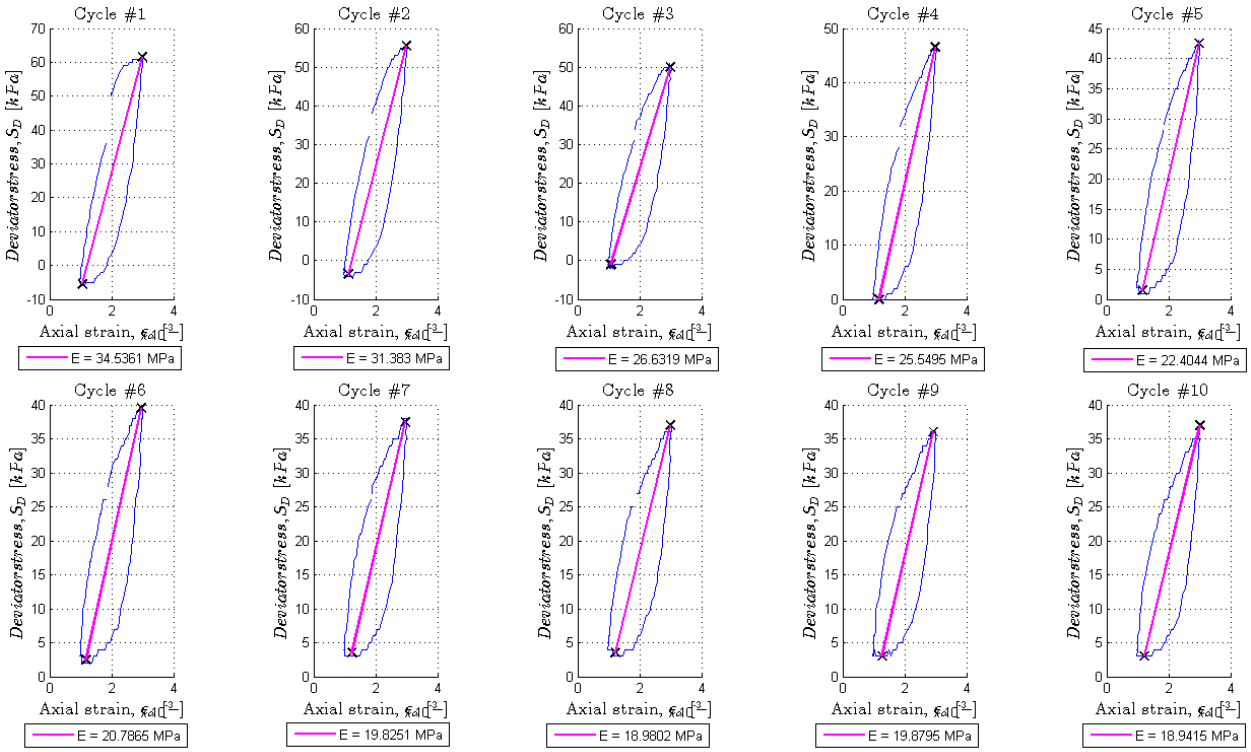

Figure 49 Young's modulus variation for 0.1% axial strain amplitude

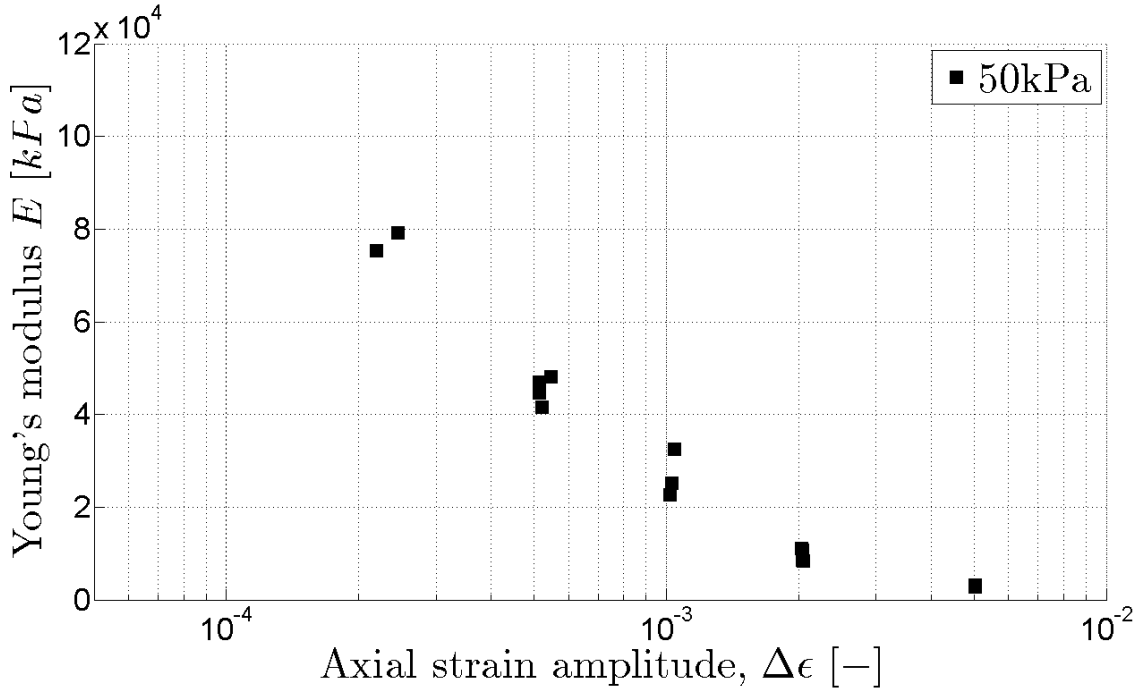

Figure 50 Young's modulus versus axial strain for 50 kPa confining pressure

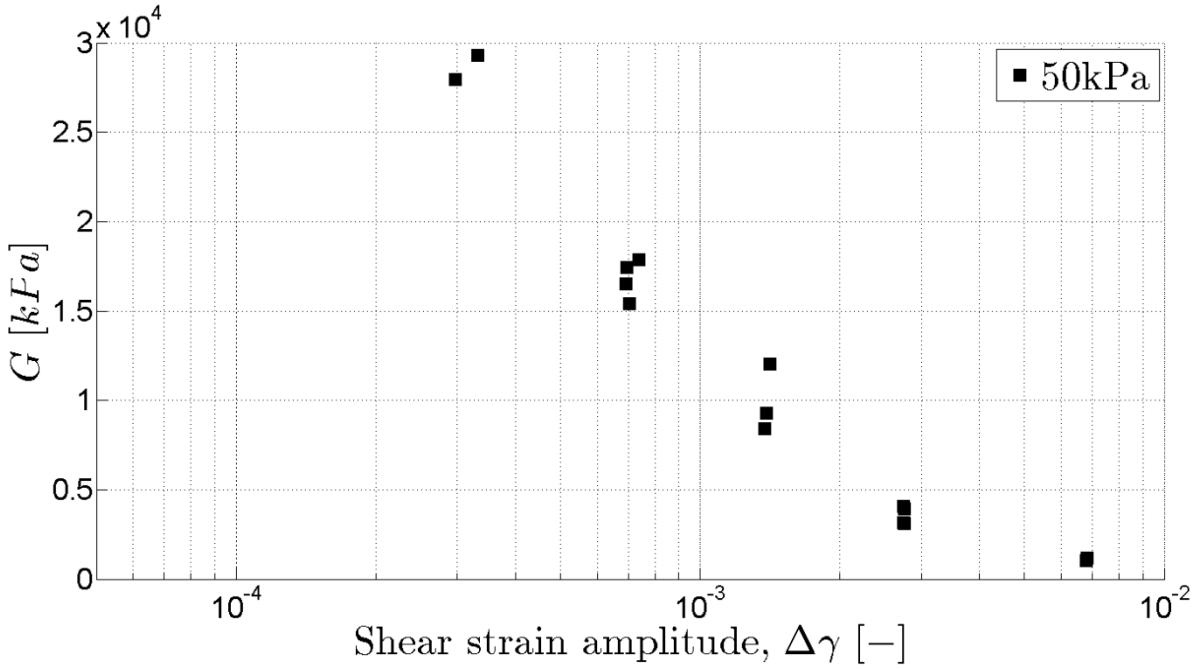

Figure 51 Shear modulus versus shear strain for 50 kPa confining pressure

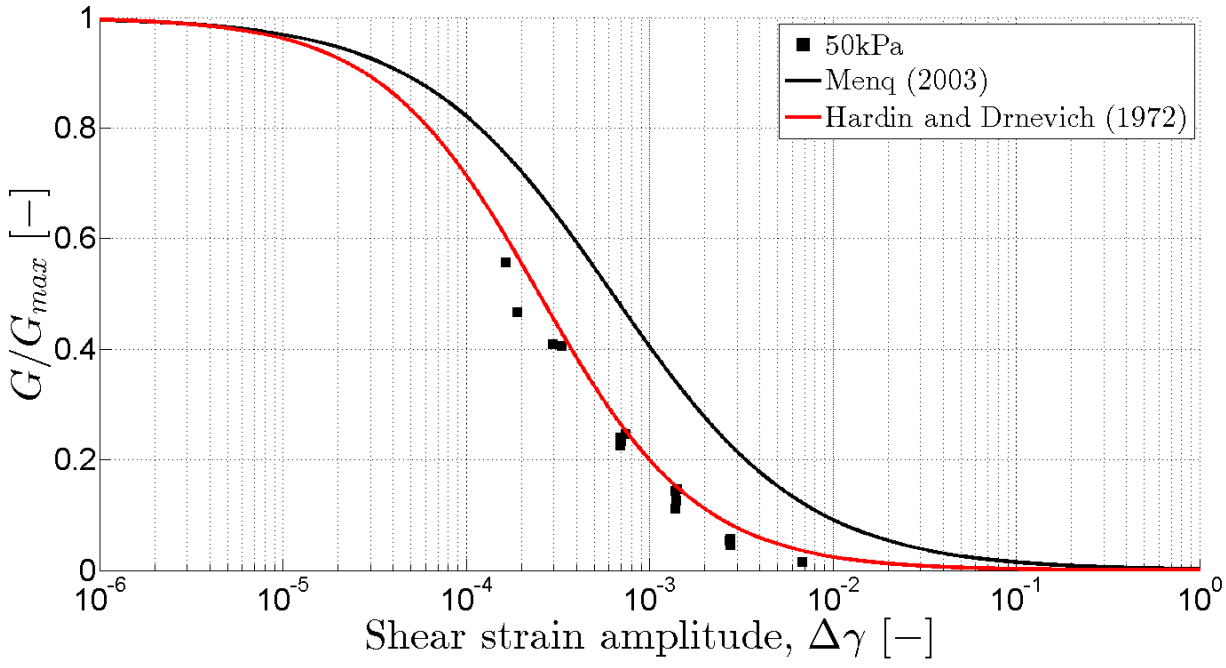

Figure 52 Normalized shear modulus versus gamma for saturated soil tests

CHAPTER IX. RESULTS: STRAIN-CONTROLLED TESTS ON PARTIALLY SATURATED SAND

The main goal of this study was to investigate the effect of the level of saturation on dynamic soil properties. As described in Chapter 6, sand specimens were fully saturated prior to application of matric suction. After that, the DigiFlow Flow Pump was operated in pressure control mode to impose negative pore pressure to the bottom of the specimen.

Depending on the target value of matric suction, different times were needed for the system to equilibrate. The most challenging task was to achieve constant matric suction when soil specimen was undergoing transition regime, meaning that water in the pores of the specimen started to drain. Because of the considerably large size of the specimen water would keep moving through the soil at a very slow rate, and much longer time was needed to reach equilibrium condition.

In order to study the change of soil properties of the specimen on the drying path of hydraulic hysteresis, tests with the following matric suction were performed: 2, 2.5, 3, 3.5, 4.5, 6, and 10 kPa. The corresponding effective stresses and the mean effective stresses values for unsaturated soil specimens were calculated using Equations 32 and 7, respectively.

As mentioned earlier, axis translation technique was implemented for suction control and the Flow Pump was used to maintain the negative pore pressure at the bottom of the specimen, while the top of the specimen was open to the atmosphere. Because the tests were conducted on the soil with a very high permeability, all specimens were very sensitive to any influence of motion.

Even minor disturbance (e.g. aligning the triaxial cell under the load frame) would cause water to move inside the specimen. During rapid dynamic loading the soil specimen would experience increase in pore pressure (or decrease in suction), which is demonstrated in Figure 53. If a soil specimen undergoes a higher strain level, the pore pressure inside will increase more significantly. The Flow Pump would respond immediately and withdraw extra water from the specimen to bring back pore pressure and reach target matric suction again. Similar to fully saturated tests, even with the consideration of change in suction, by definition, the tests were performed in drained condition as the negative pore pressure on the specimen was forced to stay constant.

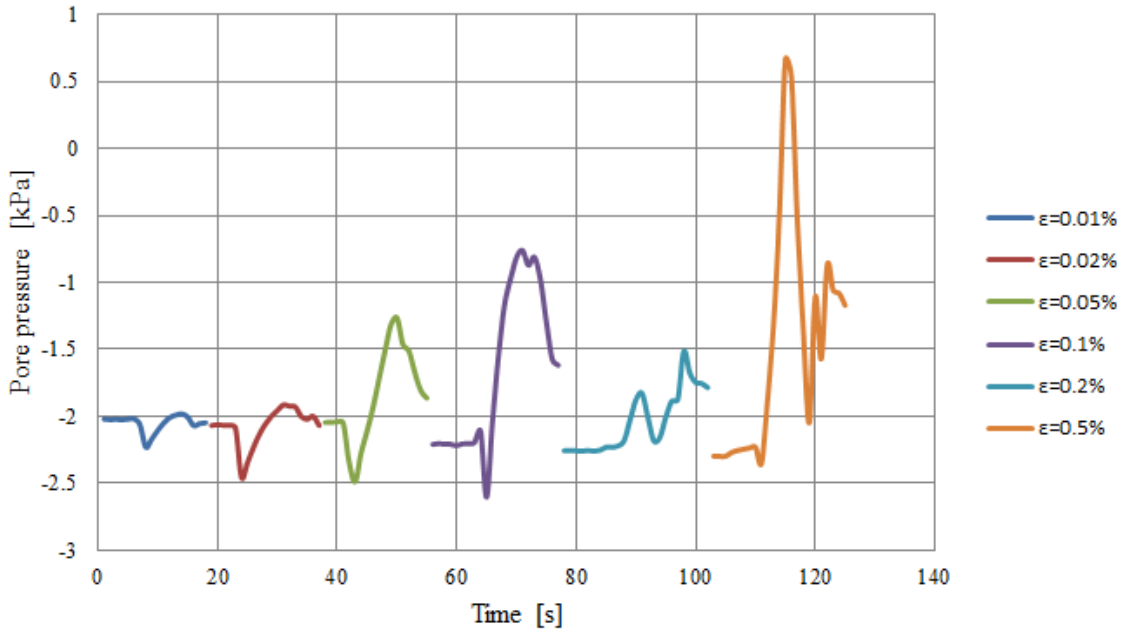

Figure 53 Change in pore pressure during cyclic test with different strain amplitudes

The calculated Youngs's modulus and shear modulus are presented in Figures 54-67 for different suction levels. Based on these data the shear modulus variation with respect to shear strain for different suction levels is shown in Figures 76, 77, 78 and 79. Later, similar to that of dry and saturated soils, the shear modulus reduction values were formed and shown in Figures 68-74.

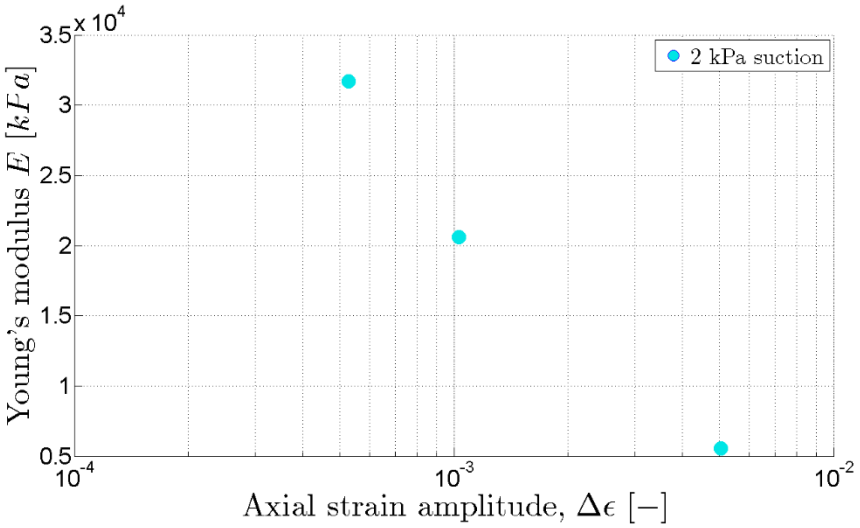

Figure 54 Young's modulus versus axial strain amplitude for 2 kPa suction

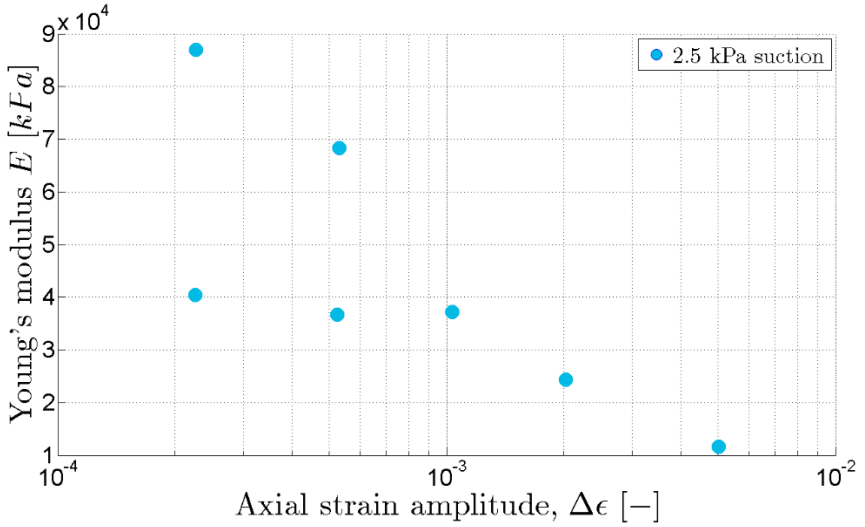

Figure 55 Young's modulus versus axial strain amplitude for 2.5 kPa suction

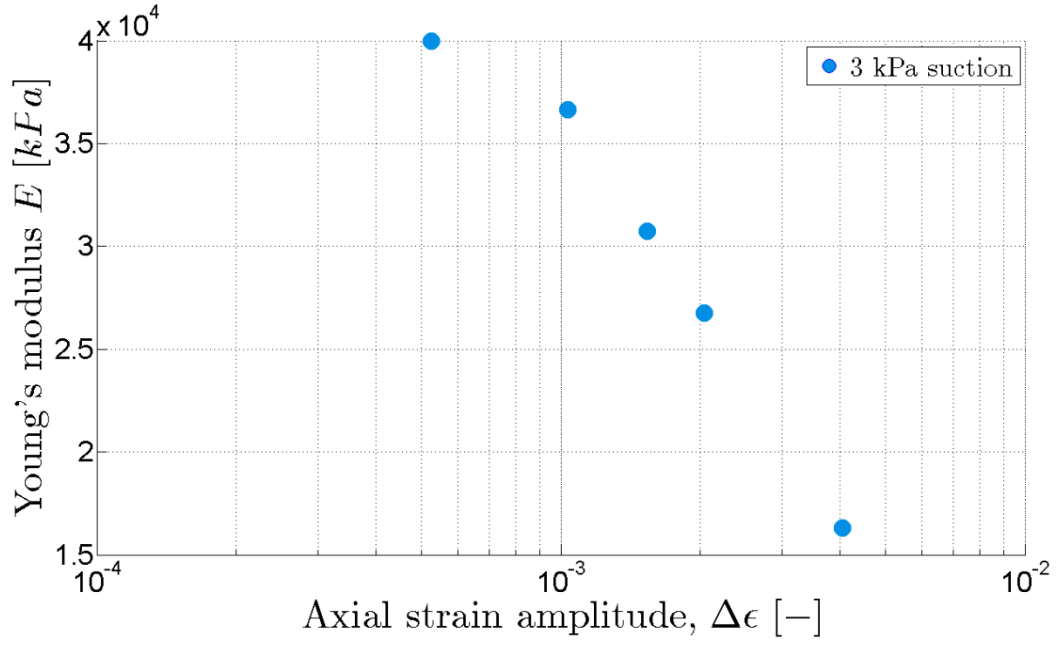

Figure 56 Young's modulus versus axial strain amplitude for 3 kPa suction

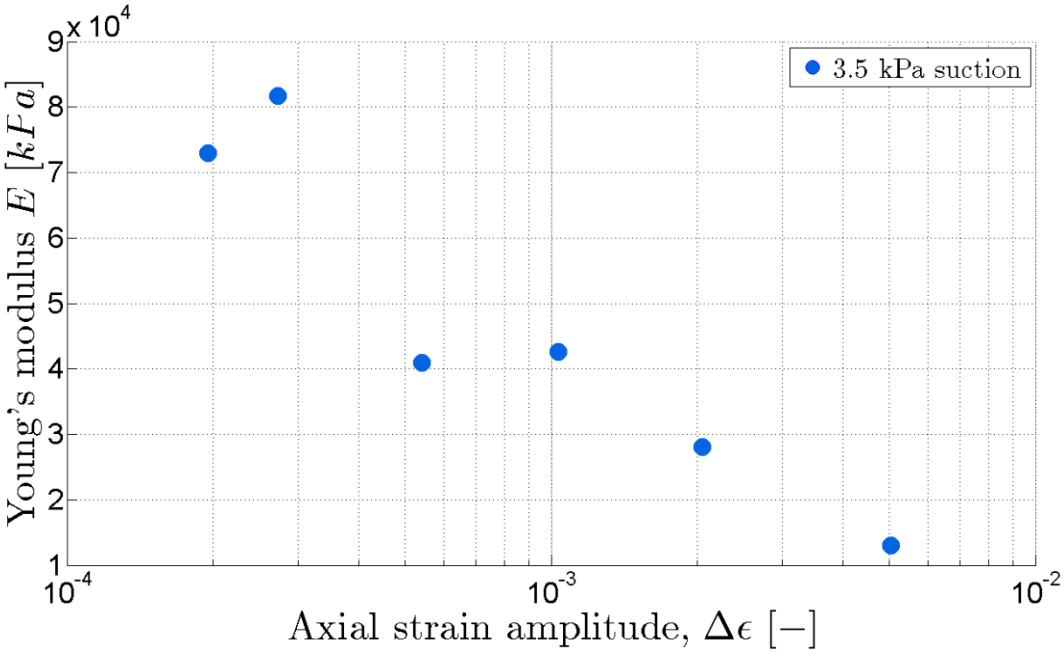

Figure 57 Young's modulus versus axial strain amplitude for 3.5 kPa suction

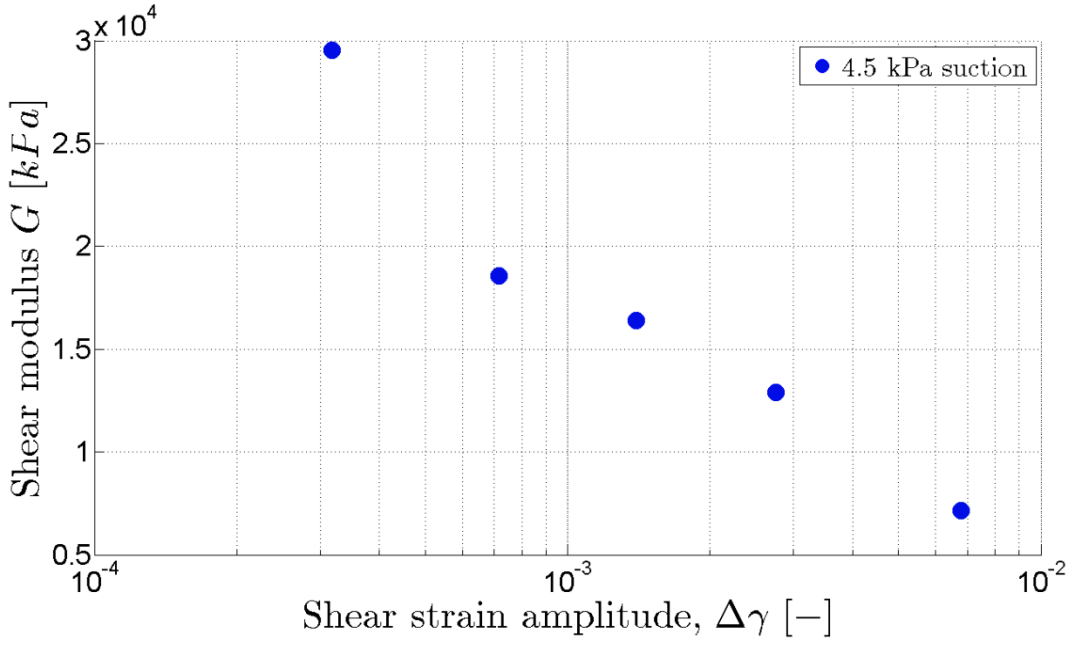

Figure 58 Young's modulus versus axial strain amplitude for 4.5 kPa suction

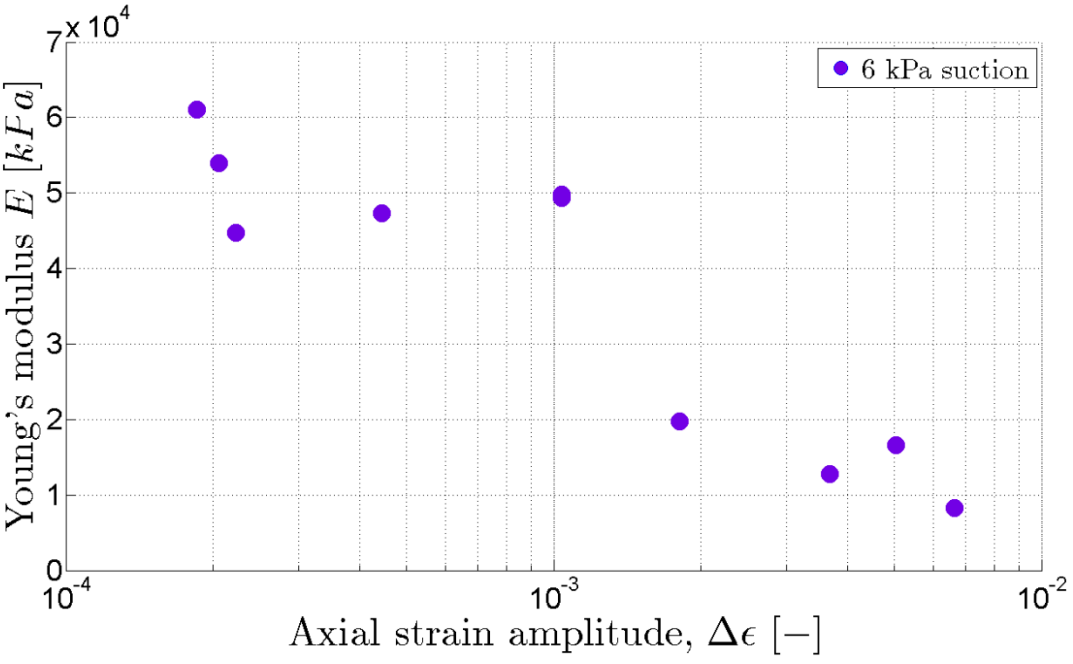

Figure 59 Young's modulus versus axial strain amplitude for 6 kPa suction

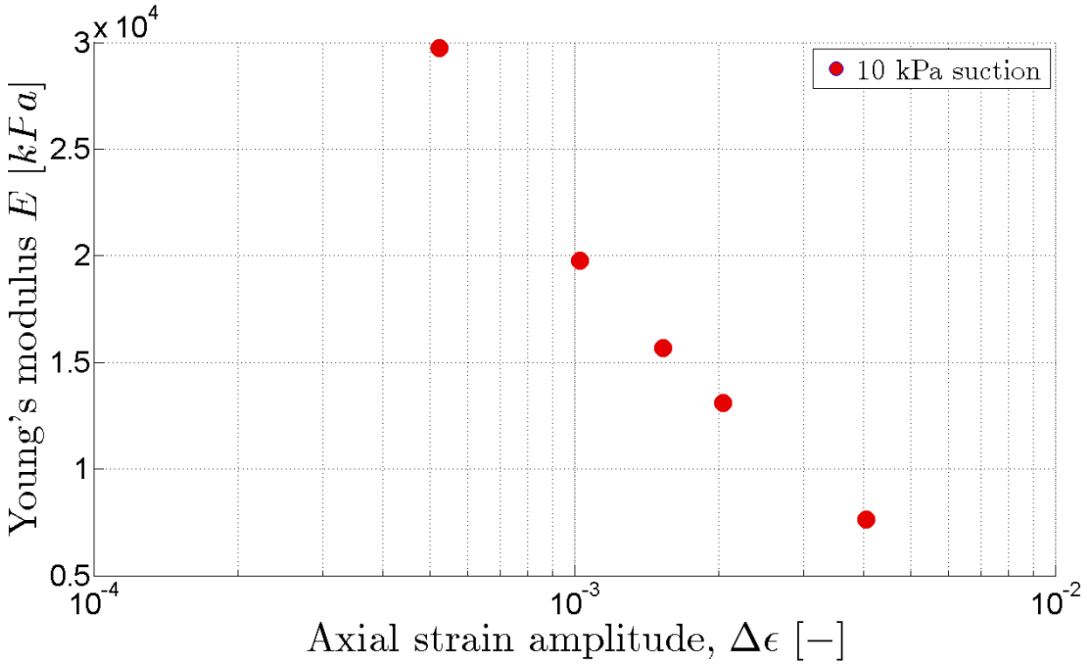

Figure 60 Young's modulus versus axial strain amplitude for 10 kPa suction

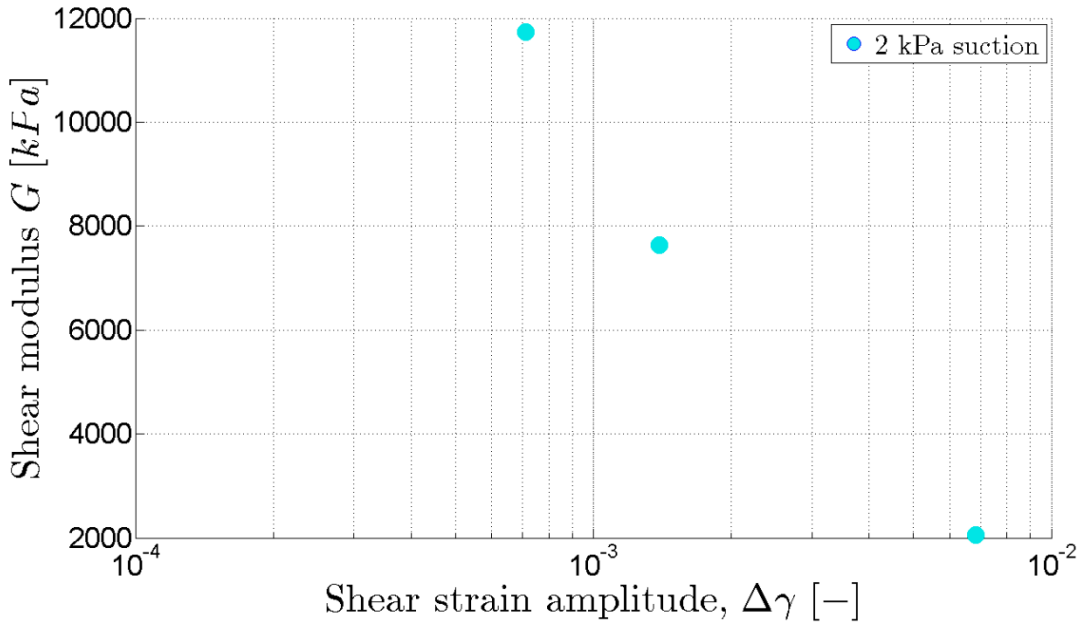

Figure 61 Shear modulus versus axial strain amplitude for 2 kPa suction

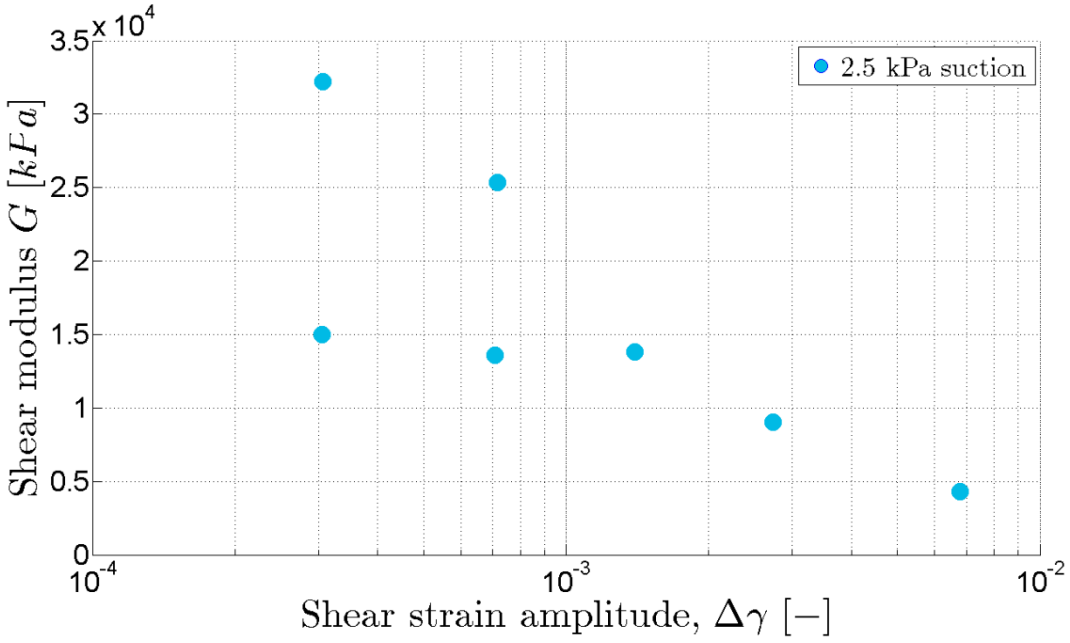

Figure 62 Shear modulus versus axial strain amplitude for 2.5 kPa suction

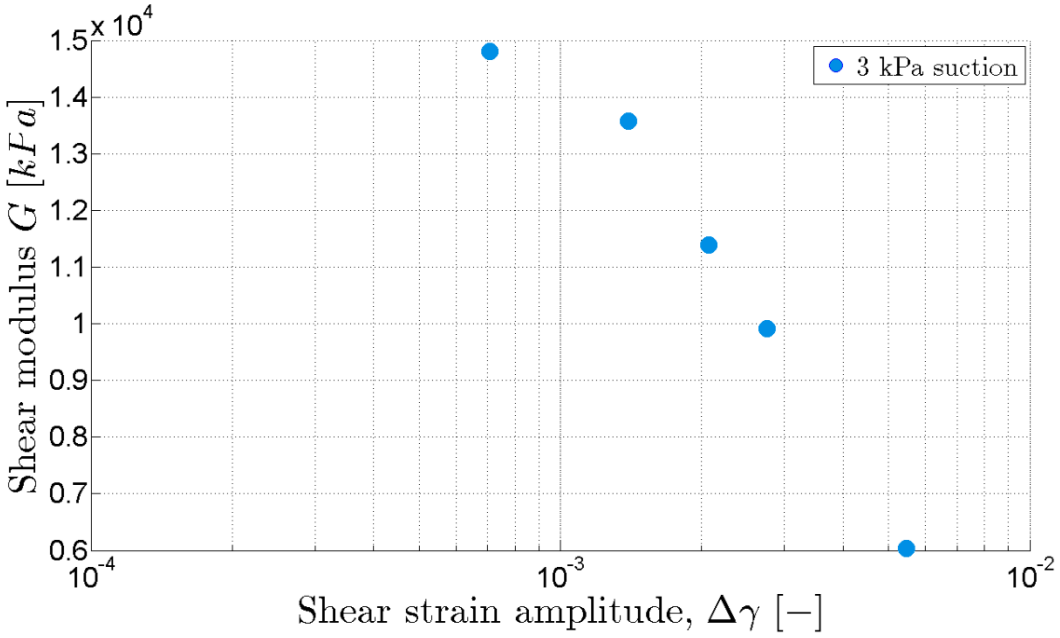

Figure 63 Shear modulus versus axial strain amplitude for 3 kPa suction

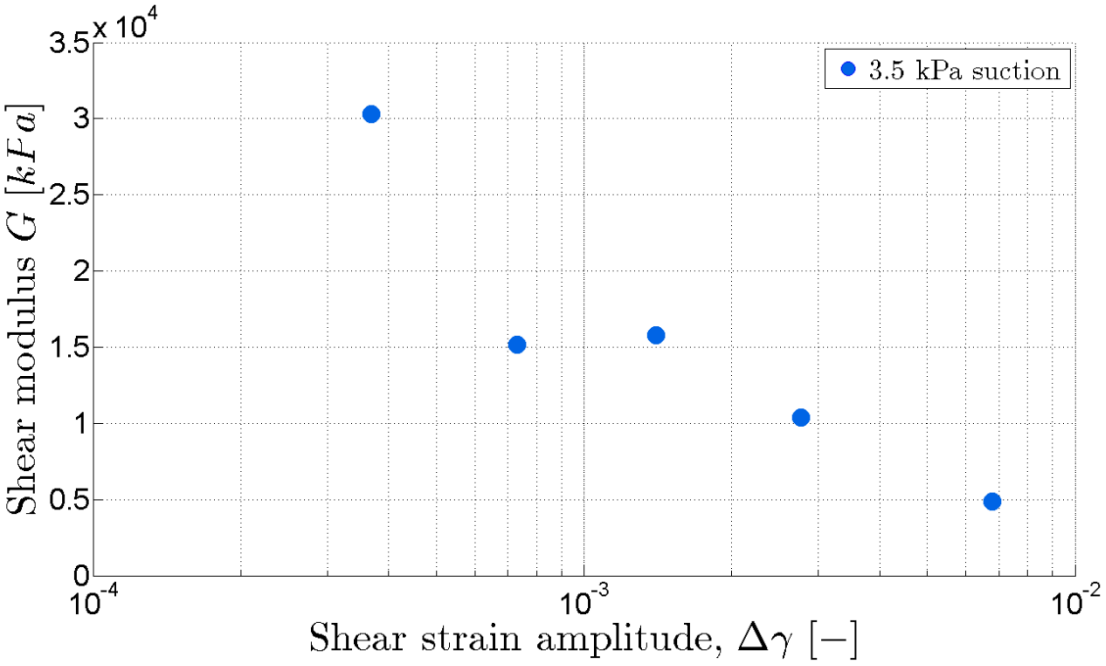

Figure 64 Shear modulus versus axial strain amplitude for 3.5 kPa suction

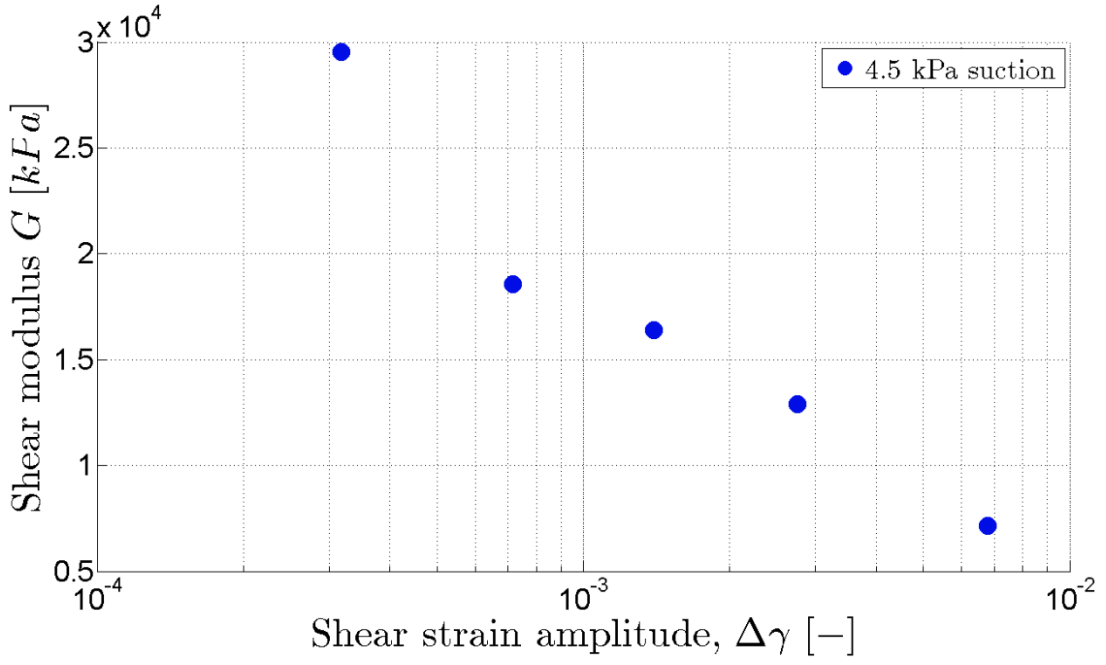

Figure 65 Shear modulus versus axial strain amplitude for 4.5 kPa suction

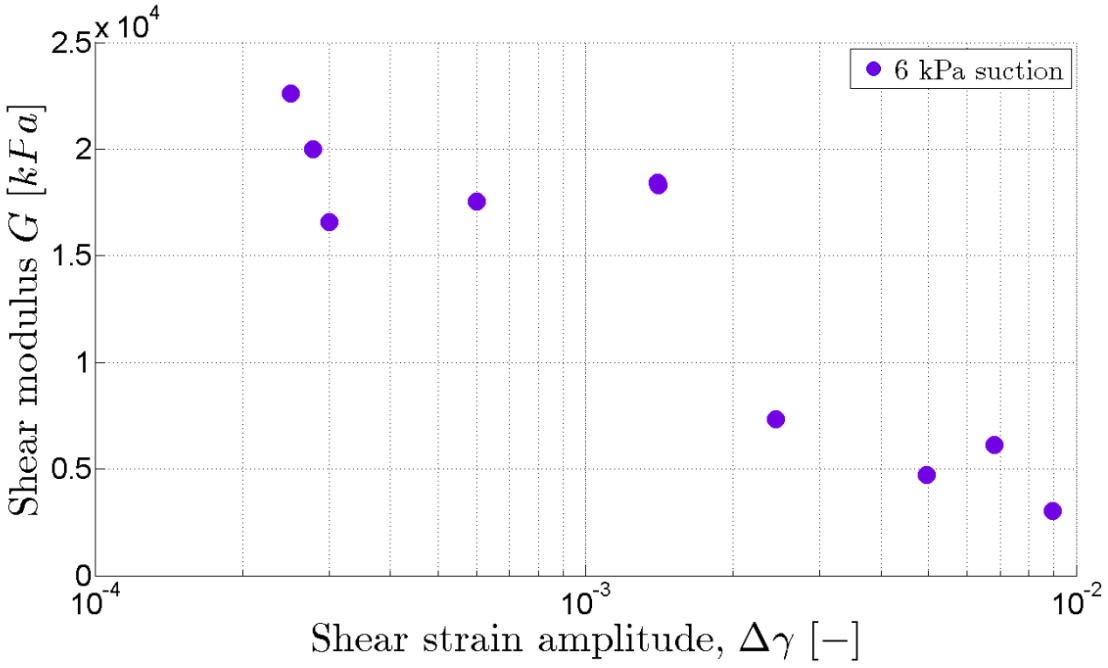

Figure 66 Shear modulus versus axial strain amplitude for 6 kPa suction

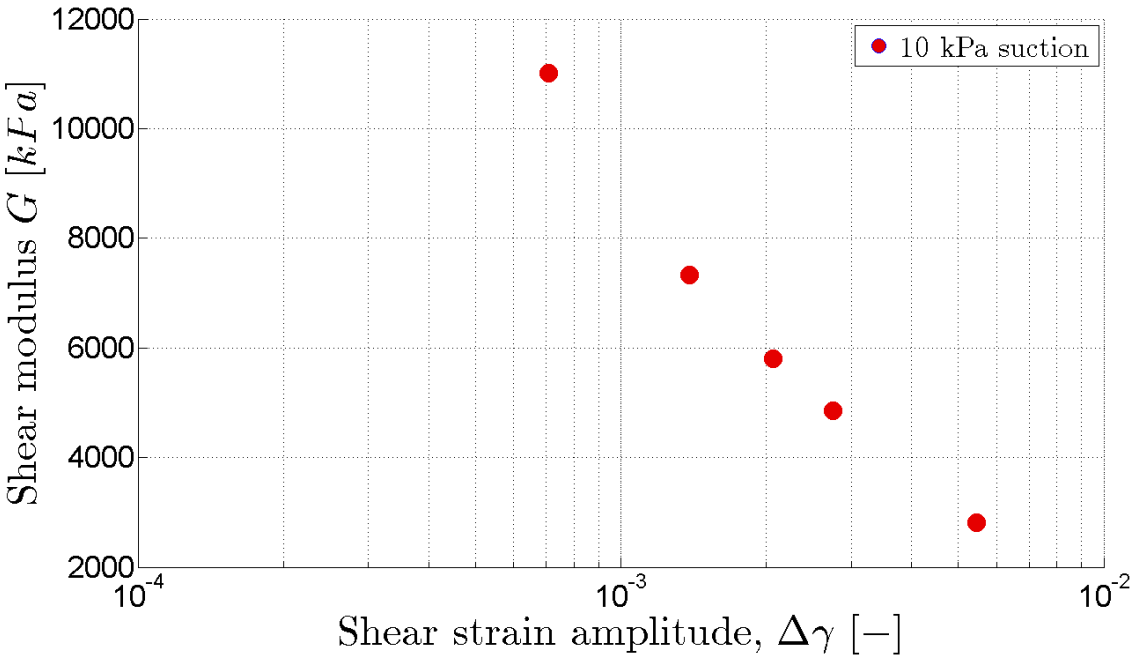

Figure 67 Shear modulus versus shear strain amplitude for 10 kPa suction

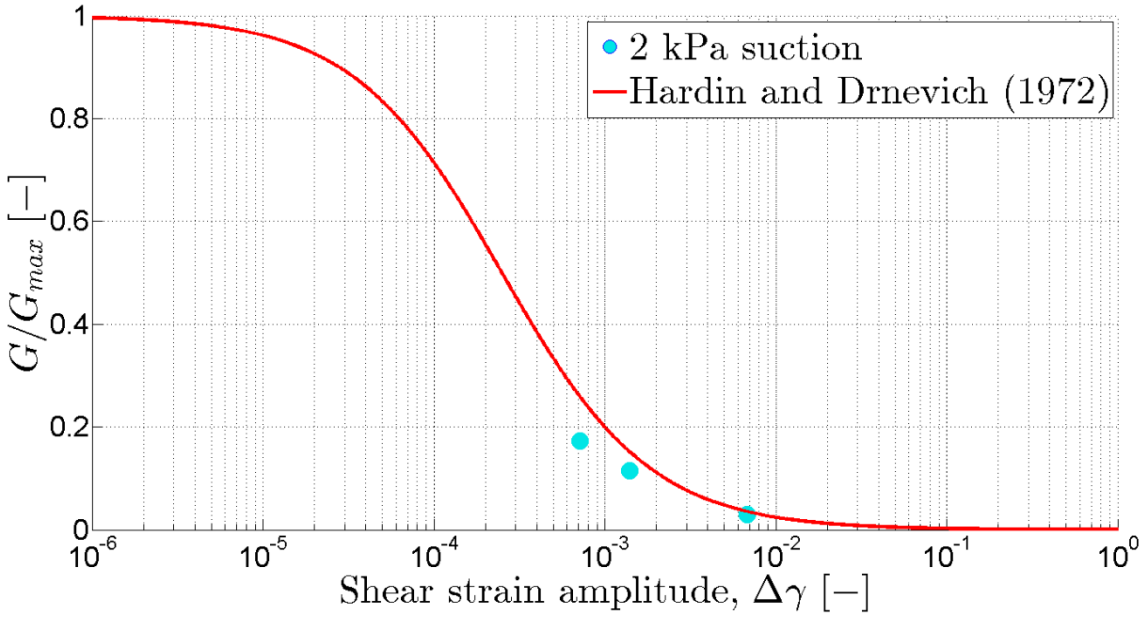

Figure 68 Normalized shear modulus versus shear strain amplitude for 2 kPa suction

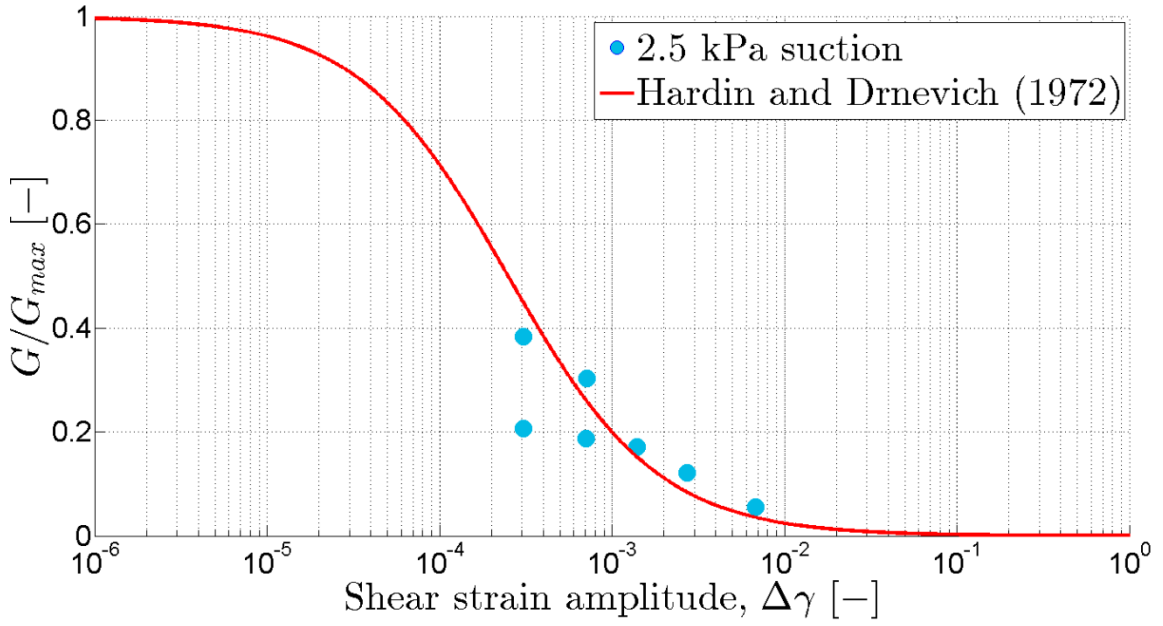

Figure 69 Normalized shear modulus versus shear strain amplitude for 2.5 kPa suction

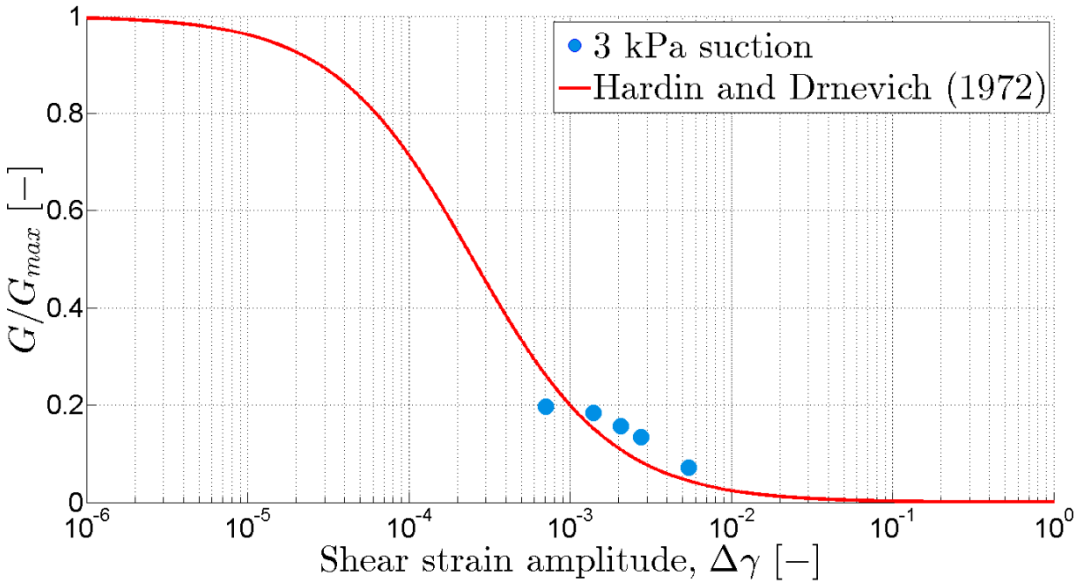

Figure 70 Normalized shear modulus versus shear strain amplitude for 3 kPa suction

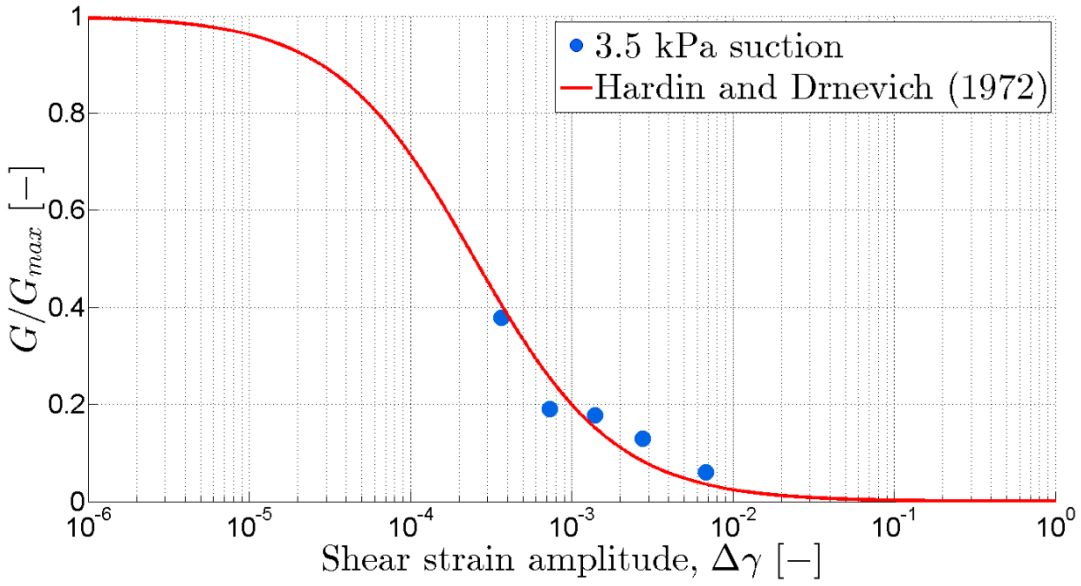

Figure 71 Normalized shear modulus versus shear strain amplitude for 3.5 kPa suction

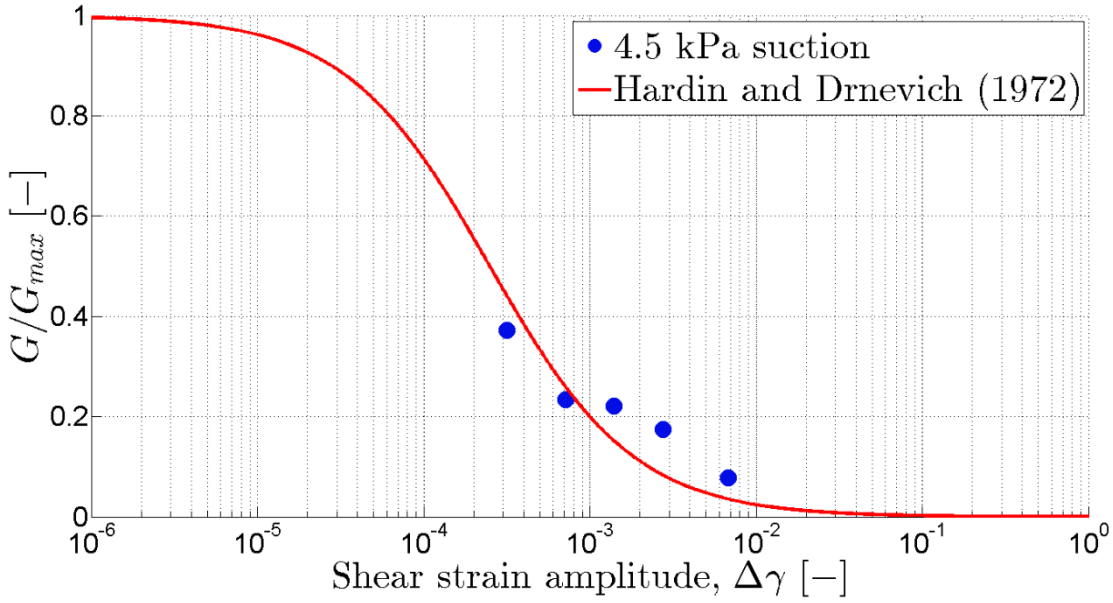

Figure 72 Normalized shear modulus versus shear strain amplitude for 4.5 kPa suction

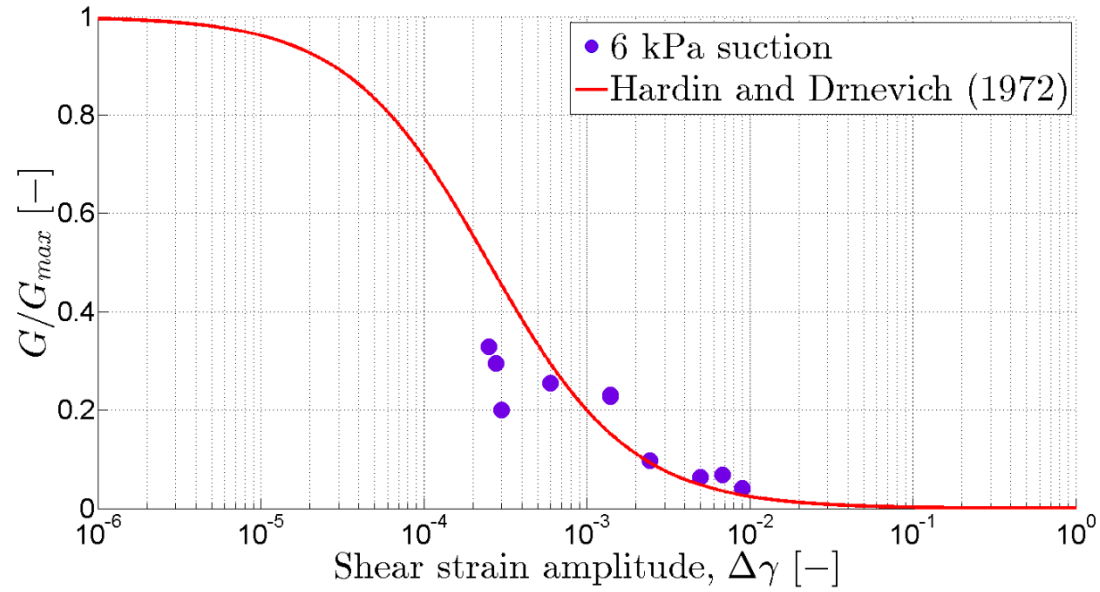

Figure 73 Normalized shear modulus versus shear strain amplitude for 6 kPa suction

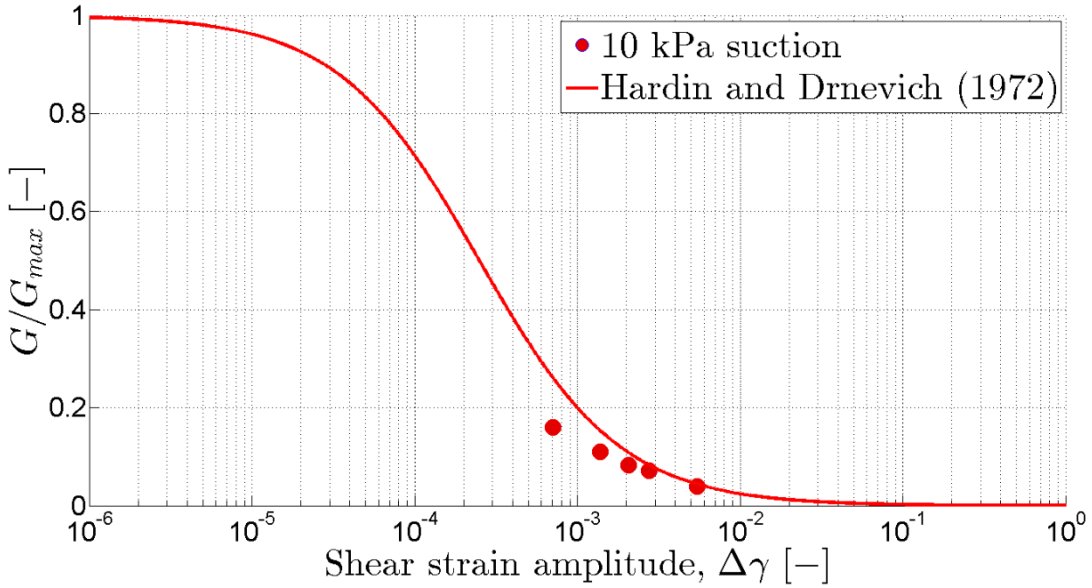

Figure 74 Normalized shear modulus versus shear strain amplitude for 10 kPa suction

Analyzing the general pattern of the measured values, one can notice that the shear modulus ratio data points are lower than the empirical relations under medium shear strain amplitudes regardless of the matric suction. Except for a few number of data points, the majority of shear modulus ratios fall nicely inside the expected shear modulus reduction band. Possible desaturation of the system under high suction range could affect the results in high suction range. Also, because of the difficulties to maintain constant negative pore pressure that are discussed in the beginning of this chapter, the response of soil specimens sometimes does not match the expected shear modulus reduction trend. Figure 76 summarizes all shear modulus reduction ratios for various degrees of saturation on one plot.

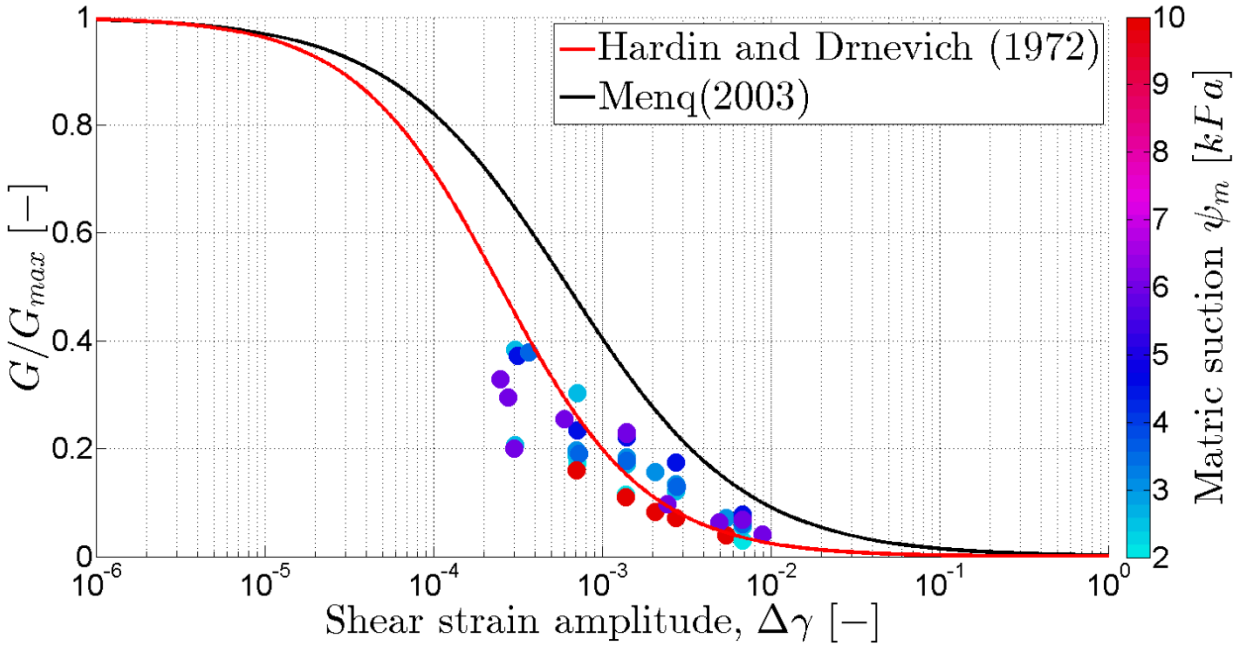

Figure 75 Normalized shear modulus versus shear strain amplitude with respect to matric suction

To show the changes in dynamic soil properties for different levels of saturation, shear modulus variation was plotted against various levels of saturation for different axial strain amplitudes. Figure 76, 77, 78, and 79 show the variation of shear modulus with respect to suction for strain amplitudes of 0.05%, 0.1%, 0.2%, and 0.5%, respectively. Ignoring the out of the ordinary data points, one can notice a general trend in the data. Typically specimens with mid-level suction levels have the highest modulus. Getting closer to fully saturated condition or residual suction values resulted in a decrease in shear modulus.

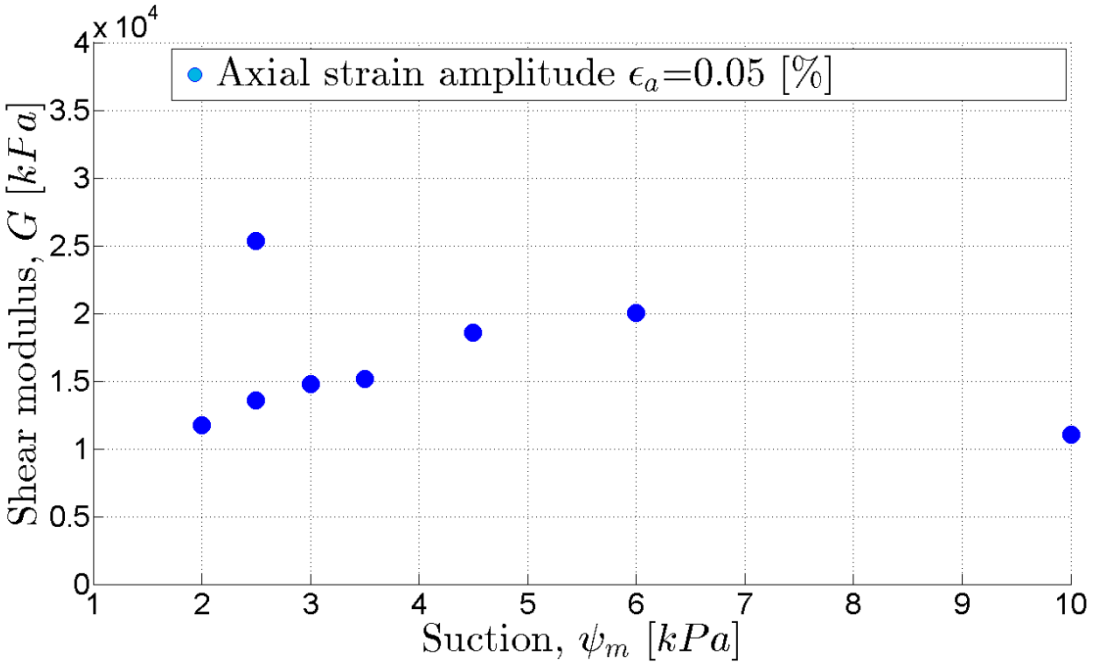

Figure 76 Shear modulus versus suction for 0.05% of axial strain amplitude

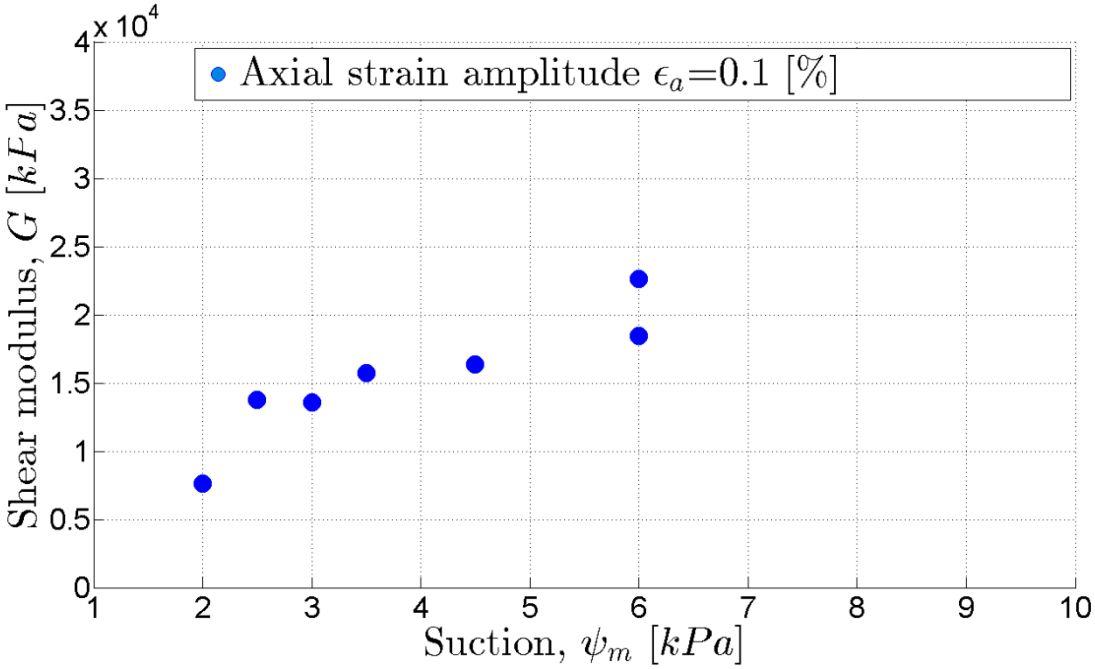

Figure 77 Shear modulus versus suction for 0.1% of axial strain amplitude

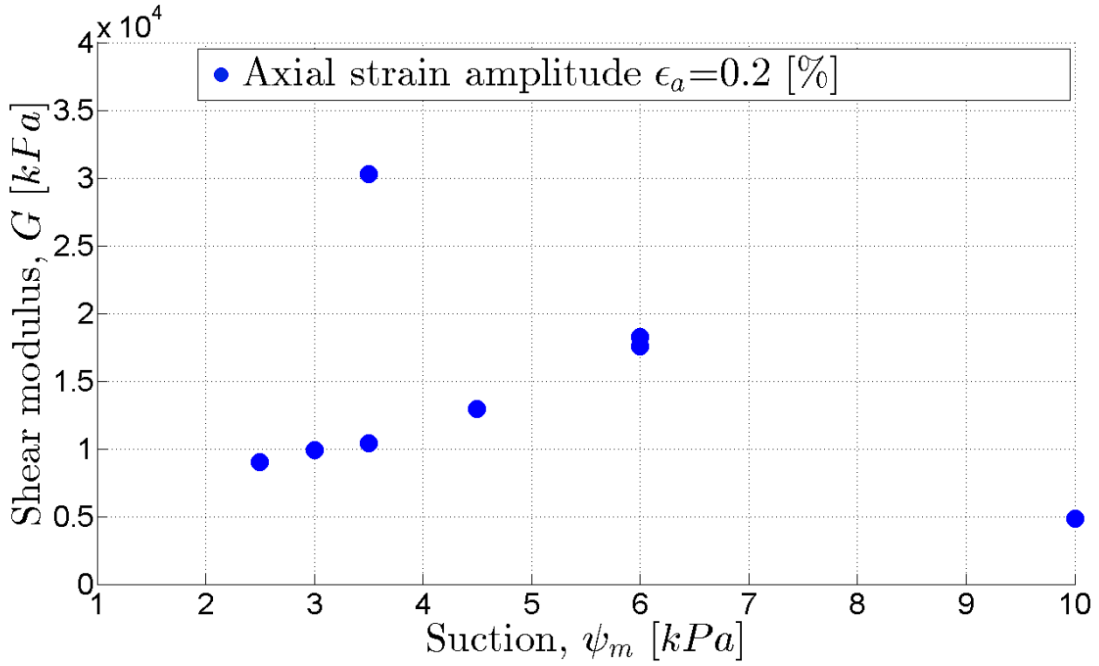

Figure 78 Shear modulus versus suction for 0.2% of axial strain amplitude

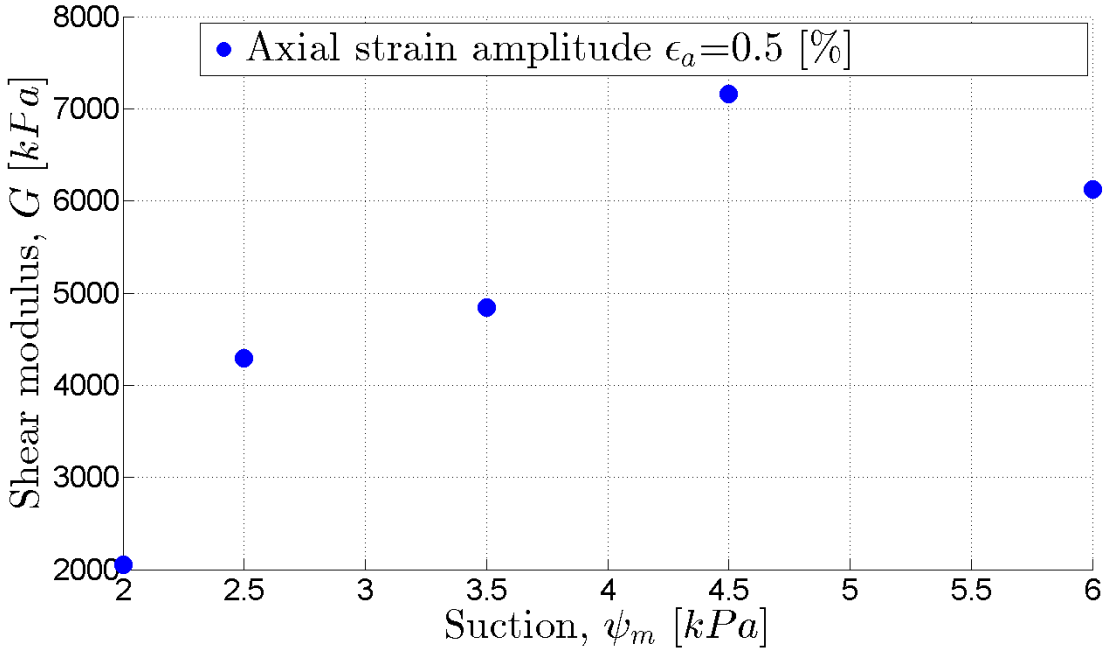

Figure 79 Shear modulus versus suction for 0.5% of axial strain amplitude

CHAPTER X. RESULTS: STRESS-CONTROLLED TESTS

In addition to strain-controlled tests, a set of stress-controlled tests were performed on dry and unsaturated soil samples. The main objective of these tests was to compare the results with strain-controlled tests presented in Chapter 7, 8 and 9 and investigate the advantages, disadvantages and consistency of the data.

Specimen preparation method was kept the same for the entire set of the tests as described in Chapter 7. Prior to the application of cyclic loading, all specimens were subjected to 50 kPa seating deviator stresses to avoid tension during stress reversals. It is expected that stress-controlled dynamic loading provides with a more representative behavior of soil properties, as it is based on the actual soil resistance. In order to study the soil dynamic properties stress-strain hysteresis loops were formed; e.g. Figure 80.

Analyzing the stress versus strain hysteresis loops, Young's moduli were calculated and plotted against amplitudes of axial strain in Figures 81,82,83,84 and 85. Further, shear modulus values were plotted against shear strain for the specimens with different matric suction values, as shown in Figures 86,87,88,89 and 90. Similar to the previous section and for a better visualization of shear modulus reduction trend, G/G_{max} was plotted for different suction levels separately. Most of the measured shear modulus ratios fell inside the shear modulus reduction band, which is consistent with what was observed in strain-controlled tests.

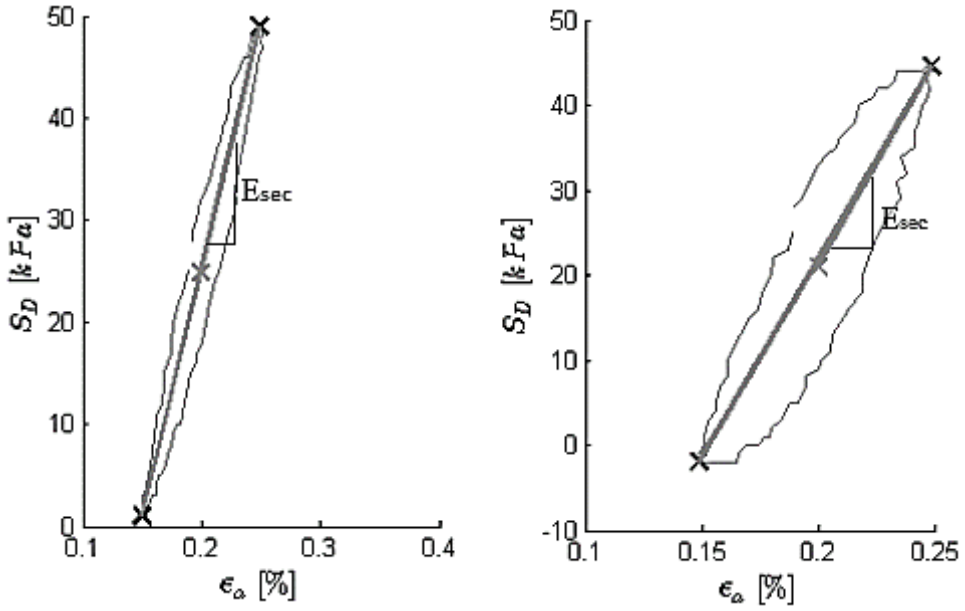

(a) (b)

Figure 80 Dynamic Hysteresis Loop for a) unsaturated; b) saturated soil

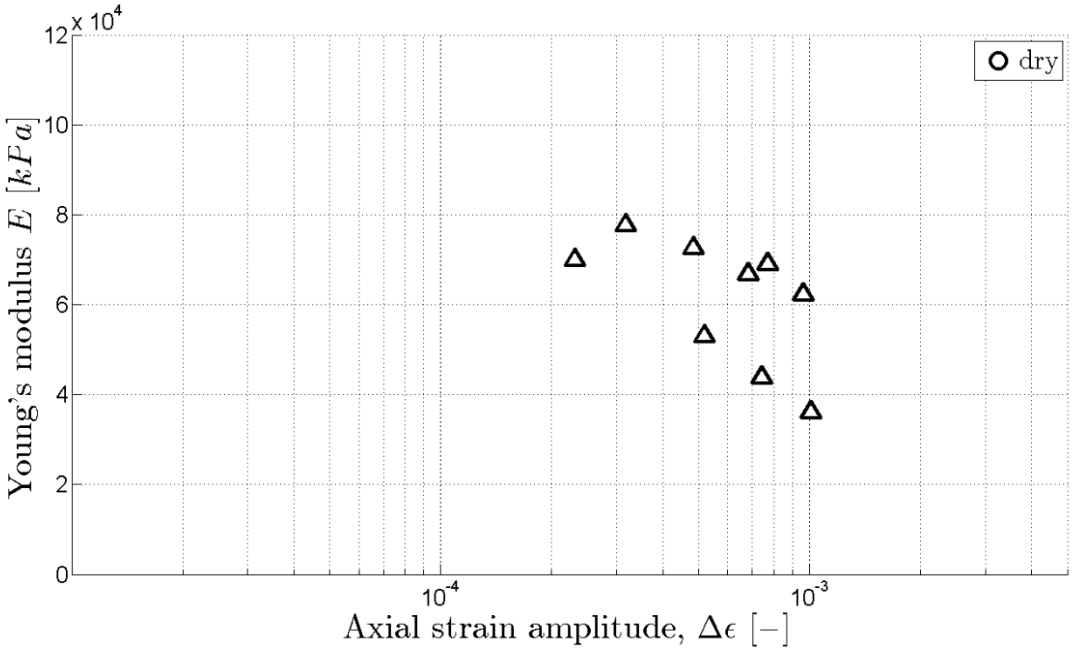

Figure 81 Young's modulus versus axial strain for dry stress controlled tests

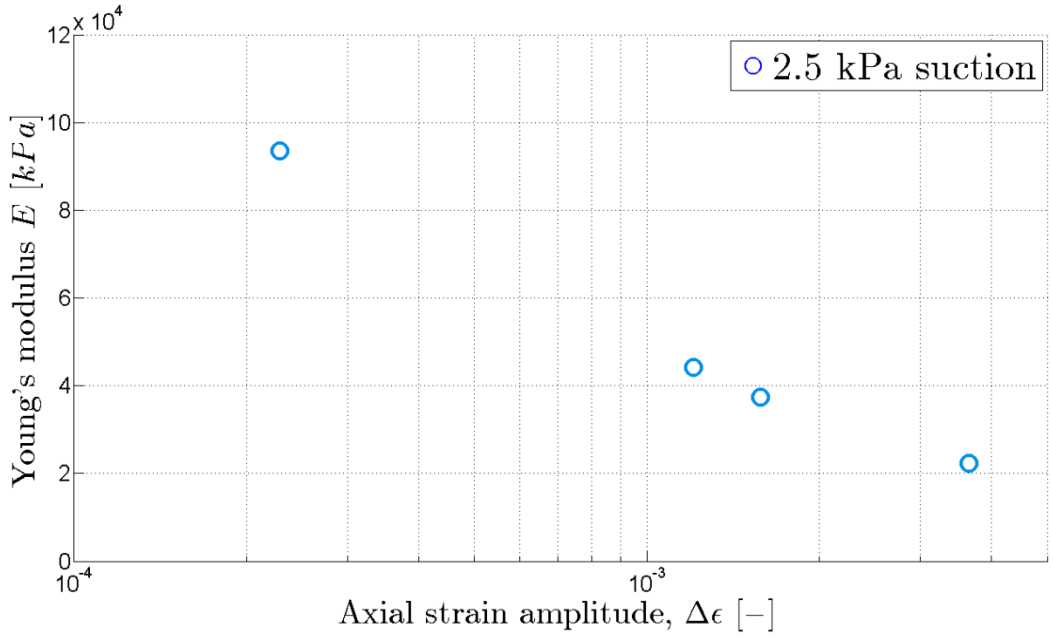

Figure 82 Young's modulus versus axial strain for specimens with 2.5 kPa matric suction

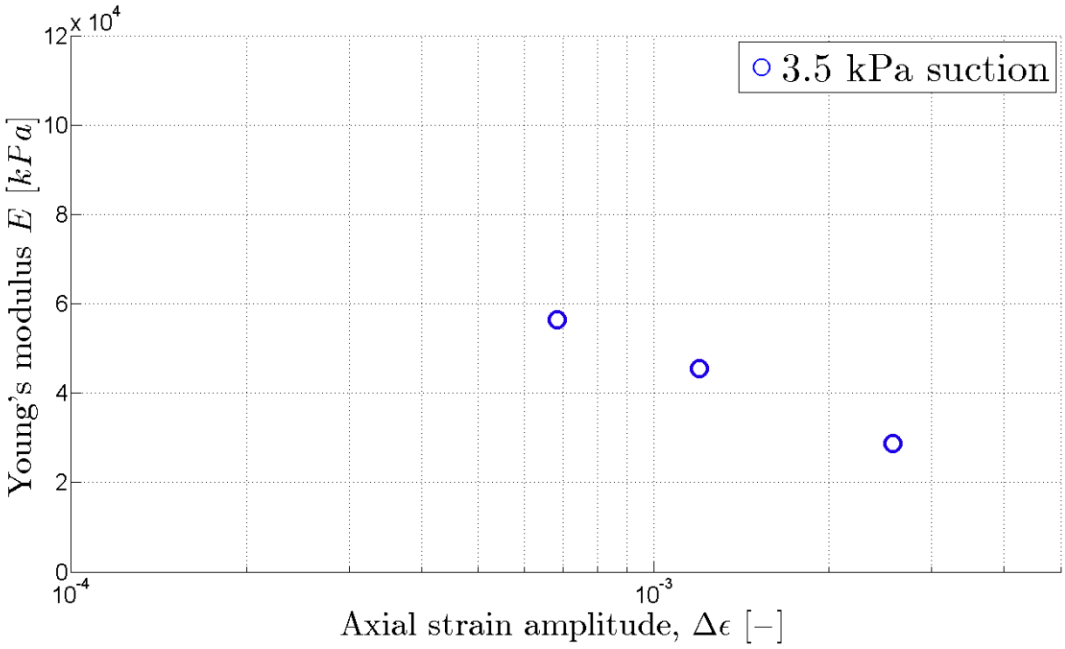

Figure 83 Young's modulus versus axial strain for specimens with 3.5 matric suction

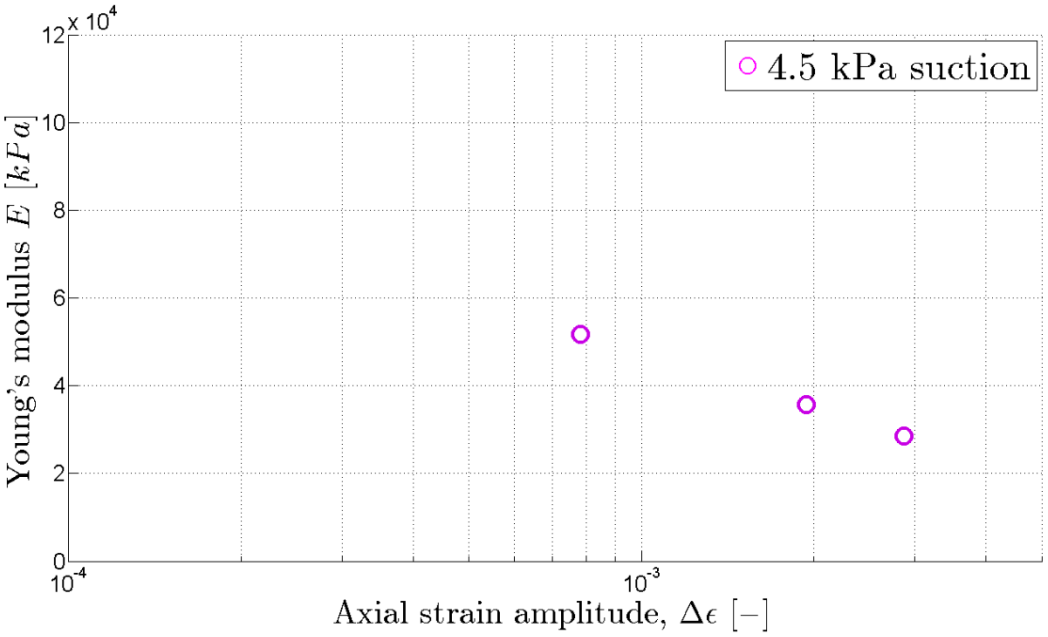

Figure 84 Young's modulus versus axial strain for specimens with 4.5 matric suction

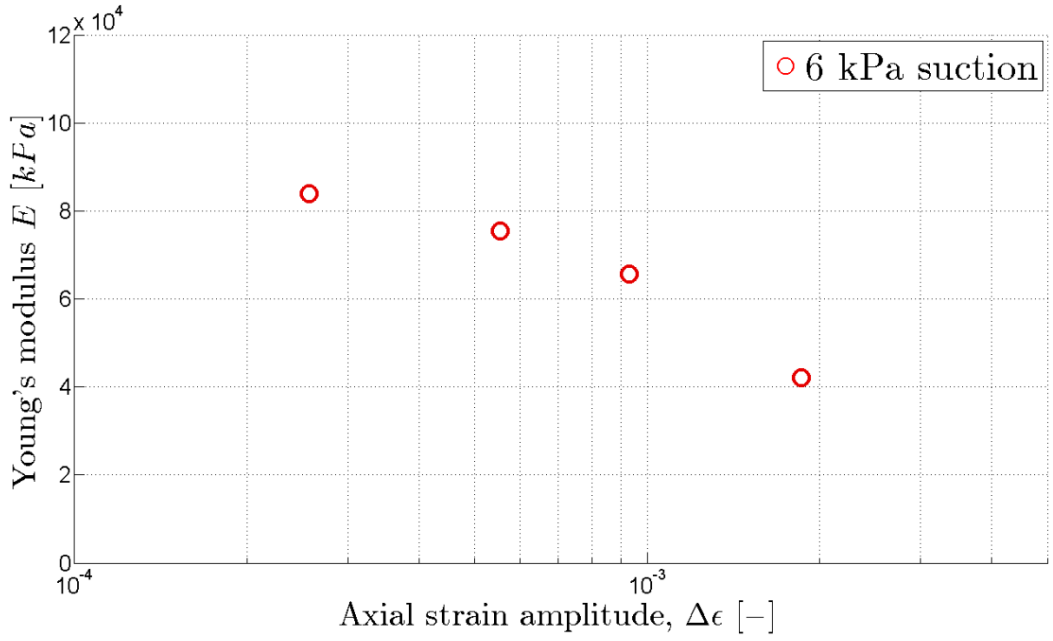

Figure 85 Young's modulus versus axial strain for specimens with 6 kPa matric suction

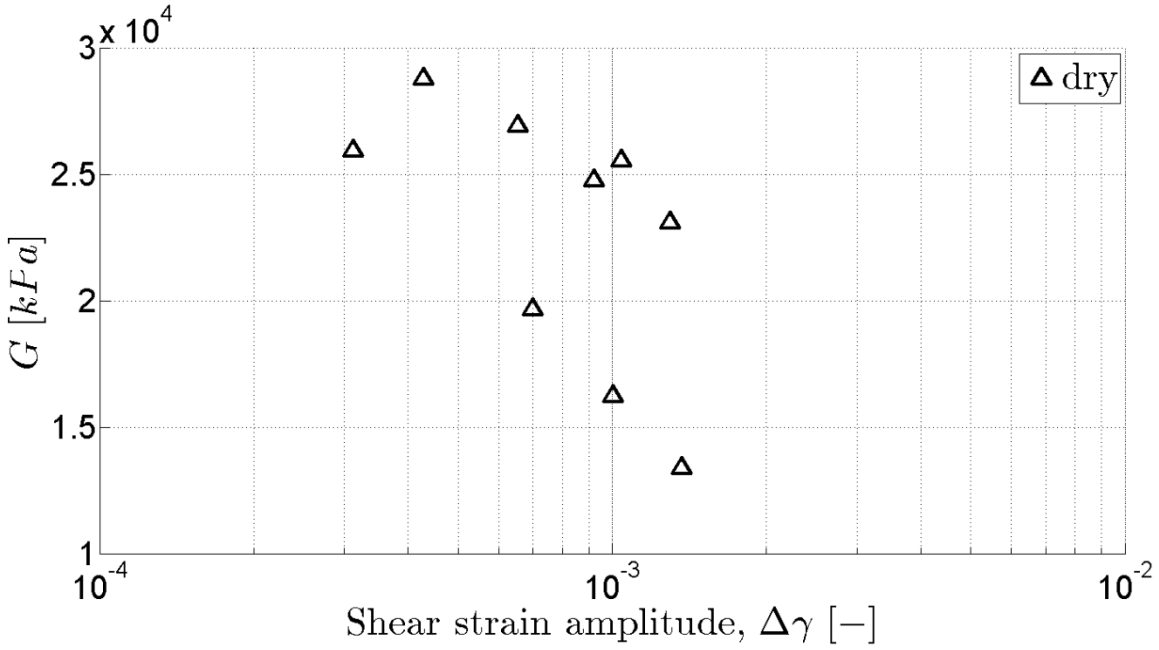

Figure 86 Shear modulus versus shear strain for dry specimens under stress controlled dynamic loading

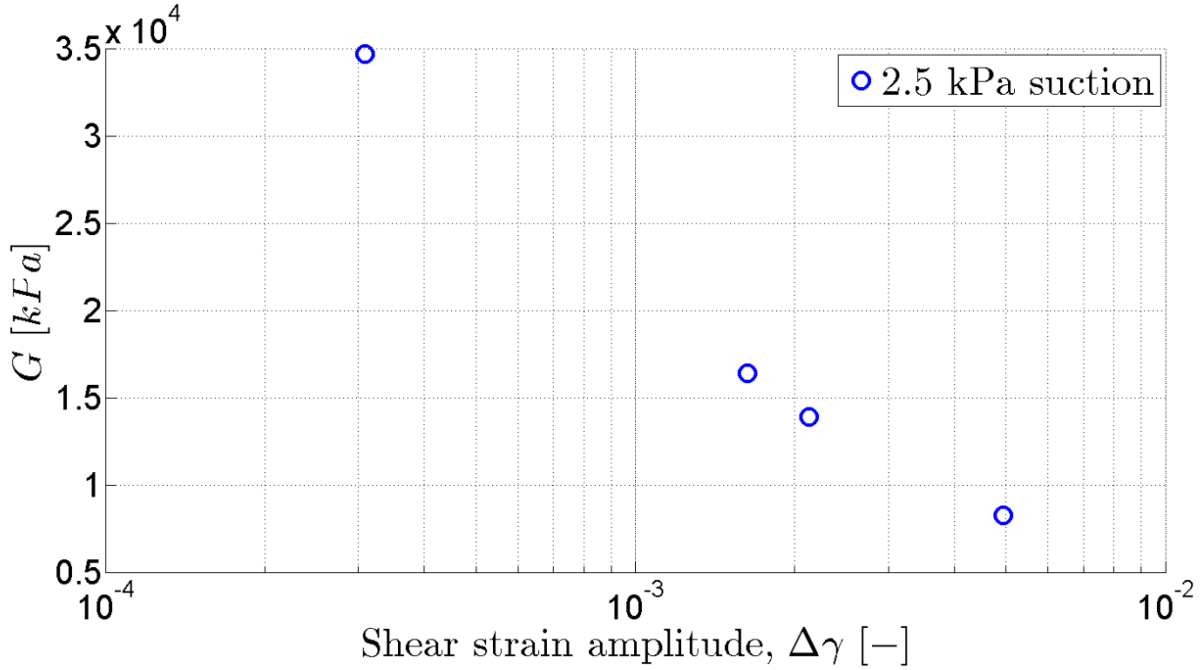

Figure 87 Shear modulus versus shear strain for specimens with 2.5 kPa matric suction under stress controlled dynamic loading

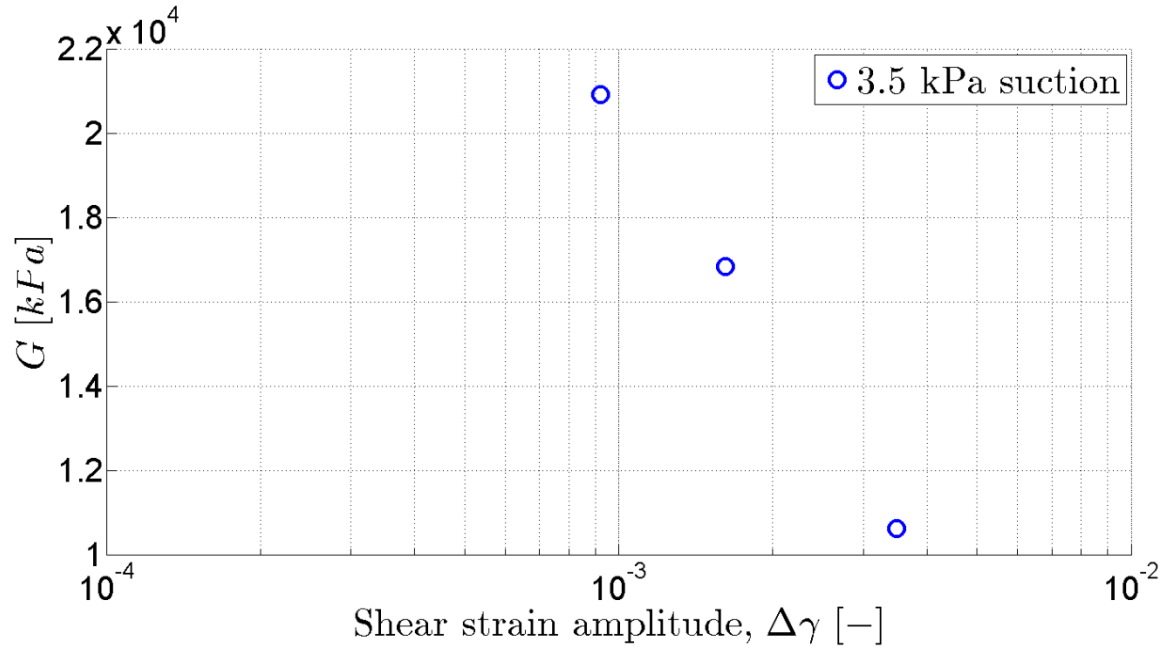

Figure 88 Shear modulus versus shear strain for specimens with 3.5 kPa matric suction under stress controlled dynamic loading

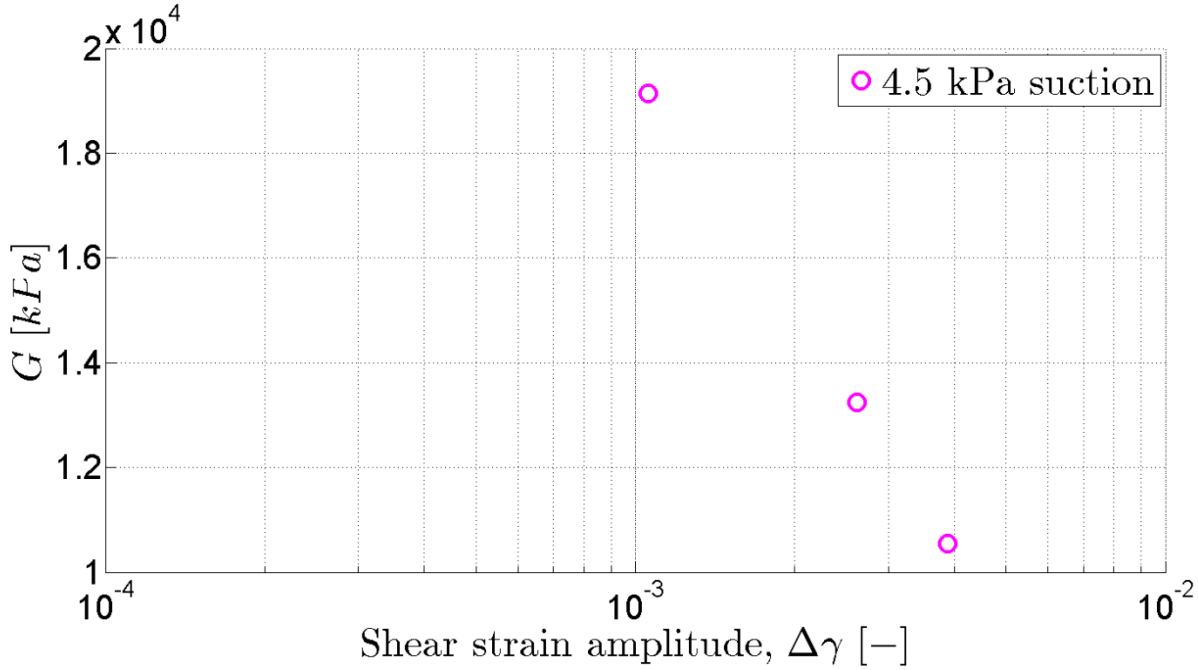

Figure 89 Shear modulus versus shear strain for specimens with 4.5 kPa matric suction under stress controlled dynamic loading

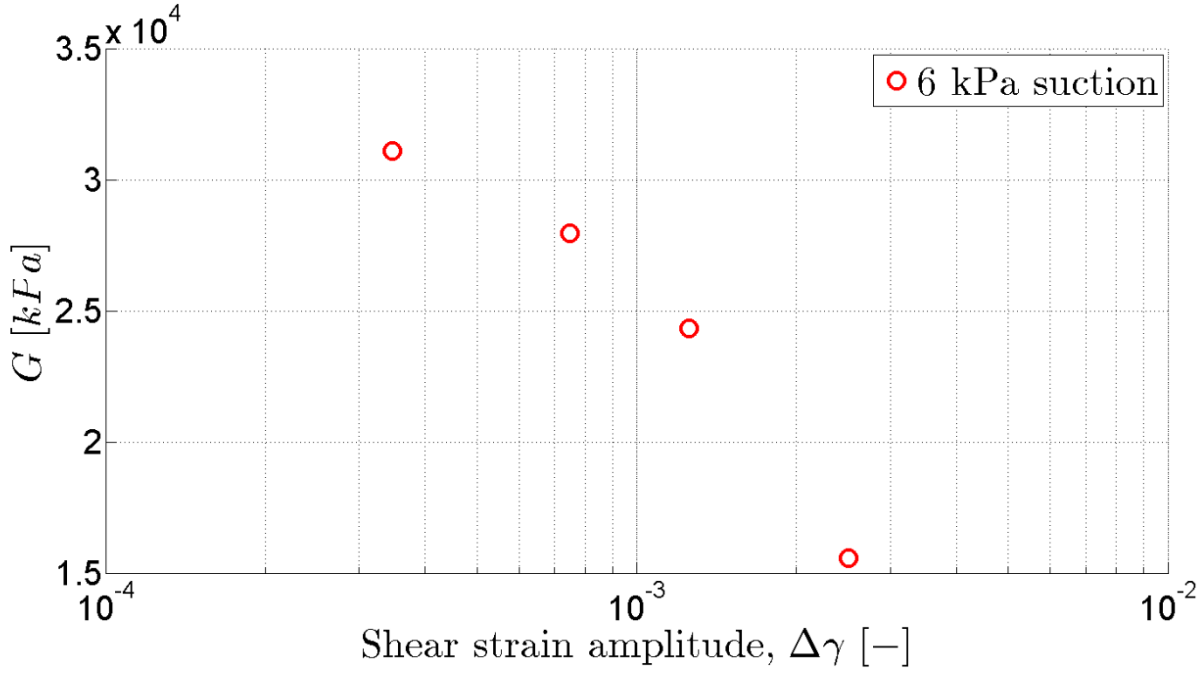

Figure 90 Shear modulus versus shear strain for specimens with 6 kPa matric suction under stress controlled dynamic loading

To summarize the results, all the acceptable data points for stress controlled cyclic triaxial tests were plotted in the Figure 91. The general trend aligns well with the curves based on empirical relations.

Analyzing the loops of stress-controlled test, the decrease of the slope (Young's modulus) within the test is much lower than for strain-controlled test. Therefore, it yielded in higher average modulus values that were taken for calculation of shear modulus. Typical loops with corresponding Young's modulus values are presented in Figure 91.

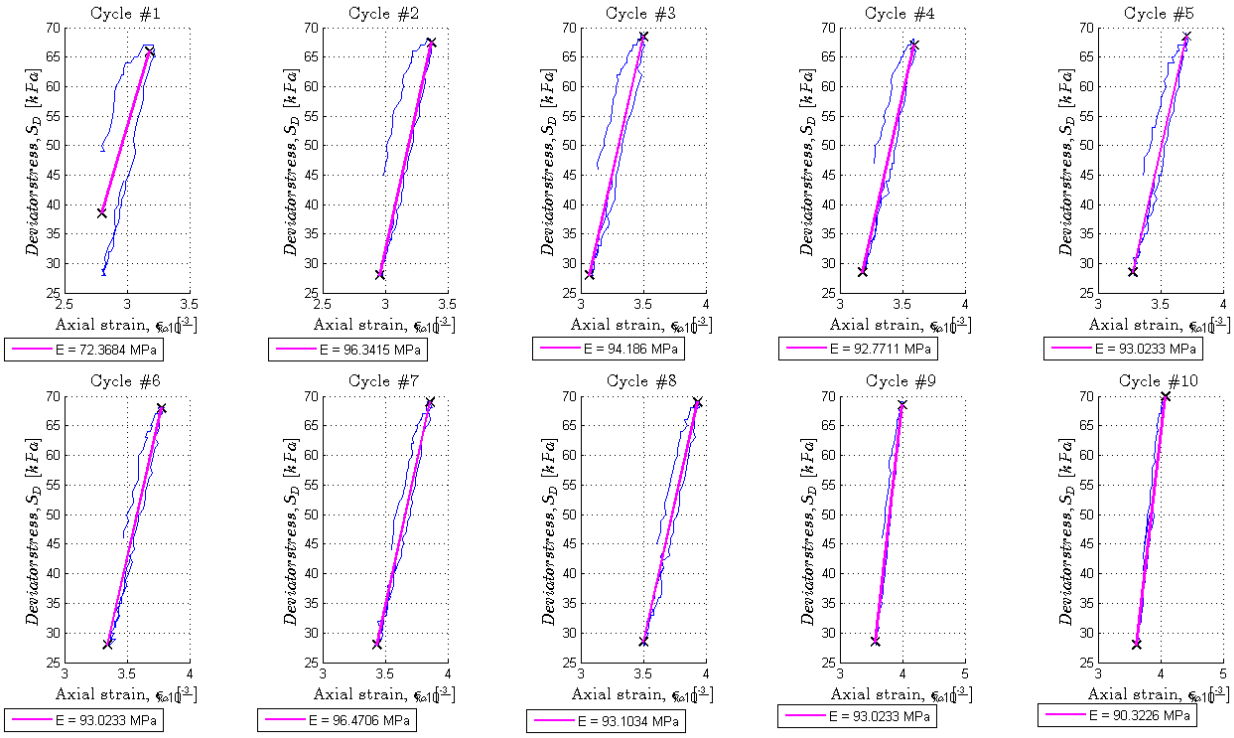

Figure 91 Young's modulus values for different cycles of the stress-controlled test

In addition, in order to revisit the effect of suction on the shear modulus the variation of modulus with suction was investigated, as shown in Figure 92 and 93. Again, an increasing trend in modulus in higher suction up to a certain suction level is noticeable.

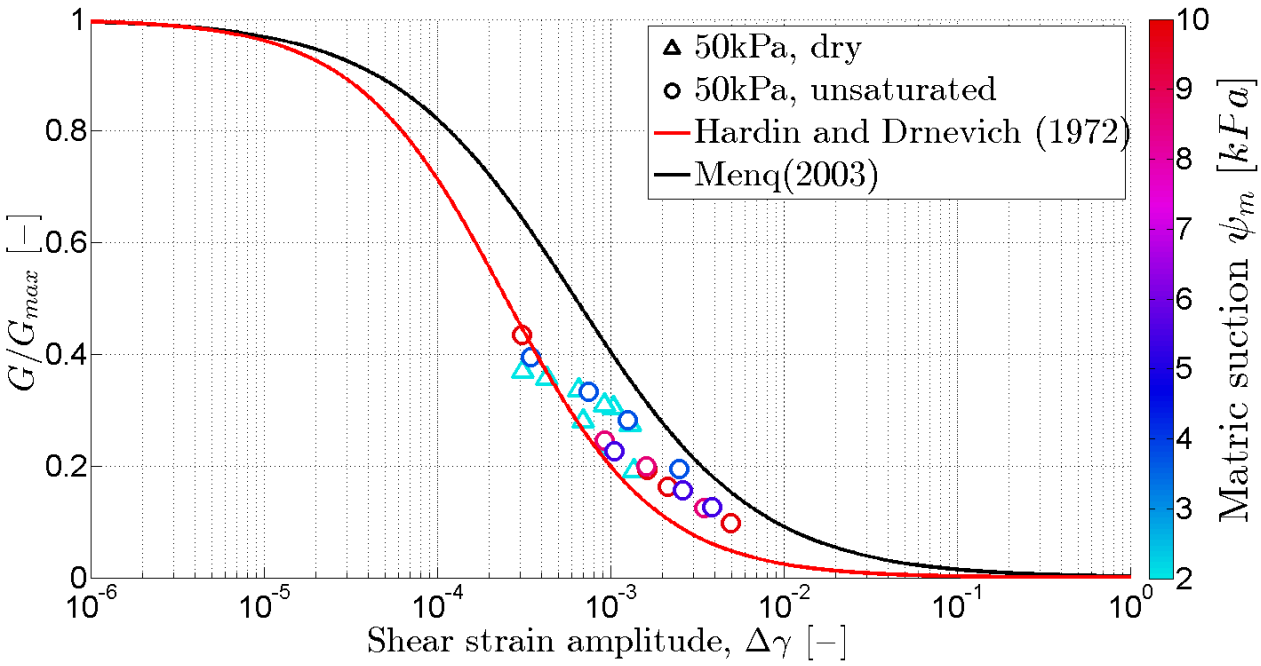

Figure 92 Shear modulus reduction curve for dry and unsaturated soil under cyclic stress application

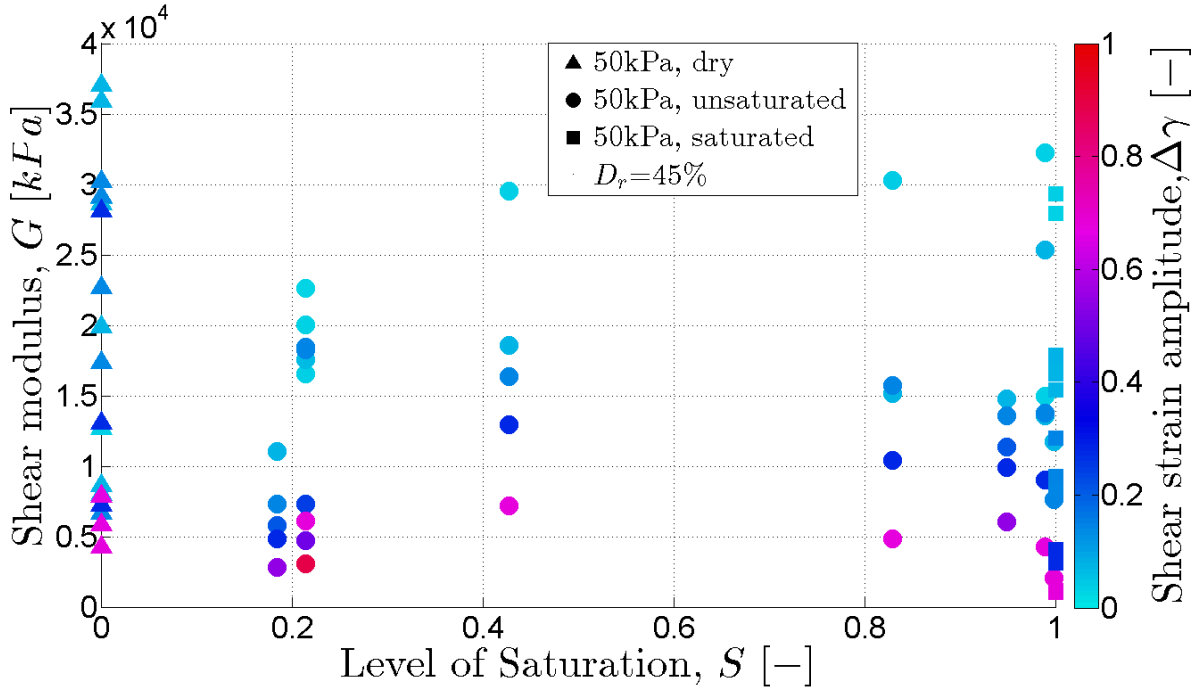

Figure 93 Shear modulus for soils with different levels of saturation

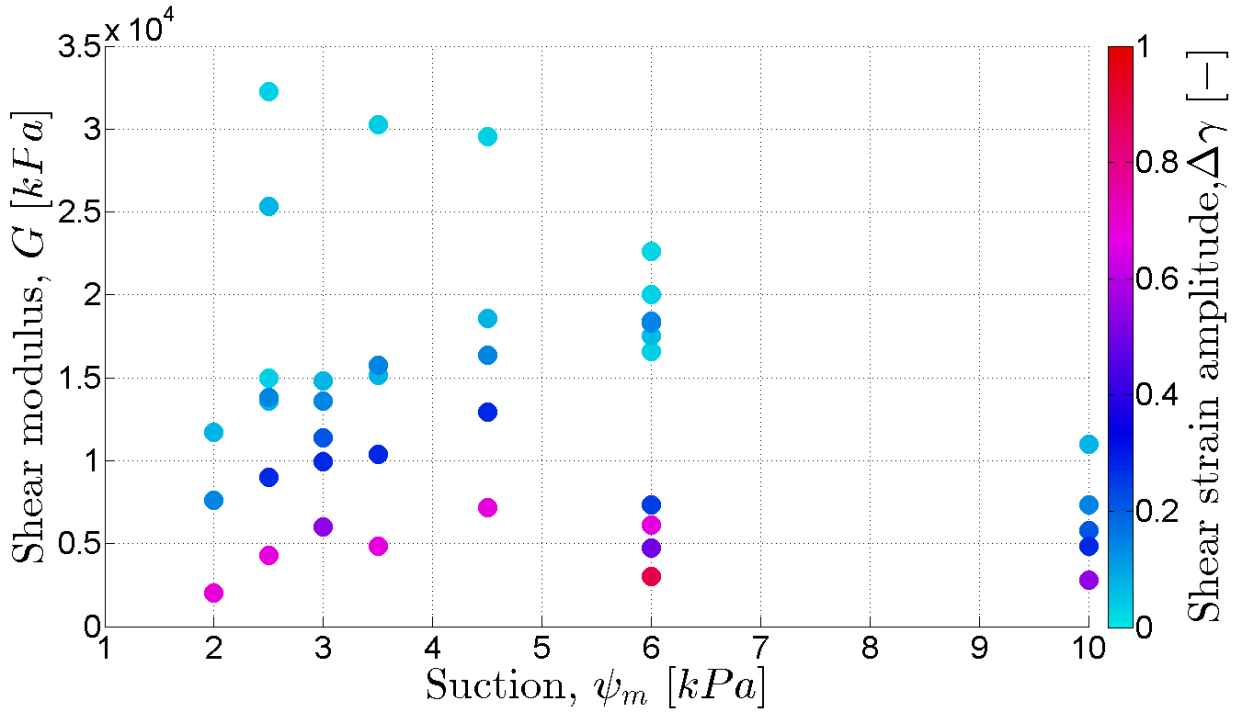

Figure 94 Shear modulus for unsaturated soil under dynamic loading

CHAPTER XI. DISCUSSION AND DATA SUMMARY

The main objective of this study was to investigate the dynamic modulus of sandy soils with different degrees of saturation and induced shear strain levels. In addition to that, the tests were repeated for both stress- and strain- controlled cyclic loading to understand the variation of results based on the control conditions. First, to better understand the consistency of the measured shear modulus with the state-of-the-practice, shear modulus reduction plots containing all data points for different saturation conditions but 50 kPa confining pressure and the accepted empirical relations were formed, as shown in Figure 95. It can be seen from the figure that the general response of the soil is following the predicted trend. Dry, saturated, and unsaturated tests all align with the shear modulus reduction curve with acceptable variation, which confirms the validity of the measured data. The applicability of standard shear modulus reduction equations for soils with various degrees of saturation is very valuable. Accordingly, shear modulus decreases by increasing the induced shear strain. However, this is with the assumption that the calculated effective stress is used correctly and consistently for unsaturated, saturated, and dry soils. However, special attention was required during the specimen preparation, suction control, and loading that resulted in ruling out several tests.

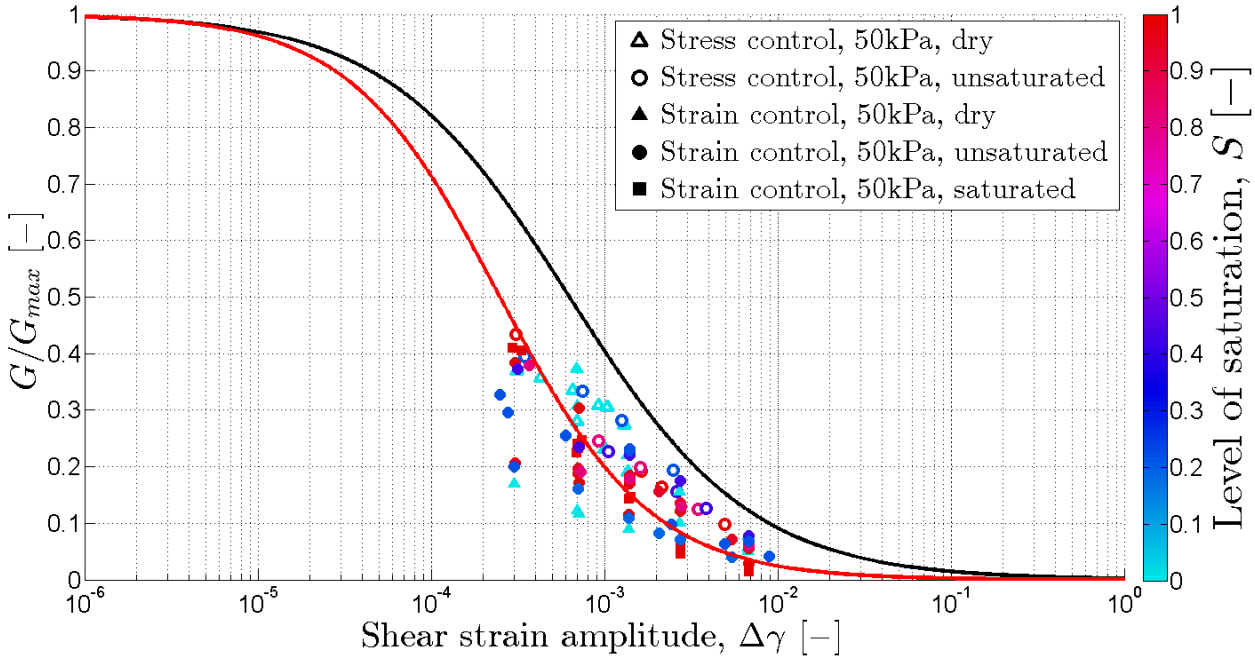

Figure 95 Shear modulus reduction curve for all the tests

To study the effect of the degree of saturation on dynamic shear modulus, all the measured modulus values for a certain strain level but different degrees of saturation were compared. Figures 96, 97, 98, and 99 show the variation of modulus from strain-controlled tests with respect to the degree of saturation for 0.05%, 0.1%, 0.2%, and 0.5% axial strains, respectively. In addition, Figures 100, 101, and 102 show the variation of modulus from stress-controlled tests with respect to the degree of saturation for 40, 60, and 80% deviator stress, respectively. In general, soils in mid-range degrees of saturation resulted in higher shear modulus values. However, some data points do not follow this general trend. For example tests on dry and saturated sands with 0.05% axial strain show a different pattern. Also, in stress-controlled tests the modulus for very low degrees of saturation are very erratic.

The general increase in mid- to large-strain shear modulus of soils by increasing suction is consistent with reported pattern for small-strain shear modulus in the literature. This is attributed to higher effective stress in midrange degrees of saturation as a result of inter-particle suction stresses. Changes in suction stress for different saturation levels were calculated using Equation 32, and shown in Figure 103. In addition, by looking at these data one can easily see the differences between the results from stress-controlled and strain-controlled tests. In most cases stress-controlled tests resulted in higher modulus values than that of strain-controlled tests. This can be described by the nature of the test as stress-controlled tests rely on the soil resistance while strain-controlled test control the deformation and only measure the mobilized stresses. In addition to that, the decrease of Young's modulus for stress-controlled tests was smaller comparing to strain-controlled tests as shown in Figure 91.

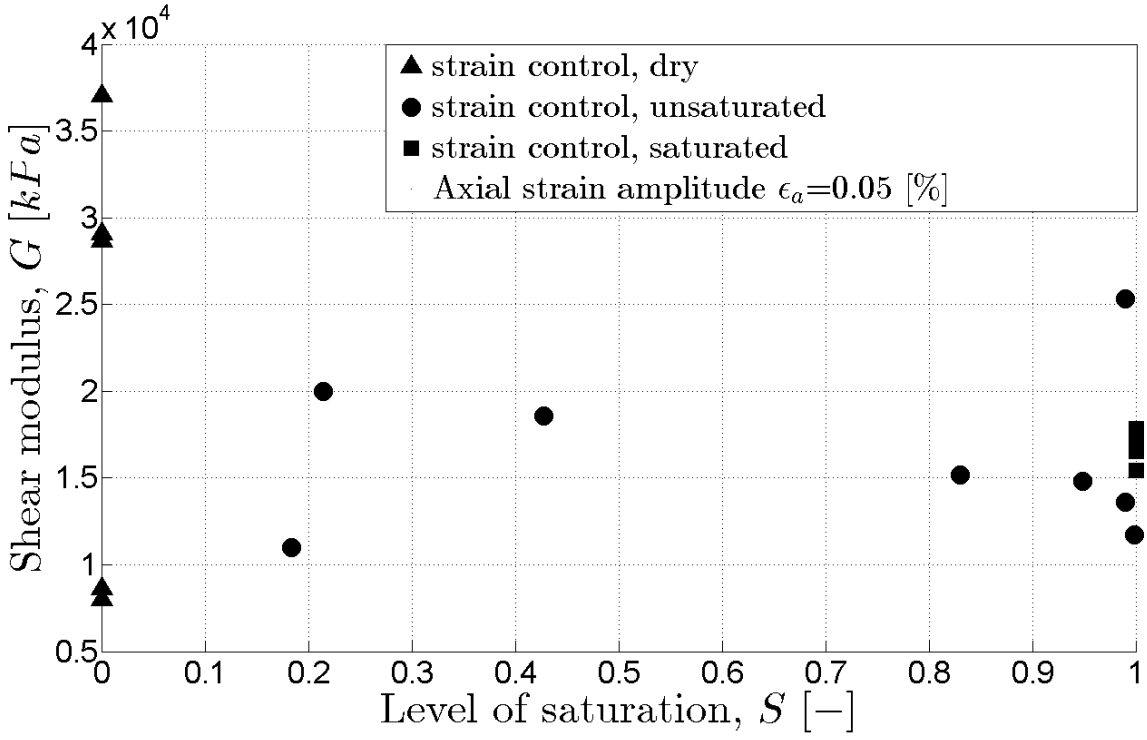

Figure 96 Shear modulus versus degree of saturation for 0.05%of axial strain

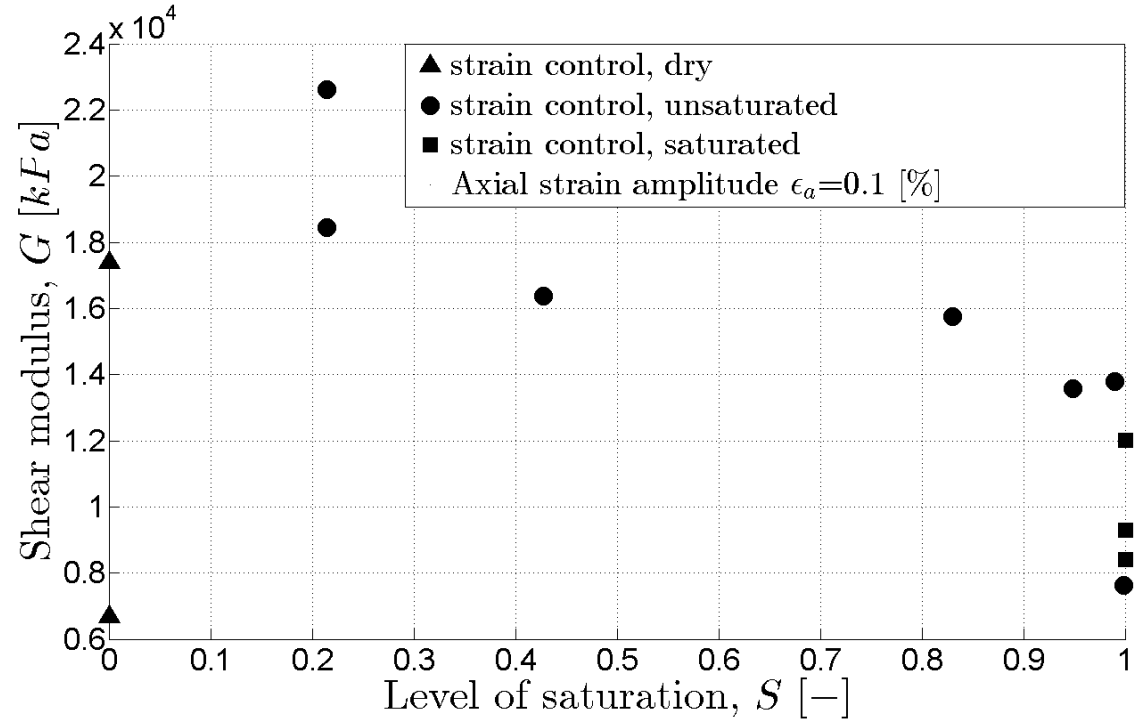

Figure 97 Shear modulus versus degree of saturation for 0.1%of axial strain

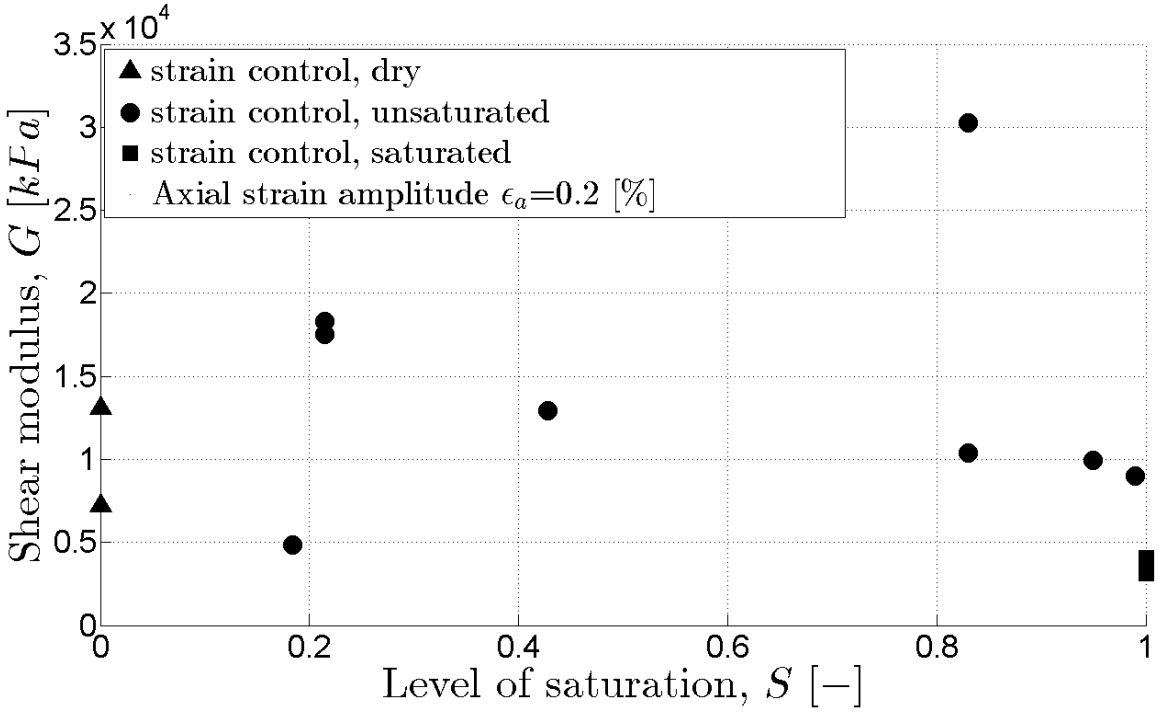

Figure 98 Shear modulus versus degree of saturation for 0.2%of axial strain

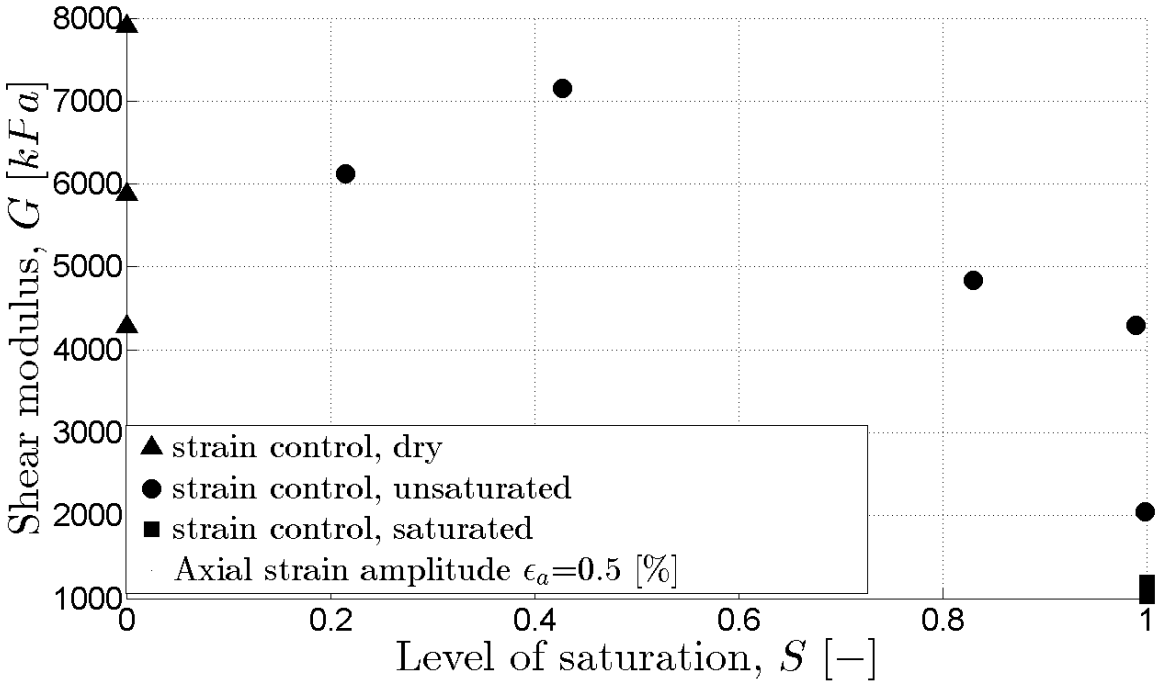

Figure 99 Shear modulus versus degree of saturation for 0.5%of axial strain

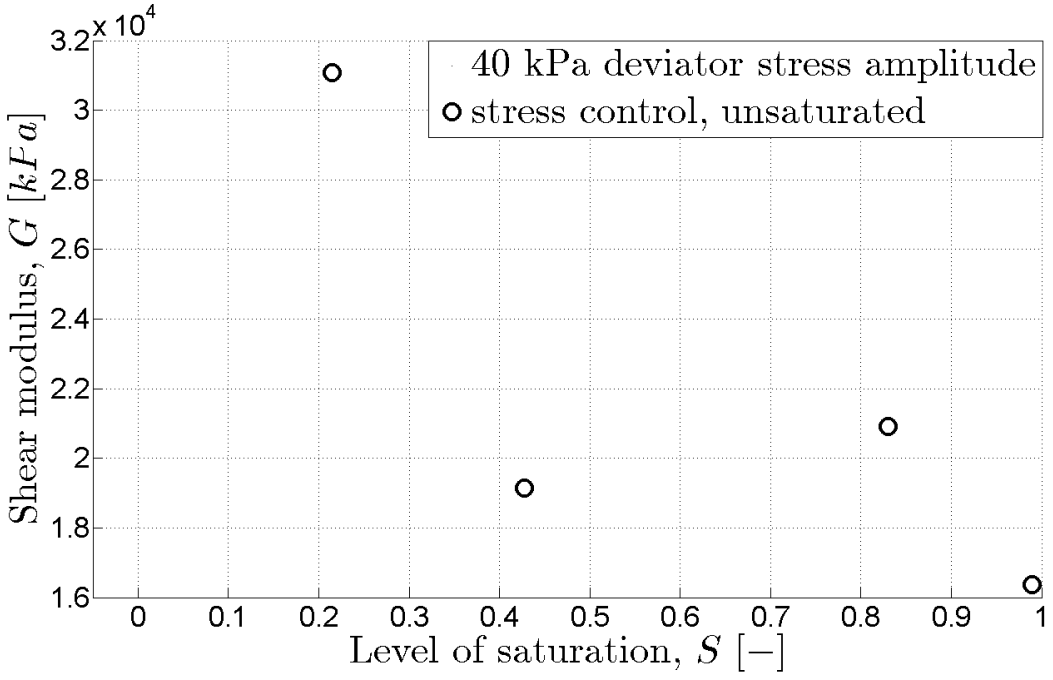

Figure 100 Shear modulus versus degree of saturation for 40 kPa deviator stress amplitude

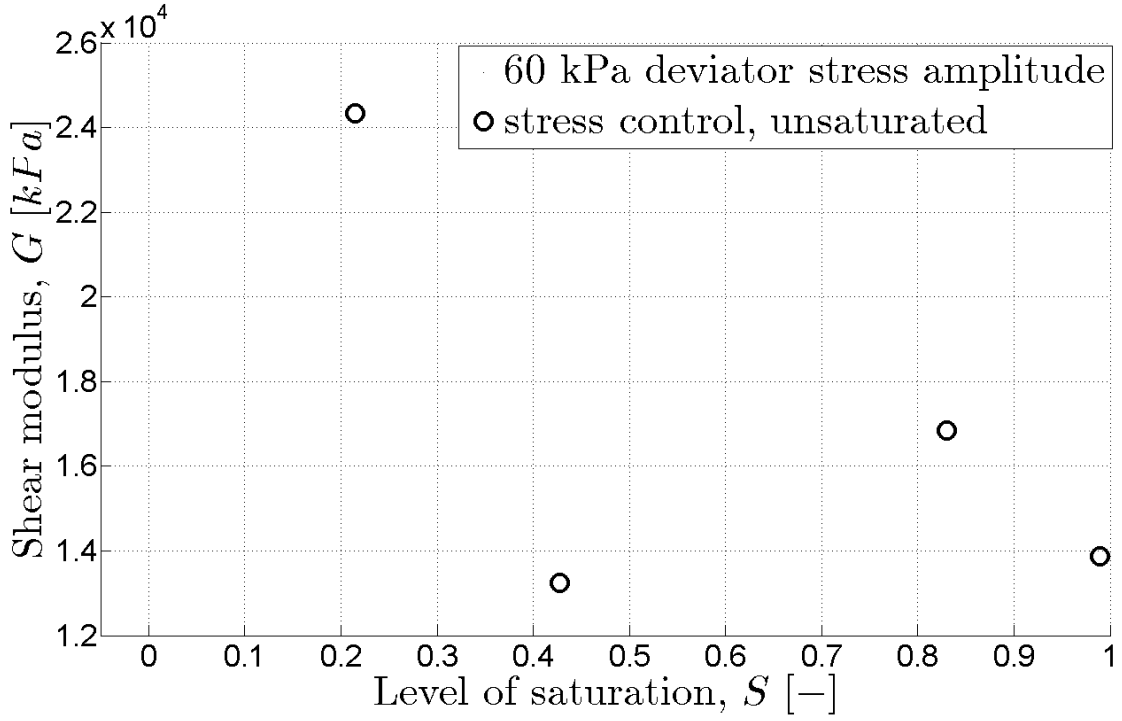

Figure 101 Shear modulus versus degree of saturation for 60 kPa deviator stress amplitude

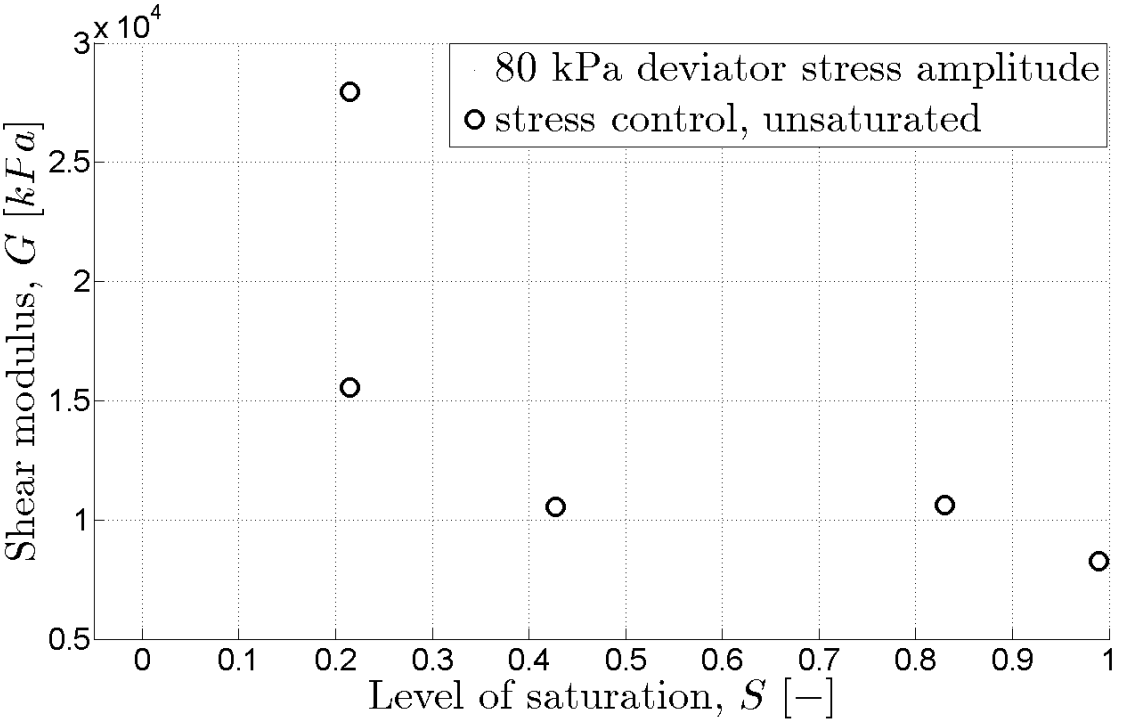

Figure 102 Shear modulus versus degree of saturation for 80 kPa deviator stress amplitude

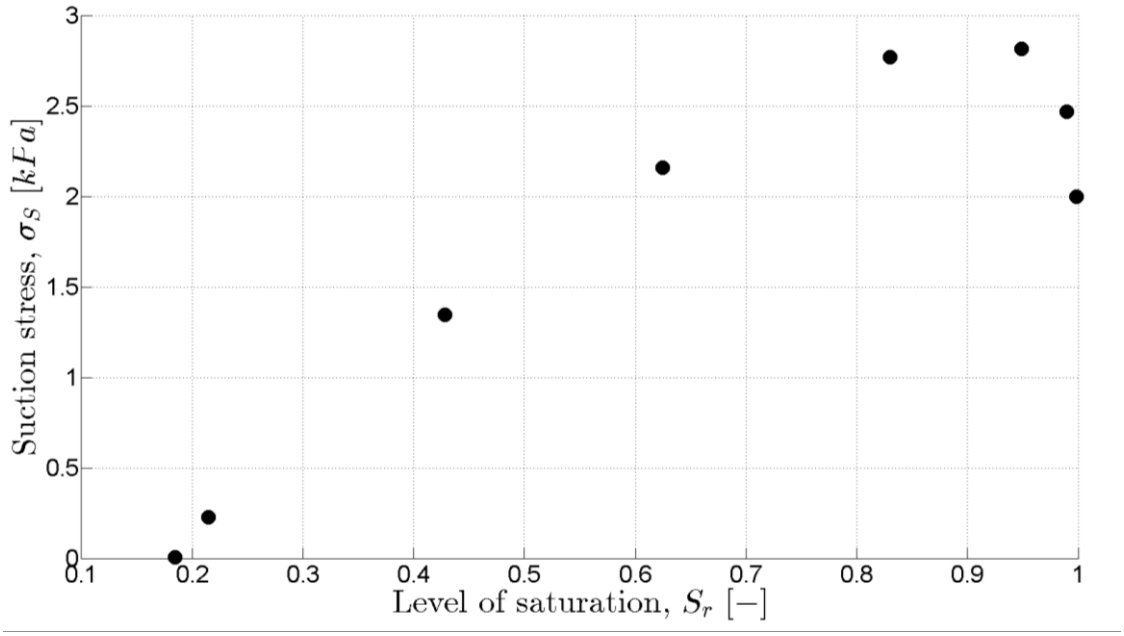

Figure 103 Suction stress versus different degrees of saturation

Some test loops for dry and unsaturated tests were not symmetrical that resulted in a lower value of Young's modulus. The reason could be uneven distribution of pressure on a soil specimen, because of the imperfect alignment of the top platen that transfers the load from the load cell to the top of the specimen. On the other hand, discontinuity of the water phase in the soil specimen could change the results of unsaturated soil tests. There could be other reasons as well, and this phenomenon should be considered in further investigation. Test loops for both dry and unsaturated tests are presented in Figure 104 and 105, respectively.

To be consistent with all calculations in this research, the slope was taken from peak to peak of the loop, but taking a slope of the compression part of the loop will provide with higher values of Young's modulus. The compression part was taken from the initial point of the test to the peak of the loop.

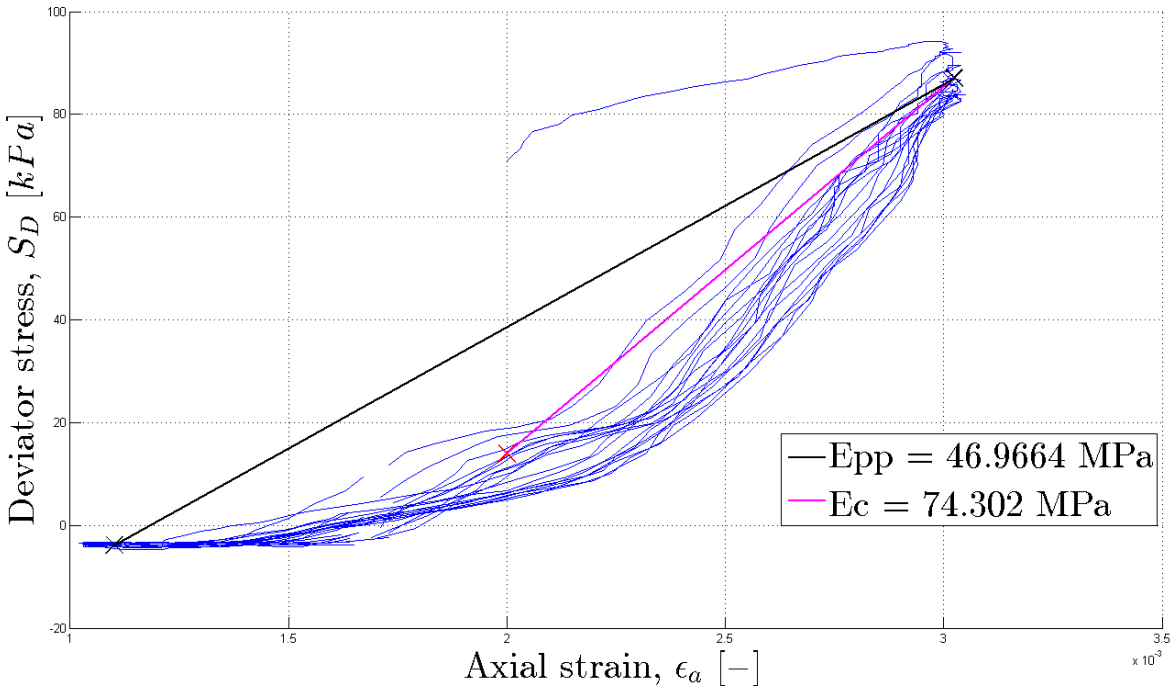

Figure 104 Different methods for determination of Young's modulus for dry specimen

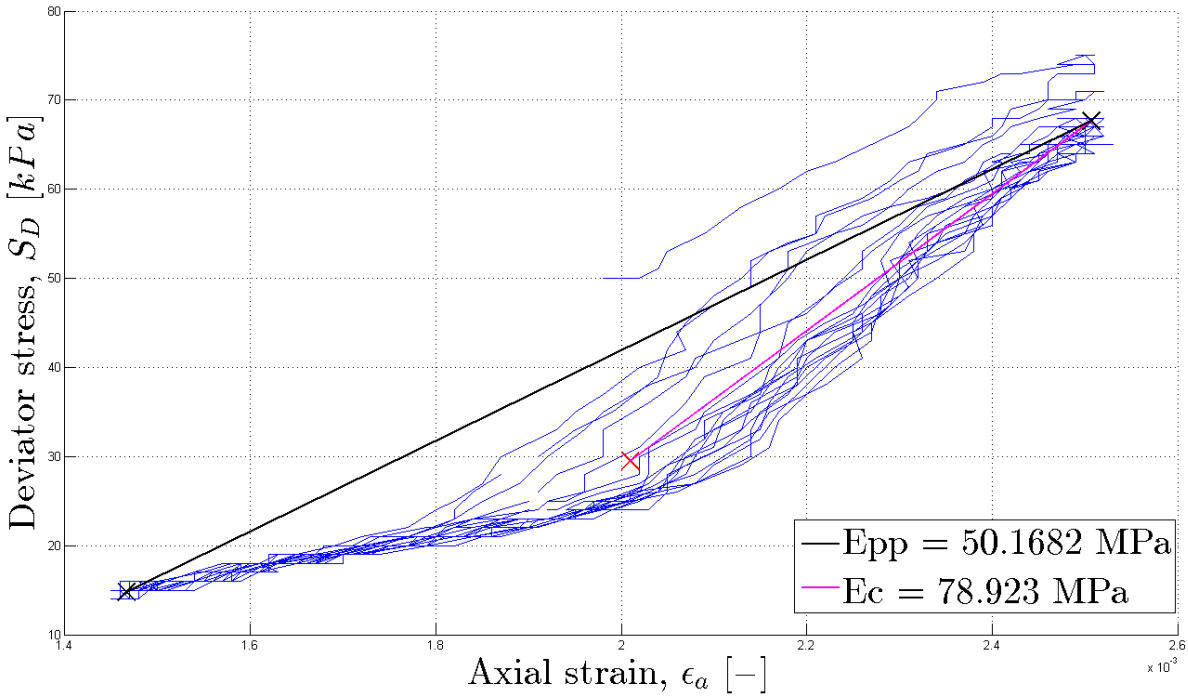

Figure 105 Different methods for determination of Young's modulus for unsaturated specimen

CHAPTER XII CONCLUSIONS AND FUTURE RESEARCH

12.1 Conclusions

- Suction-controlled dynamic triaxial system was successfully developed and used to measure dynamic shear modulus of soils.
- Tests on dry, saturated, and unsaturated soils consistently showed that increasing the shear strain will reduce the shear modulus.
- The measured data were approximately close to the predicted values from the state-of-the-practice shear modulus reduction equations. However, for consistent results in various degrees of saturation, the effective stress in unsaturated soils must be calculated based on Bishop's formula.
- Increasing the confining pressure increased the shear modulus of dry sand proportional to half power of the effective stress.
- Increasing the suction from zero at fully saturated condition resulted in shear modulus. However, by further increasing the suction towards the residual suction, the modulus decreased predicting a peak modulus at middle-range degree of saturation.
- Stress-controlled tests mostly led to higher values of shear modulus comparing to strain-controlled tests. As it has been stated before, the method relies on the resistance of the soil, not on the deformation. External Linear Variable Differential Transformer (LVDT) is placed on the load frame and measures the displacement of the loading bar.

- System performance and unit stability plays a vital role in accuracy of the final results. To this end, continuous calibration of the system, cleaning the residue left in the connections and the tanks, and precise performance of the tests are very critical to the success of the project.

12.2 Recommendations for future research

- Improving the pressure control system is certainly the main improvement that one can do in order to advance this research. Although, the tests were performed in "drained condition", still excess pore pressure was developed. This was more significant percentage-wise for unsaturated soil. Increasing the air pressure and water pressure, keep the difference (suction) the same, would resolve this issue.
- One of the biggest difficulties in data analysis was combining values from the Flow Pump and GCTS data acquisition systems. It is recommended to unify those in order to eliminate human error and automate the test process.
- The connection between the loading bar and the specimen was designed and manufactured in the machine shop at the University of New Hampshire. The drawing is presented in the Appendix E. However, for future research this design should be improved to reduce time needed for alignment of 4 screws under the load cell of the triaxial system.
- A new algorithm for data analysis of non-symmetrical loops should be created to study the soil response in a more precise manner.
- Running the tests on Direct Simple Shear device would certainly provide us with more reliable data due to the direct measurement of stress and strain values. It also can serve to measure the seismic compression.

REFERENCES

ASTM D3999 “Standard Test Methods for the Determination of the Modulus and Damping Properties of Soils Using the Cyclic Triaxial Apparatus”

ASTM D4253 “Standard Test Method for Maximum Index Density and Unit Weight of Soils Using a Vibratory Table”.

ASTM D4254 “Standard Test Method for Minimum Index Density and Unit Weight of Soils and Calculation of Relative Density”

ASTM D5311/D5311M “Standard Test Method for Load Controlled Cyclic Triaxial Strength of Soil”

Bernier, F., G. Volckaert, E. Alonso, and M. Villar. "Suction-controlled Experiments on Boom Clay." Engineering Geology 47.4 (1997): 325-38. Web.

Bishop, A. W. "The Use of Pore-Pressure Coefficients in Practice." Géotechnique 4.4 (1954): 148-52.

Brooks, R. and Corey, A., (1964), “Hydraulic properties of Porous media,”

Christakos, “Soil behavior under dynamic loading conditions: experimental procedures and statistical trends”. Stochastic Environmental Research and Risk Assessment Vol. 17 Issue 3, p175 (2003).DOI 10.1007/so477-003-0132-x.Print

Cohesive Soils. Ph.D. Dissertation. University of Colorado, Boulder, Colorado State University, Fort Collins. Hydrology Paper No.

Darendeli, B. M. (2001) “Develope of a new family of normalize modulus reduction and material damping curves” Ph. D. Dissertation, Univ. of Texas at Austin, 362 p.

Das, Braja M. Principles of Soil Dynamics. Boston: PWS-Kent Pub., 1993. Print.

Dashti, Shideh, Jonathan D. Bray, Juan M. Pestana, Michael Riemer, and Dan Wilson. "Mechanisms of Seismically Induced Settlement of Buildings with Shallow Foundations on Liquefiable Soil." Journal of Geotechnical and Geoenvironmental Engineering 136.1 (2010): 151.

Delage, P., and Y. J. Cui. "An Evaluation of the Osmotic Method of Controlling Suction." Geomechanics and Geoengineering 3.1 (2008): 1-11. Web.

Fredlund, D. G., and H. Rahardjo. Soil Mechanics for Unsaturated Soils. New York: Wiley, 1993. Print.

Fredlund, Delwyn G. "Unsaturated Soil Mechanics in Engineering Practice." Journal of Geotechnical and Geoenvironmental Engineering 132.3 (2006): 286.

Gardner, W. R. "Calculation of Capillary Conductivity from Pressure Plate Outflow Data1." Soil Science Society of America Journal 20.3 (1956): 317.

Genuchten, M. Th. Van. "A Closed-form Equation for Predicting the Hydraulic Conductivity of Unsaturated Soils1." Soil Science Society of America Journal 44.5 (1980): 892.

Ghayoomi, M. and McCartney, J.S. (2011) "Measurement of the Small-Strain Shear Moduli of Partially-Saturated Sands During Infiltration in a Geotechnical Centrifuge." Special Issue on Advances in Experimental Characterization of Unsaturated Soils, Volume 1. ASTM Geotechnical Testing Journal. 34(5), 503-513.

Hardin, B. O. (1978). "The Nature ofStress-Strain Behavior of Soils," Proceedings, Geotech. Eng. Div. Specialty Conference on Earthquake Eng. and Soil Dynamics, Vol. 1 ASCE, Pasadena, June, pp. 3-90

Hardin, B. O. (1978). "The Nature ofStress-Strain Behavior of Soils," Proceedings, Geotech. Eng. Div. Specialty Conference on Earthquake Eng. and Soil Dynamics, Vol. 1 ASCE, Pasadena, June, pp. 3-90

Hardin, Bobby O., and Vincent P. Drnevich. "Shear Modulus and Damping in Soils: Measurement and Parameter Effects." Journal of the Soil Mechanics and Foundation Division (1972.): 603-624.

Hardin, Bobby O., and Vincent P. Drnevich. Shear Modulus and Damping in Soils: II Design Equations and Curves. Lexington, Ky: University of Kentucky, 1972. Print.

Hilf, J.W. "An Investigation of Pore-Water Pressure in Compacted Cohesive Soils", Thesis (pH.D.) University of Colorado, Denver, 1956

Houston, Sandra L., and Warren K. Wray. Unsaturated Soils: Proceedings of Sessions Sponsored by the Subcommittee on Unsaturated Soils (Committee on Soil Properties) and the Committee on Shallow Foundations of the Geotechnical Engineering Division of the American Society of Civil Engineers in Conjunction with the ASCE Convention in Dallas, Texas, October 24-28, 1993. New York: American Society of Civil Engineers, 1993. Print.

Ishibashi, I. and Zhang, X. (1993). “Unified Dynamic Shear Moduli and Damping Ratios of Sand and Clay,” Soils and Foundations, Vol. 33, No. 1, pp.182-191.

Khosravi, A. and McCartney, J.S. (2011). “ Resonant Column Test for Unsaturated Soils with Suction–Saturation Control.” ASTM Geotechnical Testing Journal. 34(6), 1-10.

Kokusho, T. (1980): Cyclic Triaxial Test of Dynamic Soil Properties for Wide Strain Range, Soils and Foundations, Vol. 20, No. 2, pp. 45-60

Kramer, Steven Lawrence. Geotechnical Earthquake Engineering. Upper Saddle River, NJ: Prentice Hall, 1996. Print.

Kunze, Raymond J., and Don Kirkham. "Simplified Accounting for Membrane Impedance in Capillary Conductivity Determinations1." Soil Science Society of America Journal 26.5 (1962): 421. Web.

Lu, Ning, and William J. Likos. Unsaturated Soil Mechanics. Hoboken, NJ: J. Wiley, 2004. Print.

Lu, Ning, Bailin Wu, and Chee P. Tan. "Tensile Strength Characteristics of Unsaturated Sands." Journal of Geotechnical and Geoenvironmental Engineering 133.2 (2007): 144. Web.

Mancuso, C., Vassallo, R., and d’Onofrio, A. (2002). “Small Strain Behavior of a Silty Sand in Controlled-Suction Resonant Column-Torsional Shear Tests.” Canadian Geotechnical Journal. 39(1), 22-31

Manual CATS Advanced and Universal 1.96 User’s Guide and Reference by GCTS Testing Systems.

Manual CATS Triaxial Test Mode 1.85 User’s Guide and Reference by GCTS Testing Systems.

Marinho, E. A. M., Chandler, R. J., and Crilly, M. S., 1995, “Stiffness Measurements on an Unsaturated High Plasticity Clay using Bender Elements,” Proceedings of the First International Conference on Unsaturated Soils, UNSAT ’95, Paris, France, 6–8 Sep. 1995, A. A. Balkema, Ed., Rotterdam, the Netherlands, Vol. 2, pp. 535–539.

Mendoza, C.E., Colmenares, J.E., and Merchan, V.E. (2005). “Stiffness of an unsaturated compacted clayey soil at very small strains,” Advanced Experimental Unsaturated Soil Mechanics. Trento, Italy, 27-29 June. 199-204.

Menq, F.Y. (2003) “Dynamic Properties of Sandy and Gravelly Soils” Ph. D. Dissertation, Univ. of Texas at Austin, 364 p.

Ng, C. W. W., Xu, J., and Yung, S. Y., 2009, “Effects of Wetting–Drying and Stress Ratio on Anisotropic Stiffness of an Unsaturated Soil at Very Small Strains,” Can. Geotech. J., Vol. 46, pp. 1062–1076

PCP-3000 Pressure Control Panel User’s Guide and Reference Rev.1.4, December,2010

Powrie, William. Soil Mechanics: Concepts and Applications. London: Spon, 2004. Print.

Richards, L. A. "A Pressure-Membrane Extraction Apparatus For Soil Solution." Soil Science 51.5 (1941): 377-86.

Seed, H. Bolton, and I. M. Idriss. Soil Moduli and Damping Factors for Dynamic Response Analyses. Springfield, VA: Reproduced by National Technical Information JService, U.S. Dept. of Commerce, 1970. Print.

Seed, H. Bolton, Clarence K. Chan, and Kenji Mori. "Influence of seismic history on liquefaction of sands." Journal of the Geotechnical Engineering Division 103.4 (1975): 257-270.

Silver, Marshall L., and H. Bolton Seed. “The Behavior of Sands under Seismic Loading Conditions”. Berkeley, CA: College of Engineering, University of California, 1969. Print.

Vanapalli, S. K., D. G. Fredlund, D. E. Pufahl, and A. W. Clifton. "Model for the Prediction of Shear Strength with Respect to Soil Suction." Canadian Geotechnical Journal 33.3 (1996): 379-92.

Appendix A: Complete setup for dynamic testing of unsaturated soils

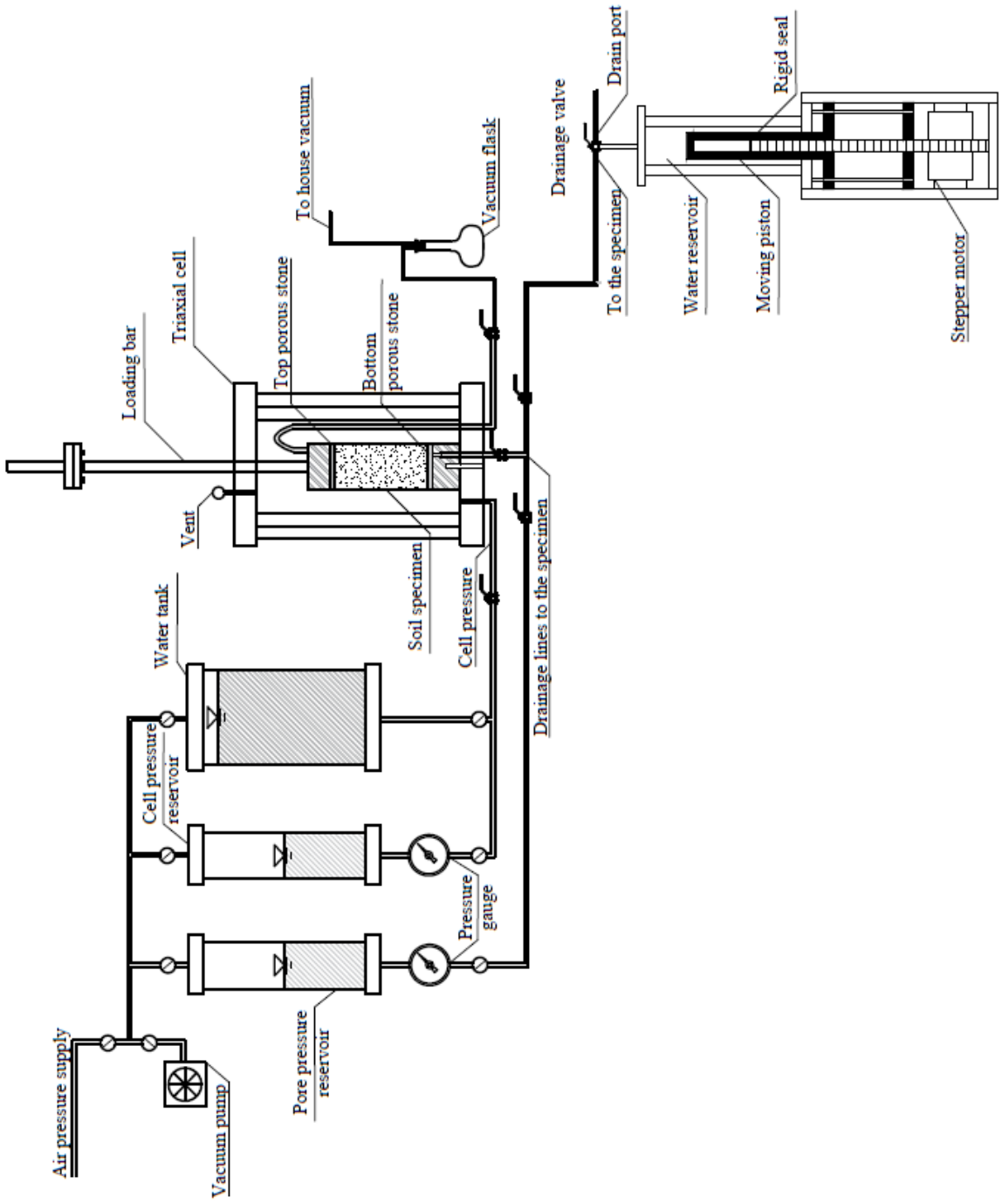

Figure A-106. Modified triaxial system at University of New Hampshire

Appendix B: View of the CATS and DigiFlow software

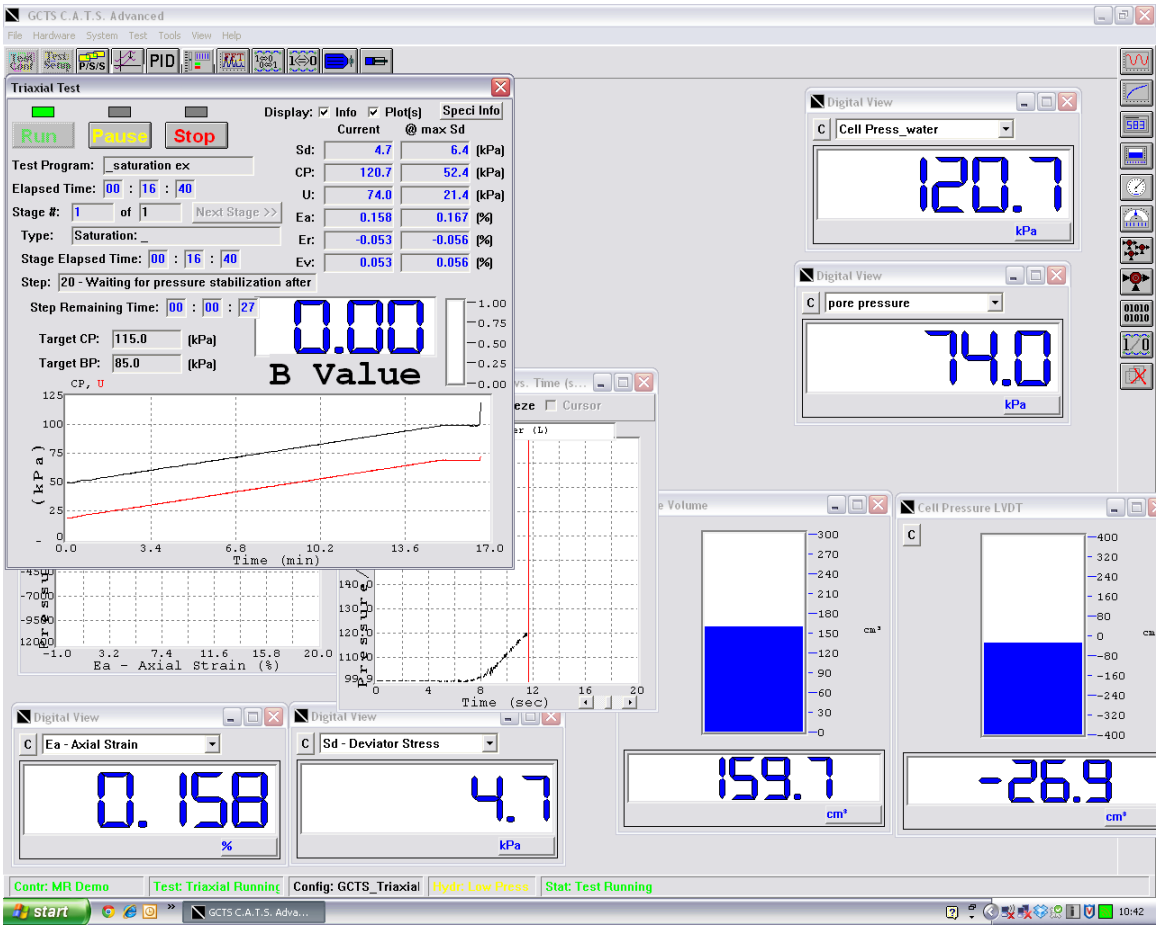

Figure B-107. CATS Software during B-value check

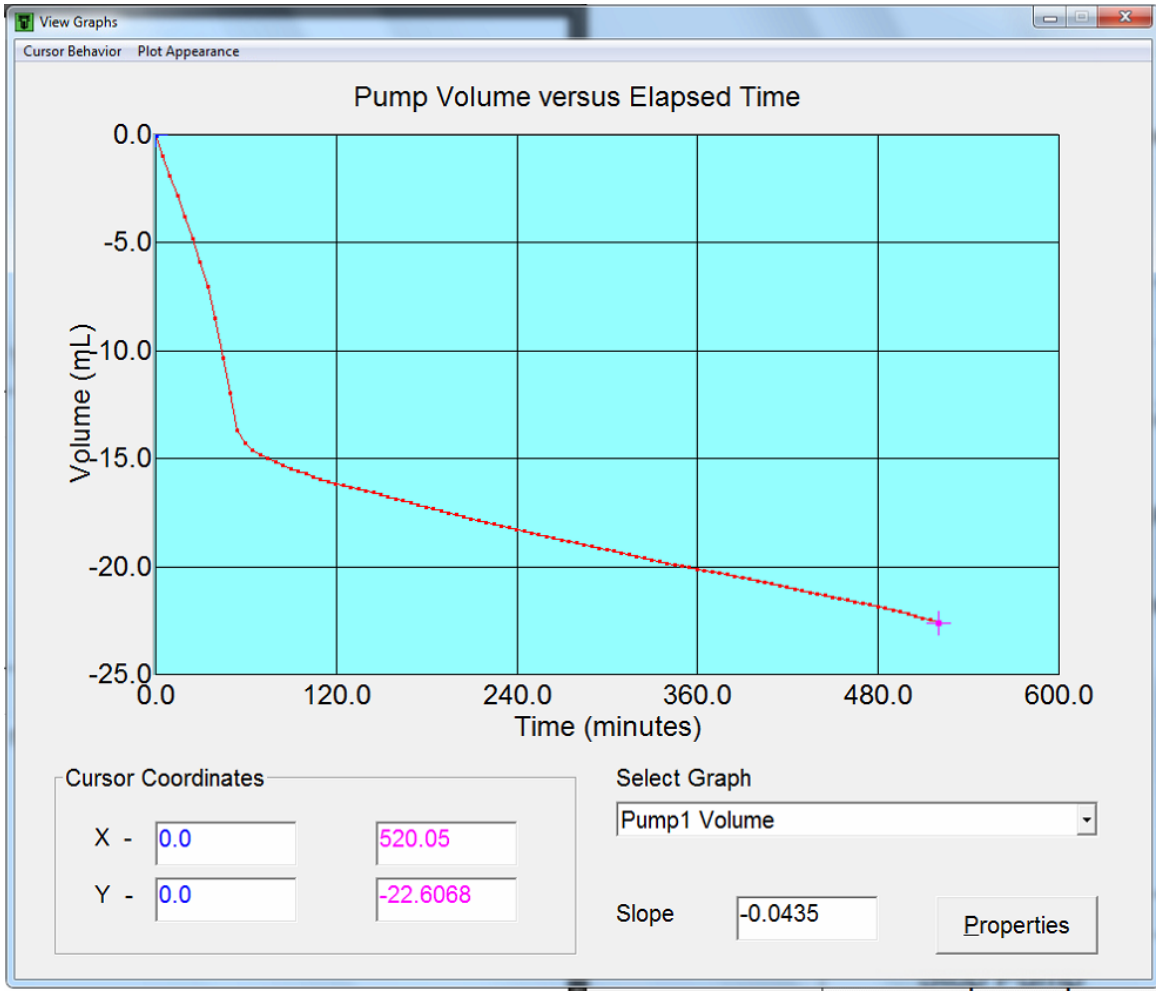

Figure B-108. Screenshot from DigiFlow Software during specimen desaturation

Appendix C: Matlab code used for data analysis

Was presented on a flash drive to Dr. Majid Ghayoomi

Appendix D: Modification of the bottom platen for triaxial cell

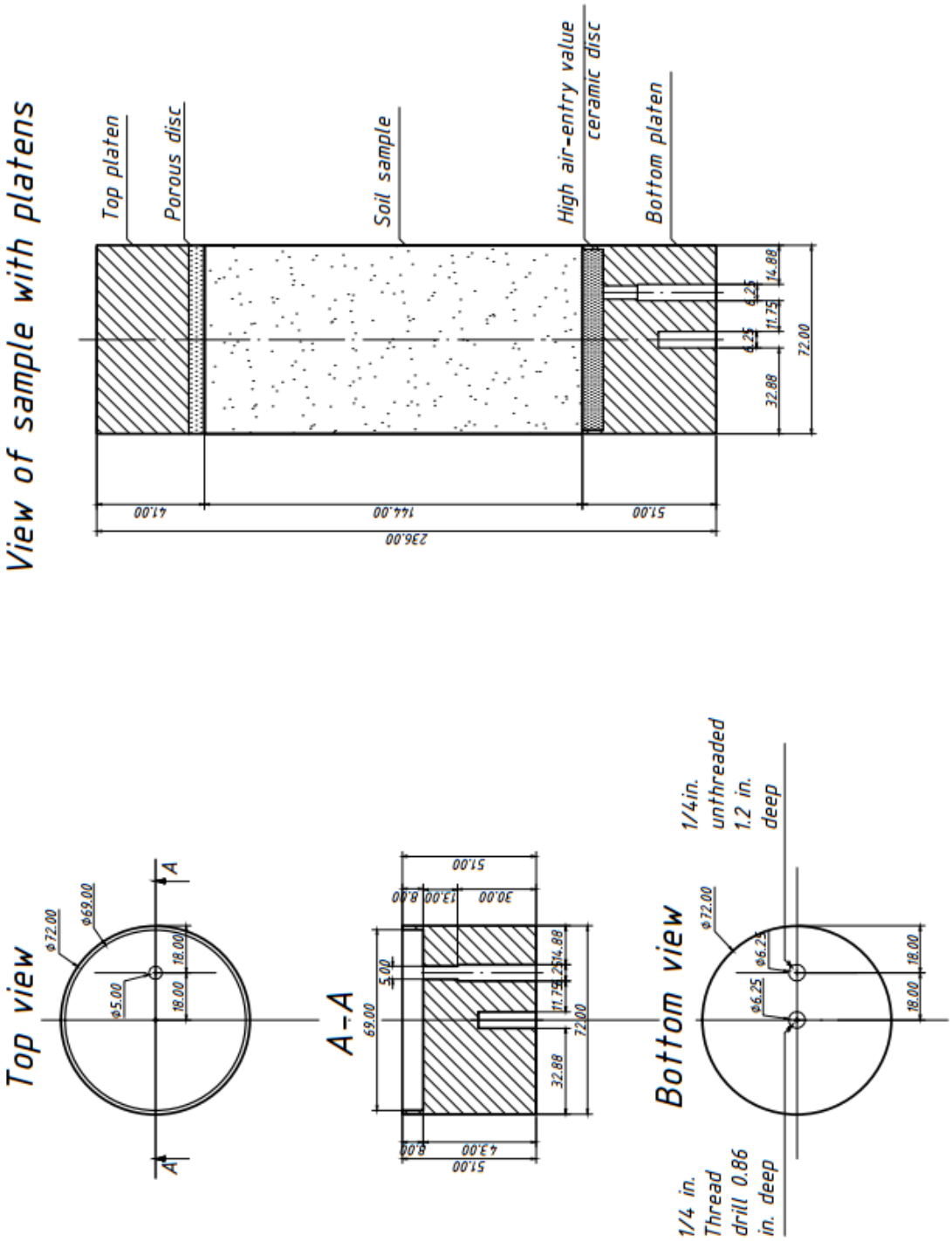

Figure D-109. Modification of the bottom platen

Appendix E: Modification of the top connection

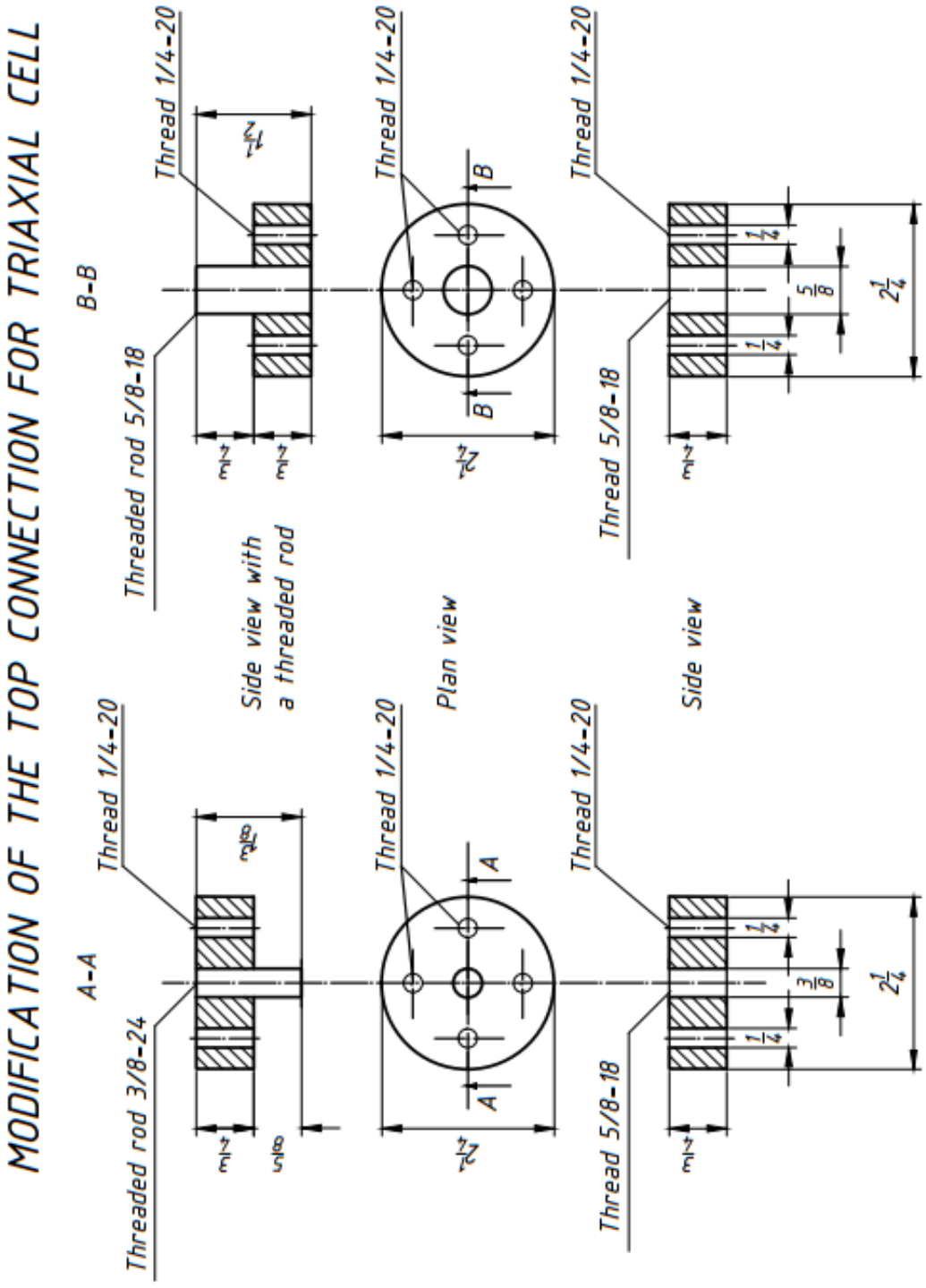

Figure E-110 Modification of the top connection

Appendix F: Guide for performing triaxial test with GCTS triaxial system

Before start of any test

Check all the connections between the system and computer.

Look inside the box with hydraulic pump and check two filters on pump itself.

Oil and filters should be changed every 5 years. The next change should be performed October 2017. If one filter will indicate that it needs to be changed -both filters should be replaced.

Oil Shell tellus46 or Mobile dte25, approximately 40 galons.

In case of emergency be ready to push the red button!

Circuit breakout: On the electricity panel near the door switches 31 33 35.

Part 1. General information

An experiment on the soil sample that is conducted in the laboratory usually simulates the actual field conditions. The data received after the test is used for predicting the behavior of soil element in the field. Consequently, it is crucial in the experiment to duplicate field conditions for more accurate results.

The main concept of triaxial test is to apply a three-dimensional stress to the soil specimen, while the pore pressure is controlled. A cylindrical specimen (2.8 in. width and 5.6 in. height) is embraced in the membrane. Rubber O-rings are used for sealing the membrane, therefore no water can trap into the specimen. Porous discs and filter paper are used to prevent soil flow into the system. The typical cell is shown in the Figure F-23.

A Plaxiglass cylinder, which is sealed on top and at the bottom), forms a cell which will have a soil specimen inside. Two valves give access to the bottom and top of the cell. Another 4 valves can be used to control soil specimen from the top and from the bottom. In a regular triaxial cell, water pressure is used for confinement pressure and a loading piston for imposing vertical stress.

Part 2. Specimen preparation

Any test outcome is highly dependent on specimen preparation. In case of inaccurate preparation, results might be flawed. Extreme care should be taken while tightening any metal pieces in the triaxial cell including rods and bolts. Vacuum grease should be applied in accordance with the instruction for creating a seal and elimination of water leakage.

In the geotechnical laboratory S 123, GCTS triaxial system includes a pedestal for triaxial cell with loading mechanism, hydraulic pump, GCTS PCS-3000 Control Panel and SCON-1000 Digital System Controller. Figure 19 shows the cell base, metal pieces for cell assembling, bolts, vacuum grease, rubber "o"-rings, hex wrenches on the pedestal with loading mechanism.

Before performing any action towards specimen preparation one has to make sure to have everything needed in easy access. All parts, as well as all grooves, must be clean of any dust or grease. Small vacuum cleaner can be used for eliminating dirt from the elements that are difficult to access.

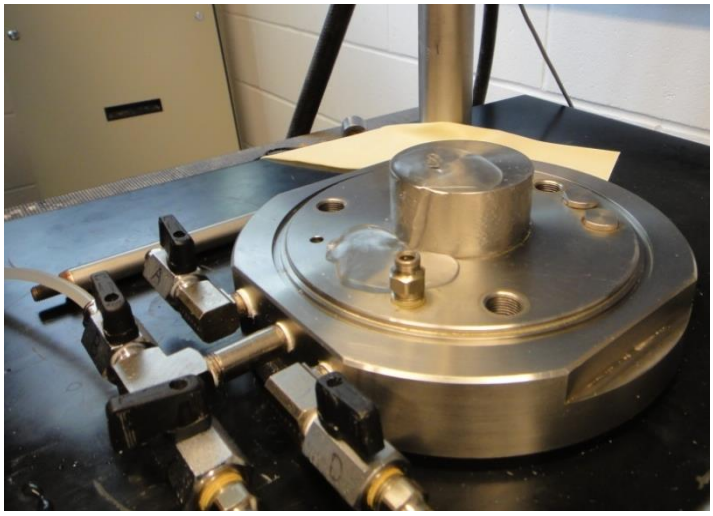

Figure F-111. Saturation of the system

In case of conducting a test on saturated or unsaturated soil, the system should be fully saturated before installing the specimen. In order to do this one should attach a hose to the connection on the Control Panel at the bottom of Reservoir (below the ball valve that says "Closed") to the valve B at the base of the cell. Open the ball valve on the cabinet and B valve on the bottom platen. Water should flow freely and no air bubbles should come out. After both conditions are met, the valves can be closed and water should be wiped from the bottom platen. However, experimental data showed that saturation of both B and C connections result in efficient performance. Repeat saturation procedure for both sides.

The next step in specimen preparation is application of the vacuum grease on the top and bottom platen. Make sure both metal pieces are clean and dry and have no sand on it. Figure below show the original GCTS bottom platen, that can be used for dry or saturated soils. However, for testing unsaturated soil specimens, the bottom platen should be changes to one shown in the Figure F-7:

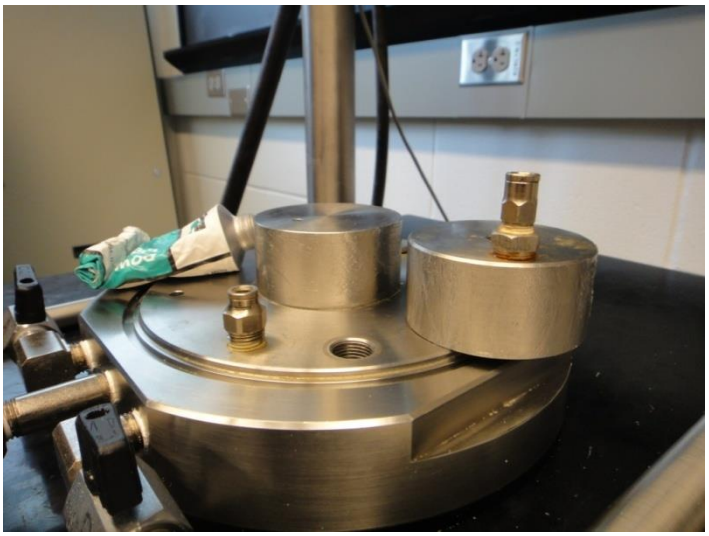

Figure F-112. Top and bottom platens with vacuum grease

The membrane should be stretched on the bottom platen and two rubber “o"-rings should be put over it. This will prevent water from the cell from entering the specimen, therefore create an isolated confinement.

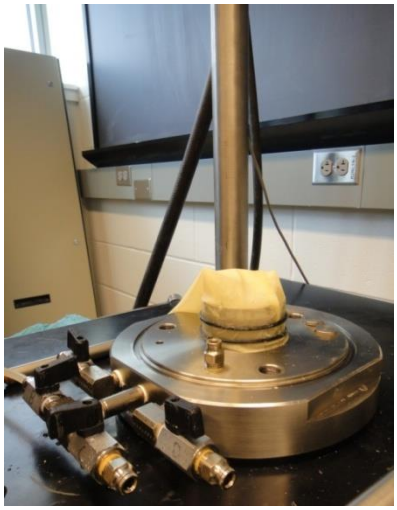

Figure F-113. Membrane stretched on the bottom of the cell

One should take the mold and install it over the membrane and rubber “o”-rings on the bottom platen. Pliers may be used for tightening the wings on the mold. The membrane should be stretched on top of the mold before applying vacuum. Connect the hose from the mold to the vacuum connection on the cabinet. Turn the vacuum regulator and open the valve that says “Vacuum”. One should feel it before connecting hose to the mold. The vacuum applied to the mold will stretch the membrane for further specimen preparation.

The arrow valve on the cabinet (to the left of Top Back Pressure regulator) should point down, which means that vacuum is applied simultaneously to the connection under “Vacuum” valve and water reservoir inside the cabinet. For water in the tank to be deared properly, leave vacuum on for 24 hours (GCTS Technical Support,2014).

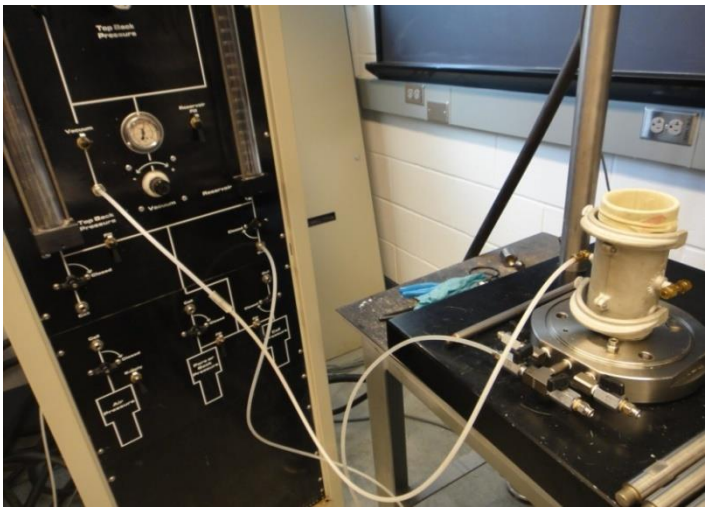

Figure F-114. Vacuum application to the mold to stretch the membrane

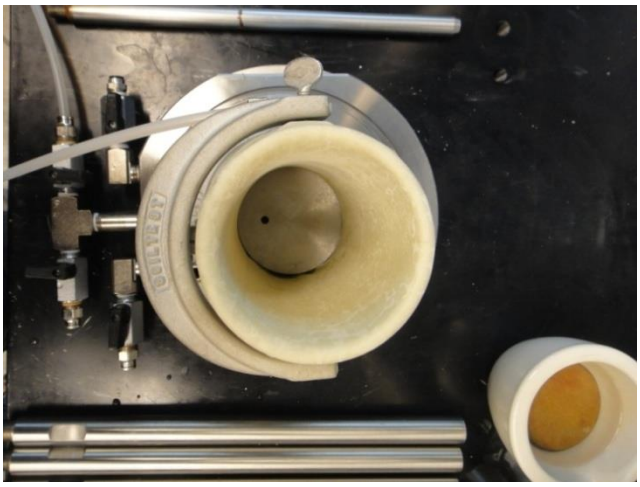

Figure F-115. Stretched membrane over the metal mold

Saturated porous stone should go on the bottom, followed by a filter paper. For an easier saturation of the specimen, porous stones need to be saturated beforehand. This can be done by soaking them in water for 24 hours, or boiling for 2 hours.

Figure F-116. Installed porous stone with filter paper on top

The next step is adding the soil to the mold. Any method may be used for sample preparation, but in this study pouring of the sand was done by dry pluviation method. Description and procedure might be found in ASTM D 4253-83: A Comparative Study "Maximum Dry Density of Cohesionless Soils by Pluviation". A funnel of a standard size is needed to pour the sand from a specified height. Ottawa F75 sand was used in this research study. Because of the fine grains involved in silica sand, it can be harmful for your health. If a respirator or mask is not used during any work with this sand it can result in lung irritation which can evolve in chronic decease called silicosis.

Silicosis has no ready treatment, and can cause severe pain or death. For this reason all materials in the lab containing more than 0.1% of silica sand must be clearly labeled.

After the specimen is installed and compacted, filter paper and porous stone should go on top. Metal platen with vacuum grease is mounted after porous stone, and membrane is flipped over it. The top platen on the specimen should strictly horizontal. Small level can be used for this purpose.

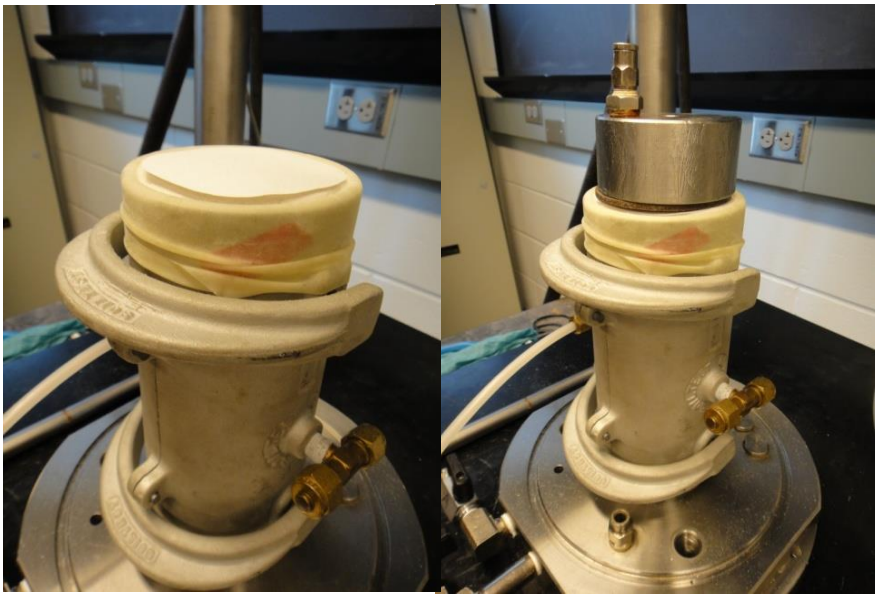

Figure F-117. Mounting the sand sample

Vacuum should be applied to the sand specimen to hold it. For this purpose, house vacuum is used and applied through an empty bottle to prevent any dirt or water to be withheld in the system. A small tube is connected to the base of the cell and the top platen. House vacuum should be open, and valve C on the base of the cell should be on.

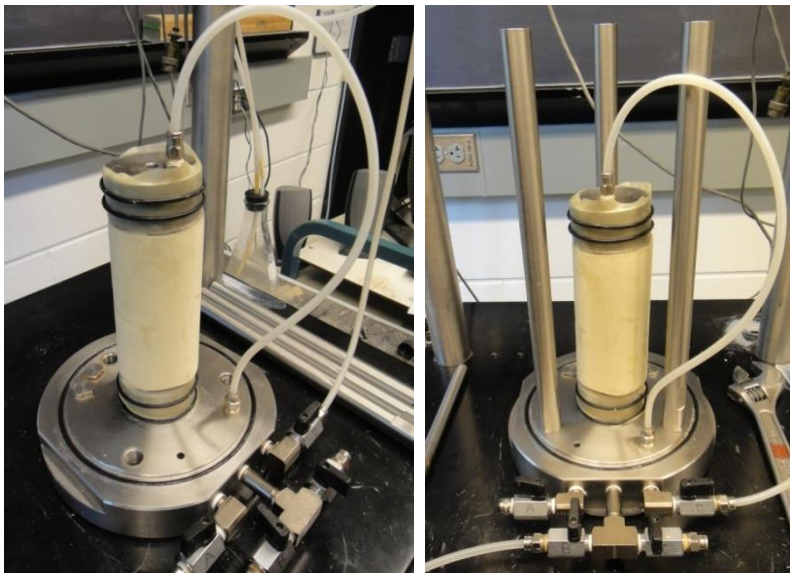

Figure F-118. Application of house vacuum

Rubber “O”-ring should be embedded in the groove at the bottom of the cell. Vacuum grease should be applied on the ring and nearby area. After vacuum application to the specimen, the metal mold can be taken apart.

Turn off the vacuum valve on the cabinet and disassemble the metal mold. Screw metal frame parts to the base of the cell by using wrench. Also, steel piston for load application should be installed on the top platen of the specimen.

After those steps are performed, metal top of the cell should be installed with three large screws and hex wrench. Plaxiglass cell can be mounted afterwards and should sit on the greased rubber “O”-ring. Metal ring for the cell should be installed on top of the Plaxiglass and screwed with four small screws.

When the cell is ready, vacuum should still be applied to the specimen. For performing triaxial test the cell should be filled with water. Ideally, deaired water must be used for this purpose. In case if house water used for this purposes air bubbles that might get inside the rubber membrane to the specimen and cause incomplete saturation.

Connect hose to valve A (which corresponds to bottom of the cell) and to the opening under reservoir on the cabinet. Open the valve and wait for the cell to be filled. Make sure there is enough water in the deaired tank to use difference in height for filling the cell. Also, the valve at the top of the cell should be open.

Performing tests for educational purposes, the cell is filled with house water through the same A valve at the bottom.

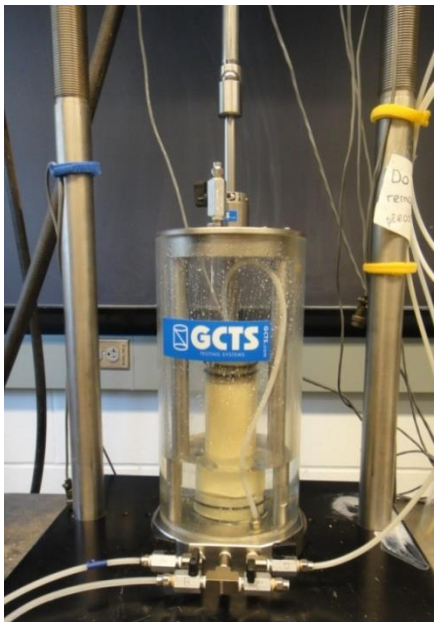

Figure F-119. Filling the cell with water

After the cell is filled with water, close A valve and valve on the cabinet or house vacuum. The specimen is ready to work with. Push the cell very carefully under the load frame, and secure the bottom of the cell to the table with two large screws to prevent any movement of the cell during the vertical loading that can cause wrong results of the test.

Part 3. Running the test

Find “Shortcut to CATS” software icon on the desktop of computer and double click left mouse button. Login and password should appear automatically. Otherwise, enter login : gcts ; password: gcts.

Figure F-120. Login icon in CATS software

The next step will be turning on hydraulic pump  on Low Presure.

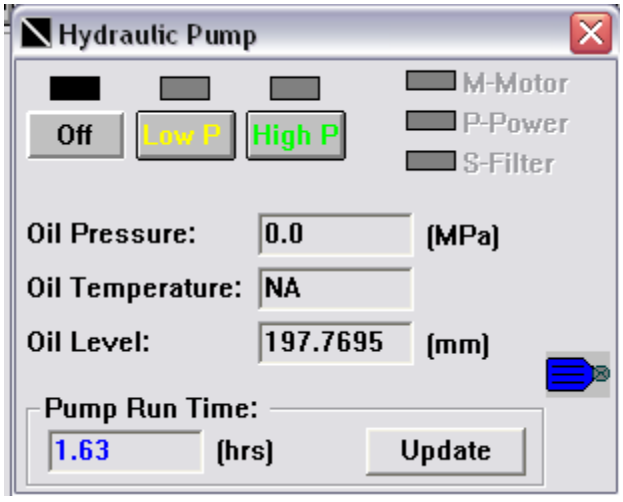

Figure F-121. Hydraulic pump icon

From this point all the controllers can be turned on. The first one would be Load Frame. Bring the piston down to touch the ball (but the ball should be able to roll)

This can be done by opening Output Functions  -Load Frame and Load Frame LVDT control and pushing arrow “down”.

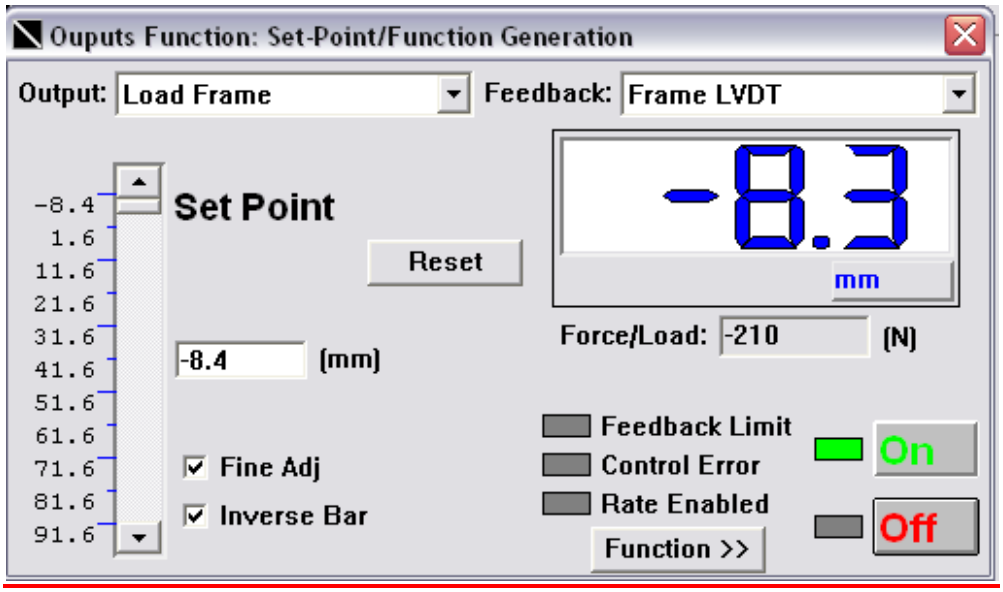

Figure F-122. Output functions

When this step is done, open Inputs Offset  window and zero Axial load and Frame LVDT

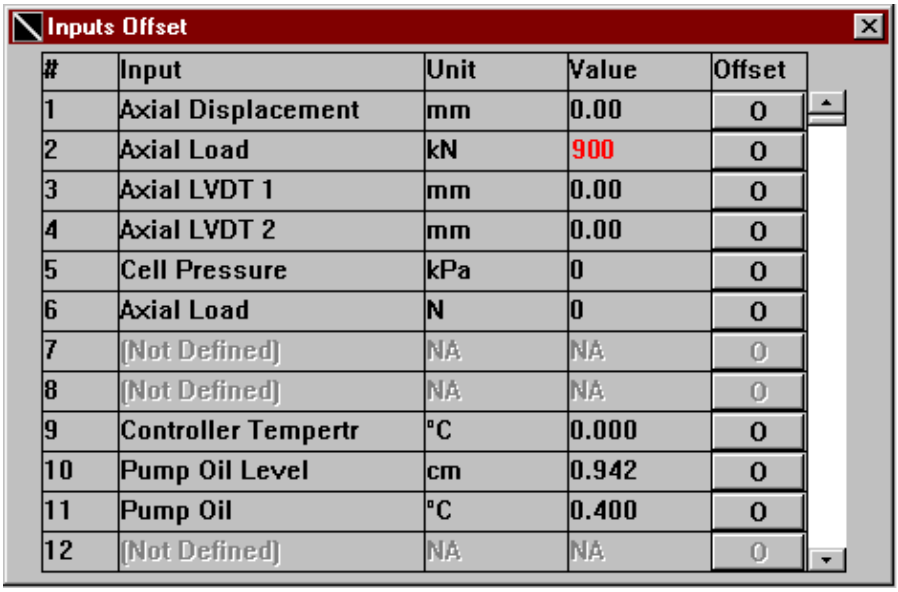

#	Input	Unit	Value	Offset
1	Axial Displacement	mm	0.00	0
2	Axial Load	kN	900	0
3	Axial LVDT 1	mm	0.00	0
4	Axial LVDT 2	mm	0.00	0
5	Cell Pressure	kPa	0	0
6	Axial Load	N	0	0
7	(Not Defined)	NA	NA	0
8	(Not Defined)	NA	NA	0
9	Controller Tempertr	°C	0.000	0
10	Pump Oil Level	cm	0.942	0
11	Pump Oil	°C	0.400	0
12	(Not Defined)	NA	NA	0

Figure F-123. Inputs icon in CATS software

For cell pressure application, switch Output to Cell Pressure and turn it on. At this time hose from the valve A should be connected to the "Cell Pressure" opening on the cabinet. For turning on Pore Pressure connect another hose to the cabinet. Switch Output to Pore Pressure and Feedback to Pore volume. Bleed the hose by pushing the arrow on the screen up before connecting it to the valve C. In the software the controller should be switched to Pore Pressure. At this point Pressure Cylinder and Specimen are connected. Make sure this pressure never exceed cell pressure. If this happens, the specimen will collapse and can not be used for further testing.

After all three controllers are turned ON, the specimen is ready to test. For performing tests on saturated specimens, B-value check should be done before.

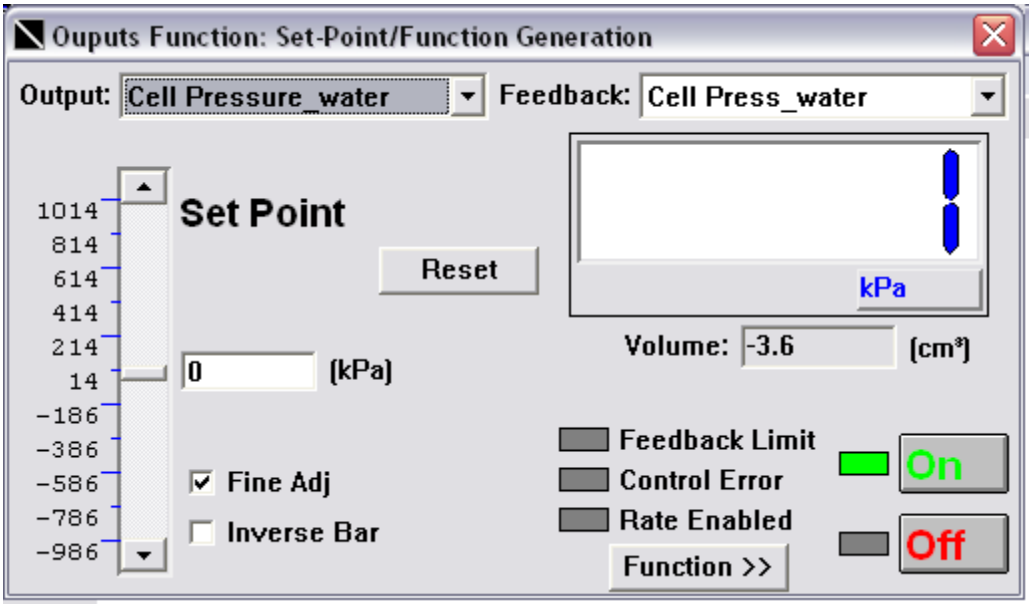

Figure F-124. Cell pressure output function

If the soil in the real conditions in the field is saturated, it is essential to saturate the specimen. The reason for this is to obtain a pore pressure response that will correspond to that of the soil deposit in the field.

Sometimes incomplete saturation of the specimen arise because of the air bubbles trapped between the soil sample and the membrane or filter paper, or device for measuring pore pressure and the drainage lines. This problem may be solved by applying back pressure through drainage lines while increasing cell pressure equally. Because of the fact that pore pressure varies through the specimen, it is vital to prevent exceeding of effective stress to the final consolidation stress at any point in the sample.

The maximum level of pressure ramping depends on the “B” value, which may be described as the change of pore pressure over the change of cell pressure.

Fill the specimen with deaired water from the same reservoir located inside the cabinet. After that turn on Pore Pressure Controller, and switch Feedback to Pore Volume. Make sure that liquid indicator inside the cylinder is in the middle position before every test.

For conducting the test, a new program should be created or chosen an existing one.

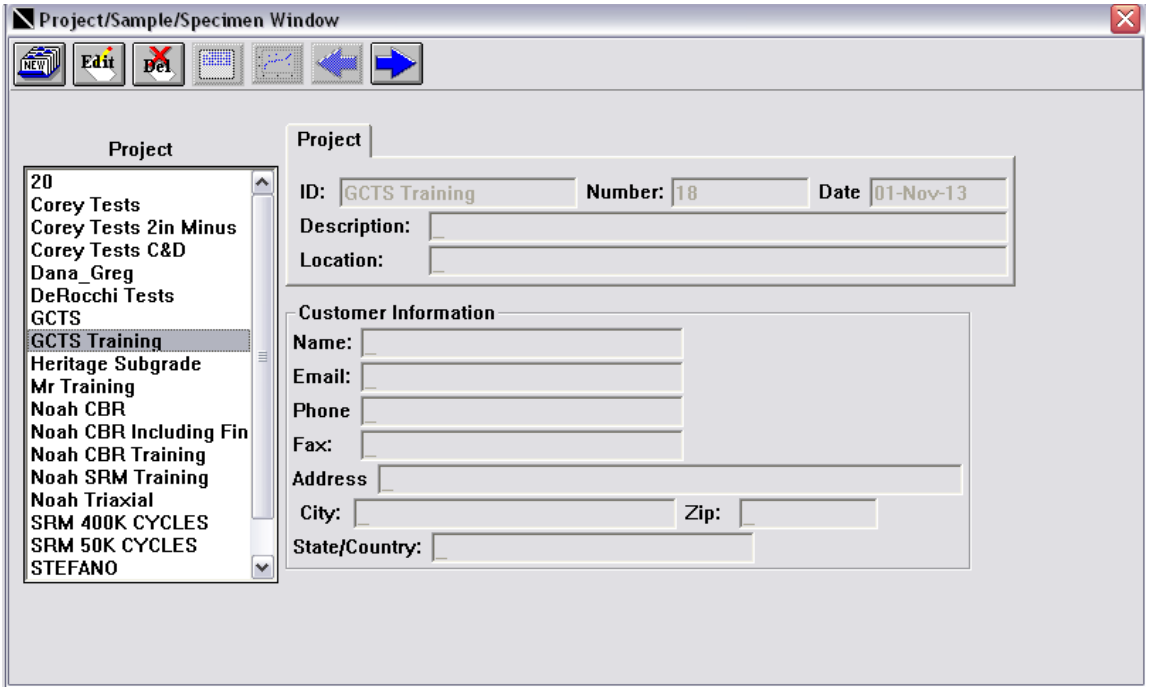

Figure F-125. Project Window in CATS software

After the program is selected, the specimen should be created with entering height of the specimen and platens, weight of the sample, specific gravity. The next step is to choose the test that should be conducted on the specimen (double click on it- see Figure 3.8)

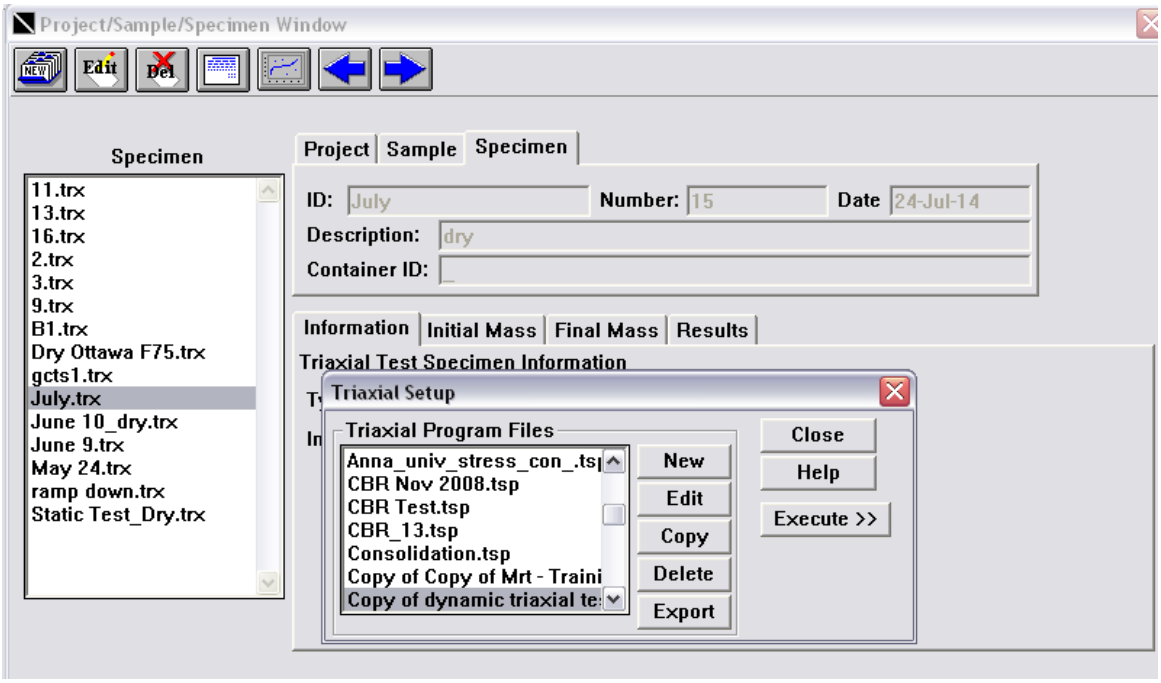

Figure F-126. Creating Specimen Window

For different programs that might be used in CATS software, see Manual CATS Advanced and Universal 1.96 by GCTS Testing Systems. For example, the test program “ramp up” was created for increasing cell pressure and axial load (or strain) before starting the test.

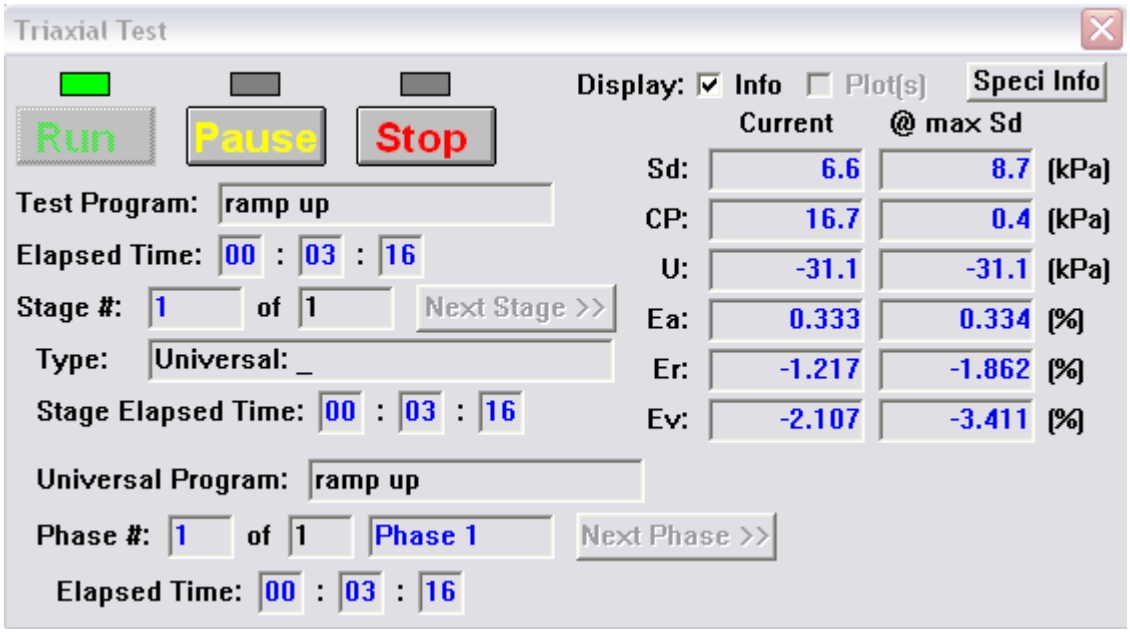

Figure F-127. Ramp up program based on Universal test

After reaching the necessary parameters, the strain controlled test has been conducted.

Programs Icon -> Choose specimen -> Strain Control -> Check all the inputs.

They should correspond the desirable test parameters. The test program can consist of several phases, deformations might be zeroed or kept as it is.

For more information about parameters see manuals for Triaxial Test.